elektronisches dokument
ULB Sachsen-Anhalt

Characterization of Rubber-filled Polymers by Solid-State NMR Spectroscopy and other Methods

Dissertation

zur Erlangung des akademischen Grades
Dr. rerum naturlalium (Dr. rer. nat.)

vorgelegt der

Mathematisch-Naturwissenschaftlich-Technischen Fakultät
(mathematisch-naturwissenschaftlicher Bereich)
der

Martin-Luther-Universität Halle-Wittenberg

von Frau

Mihaela Aluas

geb. am 27.12.1974 in Hida, Rumänien

Gutachter:

1. Prof. Dr. Horst Schneider
2. Prof. Dr. Dan Demco
3. Assoc. Prof. Dr. Simona Cinta Pinzaru

Halle (Saale), 25 October 2004

CONTENTS

Zusammenfassung

1 General Introduction 1

1.1 Motivation 2

1.2 Cross-linked Polymers and their Blends 4

1.2.1 The Nature of Polymers 4
1.2.2 The Mechanism of Sulfur Vulcanization 5
1.2.3 Thermoplastic Elastomers 8

1.3 NMR Methods used on Polymers Study 10

1.3.1 NMR Phenomenon 10
1.3.2 Magic Angle Spinning 12
1.3.3 Dipolar Decoupling 16
1.3.4 Cross Polarization 17

2. Samples and Previous Work 18

2.1 Samples and Non-NMR Methods 19

2.1.1 Ethylene Propylene Diene Monomer 19
2.1.2 The blends of Polypropylene/Ethylene-Propylene Diene Monomer 23
2.1.3 Non-NMR Methods 25
2.1.3.A. Differential Scanning Calorimetry 25
2.1.3.B. Dynamic Mechanical Analysis 26

2.2 Results and Discussions 27

2.2.1 Previous Results 27
2.2.2 Results from DSC Measurements 28

3 Proton NMR on Cross-linked Polymers 31

3.1 Residual Dipolar Coupling and Proton NMR Relaxation 32

3.1.1 Introduction 32
3.1.2 Transverse Relaxation-Background 33
3.1.3 Transverse Relaxation Function 37
3.1.4 Rescaling of the Dipolar Interaction 40
3.1.5 The Second Moment Approximation 43

3.2 Different Methods of Cross-link Density Determination from Proton NMR Relaxation 45

3.2.1 Gotlib Model 45
3.2.2 Litvinov's Method 48

3.3 Experimental Detection of Proton Transverse Relaxation 50

3.4 Results and Discussions 52

3.4.1 Determination of the Network Density for EPDM Samples 52
3.4.2 T_2 Results for PP/EPDM blends - The Influence of PP 55

4 Spin-echo, Solid-echo Double Resonance (SEDOR) and Rotational-echo Double Resonance (REDOR) applied on polymer blends 58

4.1 Introduction 59

4.2 Theoretical Background 60

4.2.1 The Principle of SEDOR 60
4.2.2 The Principle of REDOR 62

4.3 REDOR Pulse Sequence – a Practical Version for Elastomers 63

4.4 Experiments-Results and Discussions 64

5 Characterization of Cross-linking in EPDM/PP Blends from ^{1}H-^{13}C Polarization Transfer Dynamics 67

5.1 Introduction 68

5.2 Short Description of Cross-Polarization Process 69

5.3 Experimental Details 70

5.3.1 Recording Cross-polarization and Depolarization Curves 70

5.3.2 The Determination of Magnetization Transfer Efficiency 72

5.4 Results and discussions 73

5.4.1 Carbon CP-MAS Spectra 73

5.4.2 Cross-polarization and Depolarization Curves 74

5.5 Analysis and Discussions 80

5.5.1 The Thermodynamic Model 80

5.5.2 The Model of Residual Dipolar Interaction under Permanent Cross-linking 83

6. Conclusions 91

REFERENCES 94

ACKNOWLEDGEMENTS 99

CURRICULUM VITAE 100

PUBLICATIONS AND POSTERS 101

ZUSAMMENFASSUNG

Thermoplastische Elastomere stellen eine relativ neue Klasse von polymeren Materialien dar. In ihnen sind Eigenschaften von Thermoplasten (z.B. gute Verarbeitbarkeit) mit denen von vernetzten makromolekularen Systemen (z.B. Elastizität) vereint. Ein mögliches Konzept für deren Herstellung besteht darin, feinkörniges Elastomer-Pulver mit einer thermoplastischen Schmelze zu verrühren. Damit eröffnet sich gleichzeitig die Möglichkeit der Wiederverwendung von Kautschuk-Altmaterialien. Die mechanischen Eigenschaften des Materials hängen unter anderem von der Vernetzungsdichte der Elastkomponente ab, repräsentiert durch die hierzu reziproke mittlere Netzbogenlänge M_C. Es wird erwartet, dass sich dieser Wert während des Verarbeitungsprozesses noch ändert. Die Charakterisierung der dispergierten Netzwerke mit Standardmethoden ist sehr schwierig, wenn eine integrale Messmethode verwendet wird, weil hierbei der Einfluss der thermoplastischen Matrix auf die Messwerte oft kaum separiert werden kann. Das betrifft insbesondere mechanische Messungen und Quellungsexperimente.

Im Rahmen der vorgelegten Arbeit wurden Verbundsysteme aus Polypropylen (Thermoplast) und EPDM (Elast) untersucht. Die Aufgabe bestand darin, die hohe Selektivität von NMR-Verfahren zu nutzen, um allein die Elastphase zu charakterisieren. Das Ziel sind zum einen Erkenntnisse über die Art und Stärke der Veränderung der Vernetzungsdichte während der Verarbeitung (Extrudieren). Weiterhin sollen verschiedene denkbare NMR-Verfahren getestet und bezüglich der Einsatzparameter optimiert werden. Die verwendeten Proben waren im Institut für Werkstoffwissenschaften (Martin-Luther-Universität, FB. Ingenieurwissenschaften) hergestellt und dort bereits mittels DSC und dynamisch-mechanischer Verfahren charakterisiert worden.

Gemeinsames Merkmal aller hier verwendeten NMR-Verfahren ist die Erscheinung, dass infolge durch das Netzwerk verursachter topologischer Beschränkungen auch in sehr hochbeweglichen Systemen die zwischen den Kernspins bestehende dipolare Wechselwirkung nicht vollständig ausgemittelt werden kann. Die verbleibende dipolare Restwechselwirkung hängt vom Grad der Vernetzung ab und kann daher als Maß für M_C angesehen werden.

Das ^{1}H-Spin-Echo-Verfahren zur Aufzeichnung der transversalen Protonen-Relaxation ist eine vergleichsweise einfache NMR-Methode, die bereits von anderen Autoren zur Charakterisierung von Netzwerken eingesetzt wurde. Hiermit war es jedoch nicht möglich, das PP-Signal von dem uns interessierenden EPDM-Signal zu trennen, weil die chemische Verschiebung zwischen beiden weit kleiner als die Breite der ^{1}H-Resonanzen ist. Darüberhinaus kann das Gesamtsignal nicht als einfache lineare Überlagerung der Signale der reinen Komponenten angesehen werden, wofür wahrscheinlich Wechselwirkungen zwischen beiden Phasen verantwortlich sind. Somit konnte dieses Verfahren nur zur M_C-Bestimmung der Ausgangssubstanz (reines EPDM) erfolgreich eingesetzt werden.

Für die Untersuchungen der Verbundmaterialien war es daher notwendig, auf die weitaus aufwändigere ^{13}C-MAS-NMR auszuweichen. Das hohe Maß an Selektivität dieser Methode gestattet einen getrennten Nachweis von PP- und EPDM-Signalen, so dass erst auf dieser Basis eineVoraussetzung für die erfolgreiche Lösung des gestellten Problems gegeben war. Allerdings wird die dipolare Restwechselwirkung durch die schnelle Probenrotation (MAS) weiter reduziert.

Im Einzelnen wurden folgende ^{13}C-NMR-Verfahren verwendet:

^{13}C-Spin-Echo kombiniert mit ^{13}C-^{1}H-Spin-Echo-Doppelresonanz (SEDOR): Diese Methode stellt eine Übertragung der auf das Protonen-Spinsystem angewandten Methode dar. Die Methodenkombination wird genutzt, um speziell auf die ^{13}C-^{1}H-Wechselwirkung zuzugreifen und so für die Gültigkeit der bei der Auswertung verwendeten Modelle bessere Voraussetzungen zu schaffen. Die erhaltenen Relaxationskurven erwiesen sich allerdings als sehr wenig empfindlich gegenüber dem Vernetzungszustand, wodurch die Genauigkeit der hieraus abgeleiteten Parameter nur sehr gering einzuschätzen ist.

Mit ^{13}C-^{1}H-REDOR-Experimenten gelingt es, den Einfluss der dipolaren Wechselwirkung auf die Relaxationsfunktion, der durch MAS stark verringert wird, wieder zu verstärken. Unterschiedliche Grade an Vernetzung spiegeln sich im Verlauf der REDOR-Kurve wider. Jedoch war auch hier die Genauigkeit der Ergebnisse noch nicht zufriedenstellend.

^{13}C-^{1}H-Polarisationstransferexperimente erwiesen sich hier als am empfindlichsten bezüglich des Einflusses der Vernetzungsdichte. Mit Hilfe des Kreuzpolarisationsverfahrens wird Magnetisierung zwischen dem ^{1}H- und dem ^{13}C-Spinsystem übertragen; die

Übertragungsgeschwindigkeit hängt dabei von der Stärke der dipolaren Wechselwirkung ab. Dabei wurden zwei unterschiedliche Varianten genutzt:

1. Polarisation des ^{13}C-Spinsystems durch ^{1}H-Magnetisierung; der Zeitverlauf wird durch den Aufbau der ^{13}C-Resonanzen verfolgt. Durch Relaxationsvorgänge erfolgt allerdings ein allmählicher Zerfall dieser Polarisation, der dazu führen kann, dass hochbewegliche Bereiche in der Transferkurve unterrepräsentiert sind.
2. Depolarisation des ^{13}C-Spinsystems durch Abfluss der mittels $\pi/2$-Impuls erzeugten ^{13}C-Magnetisierung in das Protonensystem.

Diese Polarisationsexperimente erwiesen sich als am besten geeignet, die dipolare Restkopplung in den EPDM-Bereichen der Proben zu bestimmen.

Die Bestimmung von M_C aus der Stärke der dipolaren Restwechselwirkung kann analog zu den aus der Literatur bekannten Vorgehensweisen bei der Analyse von Protonenrelaxationsdaten erfolgen. Dabei kann eine auf der Grundlage der KUHN-GRÜN-Statistik erhältliche Beziehung genutzt werden, die eine reziproke Abhängigkei der dipolaren Restwechselwirkung von M_C beschreibt.

1 General Introduction

The topic of this thesis is the characterization of elastic phase in polymer blends by means of Solid-State Nuclear Magnetic Resonance Spectroscopy. In this chapter, after motivating the present work, a brief introduction in the field of polymers as well as in the field of NMR is given. The standard NMR methods used for studying the solid state systems are also presented.

1.1 Motivation

Thermoplastic elastomers (TPEs) are obtained by mechanically mixing soft, elastic polymers with hard, crystallisable polymers. The hard and soft segments must act as individual phases and therefore should not have thermodynamical compatibility.

Mechanical properties, and especially the level of elasticity, can be improved by dynamical cross-linking *in situ* of the elastomer during mixing with the thermoplastic material[1,2]. The resulting class of materials is called thermoplastic vulcanizates (TPVs) and presently represents the fastest growing rubber market. The material bases for commercial TPVs production are, generally, isotactic polypropylene and uncross-linked EPDM. The latter is a terpolymer of ethylene, propylene and a diene-monomer which introduces side chain unsaturation suitable for sulfur vulcanization. EPDM is becoming more and more a general-purpose rubber because of its uptake in the automotive industry and other sectors. Being used at industrial scale, the recycling of EPDM is very important and therefore the production of TPEs and TPVs based on cross-linked EPDM is considered. The macroscopic properties of these materials are intrinsically connected to the molecular motion occurring within the elastomeric phase and therefore it is important to quantify the dependence of these motions on the cross-link density.

Determining cross-link density of the elastomeric phase after the blending process with standard methods, for example swelling or dynamic-mechanical investigations, is very difficult as the contribution of the two phases (i.e. PP and EPDM) to the measured data can be hardly quantified. The same problem is encountered also by the consecrated NMR methods used for determination of cross-linked density, such as proton transversal relaxation. The resonance of PP and EPDM superimpose in a way which does not allow for an unambiguous estimation of the EPDM structural parameters. This is because in the signal superposition we observed a remarkable non-linearity: the blend signal significantly deviates from the corresponding linear superposition that we generated numerically from signals of pure PP and EPDM, respectively.

^{13}C NMR represent a solution to this problem because in carbon spectra some EPDM resonances are well separated from the PP resonances, hence giving us access to the EPDM phase of the vulcanizate. The cross-link density influences the NMR signal via residual dipolar

coupling. Some experimental schemes, like Spin-echo, Spin-echo Double Resonance (SEDOR) and Rotational-echo Double Resonance (REDOR), are proposed to estimate this parameter. The problems encountered by analyzing these results are discussed and the insensitivity of REDOR to small differences in cross-link density is proved. For determining the effect of dynamical cross-linking process upon the cross-link density of the rubber phase in our system, another experimental and theoretical approach is needed.

We demonstrate the use of cross-polarization between the ^{1}H and ^{13}C spin system in the direct version (polarization of the ^{13}C spins by protons) as well as in the indirect one (depolarization of the ^{13}C spin system towards protons). Characteristic features of the residual dipolar coupling network under intense molecular motion in elastomers at high temperatures are exploited in the present work to elaborate a more rigorous description of CP dynamics, with the purpose of making the structural information encoded in the corresponding CP build-up curves more readily available.

1.2 Cross-linked Polymers and their Blends

1.2.1 The Nature of Polymers

Plastics and rubbers are now industrially produced and universally available. These materials are build from relatively simple substances of low molecular weight, sometimes called mers, or more usually, monomers, and the reaction by which they are joined together is polymerization. The product of such reaction is a polymer.

There are two major kinetic schemes by which the polymers can be synthesized: chain and stepwise polymerization. The most important of the chain polymerization methods is free radical polymerization[3].

Polymers can be amorphous (totally lacking positional order on the molecular scale) or semicrystalline (containing both crystalline and amorphous regions in the same sample).

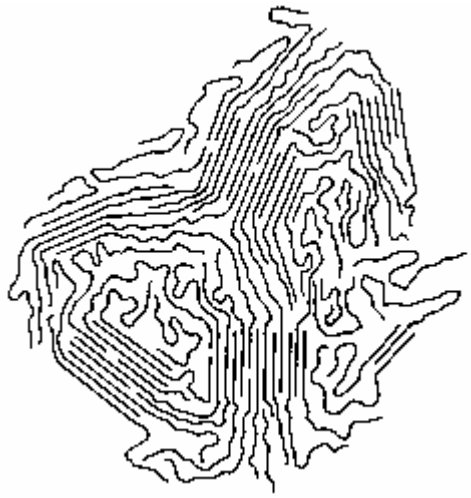

Figure 1.1 A semi-crystalline polymer containing amorphous and crystalline regions

Many of the properties of polymers can be ascribed to their organic nature or to the chain structure. The primary bonds which hold together the atoms in a polymer chain are strong: polymer degradation only occurs at relatively high temperatures (about 200^0 C). The forces

between the polymer chain, polar and induced dipolar forces, comprise dispersion. Because these forces are weak, although the fact that they operate over the hole chain length increases their effectiveness, the softening points and the strengths of polymers are comparatively low[4].

At low enough temperatures all amorphous polymers are stiff and glassy. This is the glassy state, sometimes called the vitreous state, especially for inorganic materials. On warming, the polymers soften in a characteristic temperature range known as the glass-rubber transition region. For amorphous polymers, the glass transition temperature, T_g, constitutes their most important mechanical property. Qualitatively, the glass transition region can be interpreted as the onset of long-range, coordinated molecular motion. While only a few chain atoms are involved in motion below the glass transition temperature, some more chain atoms attain sufficient thermal energy to move in a coordinated manner in the glass transition region.

The crystalline state is defined as one that diffracts x-rays and exhibits the first-order transition known as melting. Polymers crystallized in the bulk state are never totally crystalline, a consequence of their long-chain nature and subsequent entanglements. The melting temperature of the polymer, T_m, is always higher than the glass transition temperature T_g.

1.2.2 The mechanism of sulfur vulcanization

A rubber is generally defined as a material which can be stretched to at least twice its original length and which will retract rapidly and forcibly to substantially its original dimensions on release of the force. The most noticeable feature of natural rubber and other elastomers is the ability to undergo large and reversible elastic deformation. It is not unexpected that stress can cause polymeric molecules to adopt an extended configuration, but at first sight it may seem surprising that on removal of the stress the molecules retract, on average, to their initial coiled form. Simple theories of rubber-like elasticity assume, as an approximation, that both extension and retraction occur instantaneously, and neglect any permanent deformation. For example, natural rubber (cis-polyisoprene) in its native state does not satisfy this last criterion, as molecules in extended configurations tend to slide past one another and do not recover completely. Molecules need to be chemically cross-linked by sulfur bonds to prevent any

permanent flow. After cross-linking, the flow of one molecule past another (viscoelastic behavior) is suppressed. Excluding minor impurities, an object such as a rubber band can be considered as one huge molecule.

Vulcanization it is an irreversible process during which a rubber compound, through a change in its chemical structure (cross-linking) and by the formation of a three-dimensional network of polymer chains chemically bonded to one another, becomes less plastic and more elastic. It becomes more resistant to swelling by organic liquids. Elastic properties are conserved, improved, or extended over a greater range of temperature. This transformation can occur through various chemical mechanisms such as nucleophilic substitution, end-linking, addition or condensation, free radical coupling and ring opening reaction, among others[5].

In the rubber industry a sulfur-based cross-linking system is generally used. Since the vulcanization rate with sulfur alone is slow, chemical accelerators and activators are necessary, so there are two general categories of sulfur vulcanization: un-accelerated and accelerated. Un-accelerated sulfur formulations consist of rubber and sulfur, while accelerator systems contain rubber, accelerator and sulfur. In addition, zinc oxide and stearic acid are often included in both types of systems.

The exact mechanism under which accelerated sulfur vulcanization occurs is a function of the class of accelerators/activators. Typically benzothiazole or sulfenamide accelerators are used. Zinc oxide is the acctivator, and a fatty acid such as stearic acid is the co-activator. A generally accepted sequence of reactions is as follows[1, 6]

I. An interaction of the curatives occurs to form the active sulfurating agent, Ac-S_x-Ac by a reaction of accelerator (Ac) and activator with sulfur:

$$Ac + S_8 \rightarrow Ac\text{-}S_x\text{-}Ac$$ (active sulfurating agent)

II. The polymer chains interact with the sulfurating agent to form polysulfidic pendant groups terminated by accelerator groups:

$$Ac\text{-}S_x\text{-}Ac + RH \rightarrow R\text{-}S_x\text{-}Ac$$ (pendant sulfurating agent)

RH is the rubber chain.

III. Polysulfidic cross-links are formed:

$$R\text{-}S_x\text{-}Ac \rightarrow R\text{-}S_x\text{-}R \quad \text{(cross-links)}$$

IV. Network maturing and competing side reactions also occur which do not lead to effective cross-links:

$$R\text{-}S_x\text{-}Ac \rightarrow \text{cyclic sulfides} + \text{dienes} + ZnS \quad \text{(degradation)}$$

$$R\text{-}S_x\text{-}Ac \rightarrow R\text{-}S\text{-}Ac + S_{x-1} \quad \text{(desulfuration)}$$

$$R\text{-}S_y\text{–}R \rightarrow R\text{-}S\text{-}R + S_{y-1} \quad \text{(monosulfidic cross-links)}$$

$$R\text{-}S_{x+y}\text{–}R + Ac\text{-}S_z\text{-}Ac \rightarrow R\text{-}S_x\text{-}R + Ac\text{-}S_{y+z}\text{-}Ac \quad \text{(sulfur exchange)}$$

During the curing and network maturing periods, there are at least three competing reactions: cross-linking, desulfuration, and degradation reactions. The network structures formed depend on not only temperature but also accelerator types and concentration. The ratio of poly-, di-, and monosulfidic cross-links strongly depends on the ratio of sulfur to accelerator in the formulation. When accelerators and activators are used, vulcanized rubber contains sulfur cross-links of different lengths, as well as intra-molecular cycles, see Figure 1.2.

The main application and performance characteristics of a vulcanizate are determined by the chemical nature of a polymer and the type and concentration of the cross-links. So, the strength and dynamic mechanical properties of the vulcanizate depend not only on the nature of the polymer chain itself, but also is proportional to the number of network

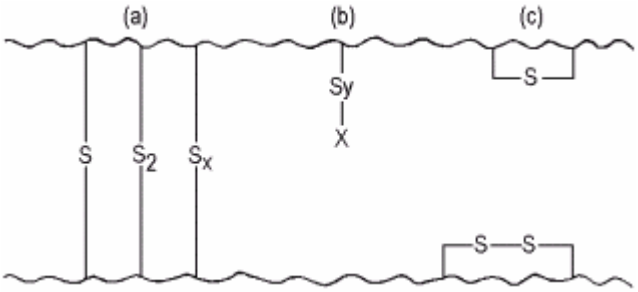

Figure 1.2 Structure of vulcanized rubber network

supporting chain in the resultant network. The cross-link density determines the number of network supporting chains; a network supporting chain is that chain between two junction points. The hardness and modulus of a vulcanizate increase with increasing cross-link density. Hysteretic properties and set characteristics decrease with increasing cross-link density[7].

1.2.3 Thermoplastic Elastomers

Thermoplastic elastomers (TPE) are relatively new polymers which, in the ideal case, combine the service properties of elastomers with the processing properties of thermoplastics. This combination of properties can be obtained through the simultaneous presence of soft, elastic segments that have a high extensibility and a low glass transition temperature (T_g value) and hard, crystallizable segments which have a lower extensibility, a high T_g value and are susceptible to association (cross-linking). The hard and soft segments must be thermodynamically incompatible with each other so that they do not penetrate each other but act as individual phases. These different segments may be present either in the same molecule, as macromolecule segments, or in the form of a micro-heterogeneous phase distribution of thermoplastics in plasticizer. This means that TPE properties are characterized more by their morphological behavior that by their chemical composition.

The ratio of soft and hard segments determines the hardness and the modulus of elasticity and also comparable properties of TPE. The chemical nature of the soft segments has an influence on elastic behavior and the low temperature flexibility, whilst the hard segments, which act as cross-link points, determine the heat resistance, the strength and the swelling behavior.

By their hardness, the TPEs can be classified as follows[2]

- Blends of rubbers with thermoplasctics, blended TPEs (e.g. EPDM/PP)
- soft block copolymers as “multi-purpose” TPEs” (e.g. SBS)
- hard block copolymers as “engineering TPEs” (e.g. thermoplastic polyurethanes, copolyesters, polyetheramides and hard elastomeric alloys)

Generally, the DSC (Differential Scanning Calorimetry) curve of a TPE shows two clear phase transition, i.e. the glass transition T_g of the elastic phase and the melting range T_m of the crystalline phase. The various TPE types, however, differ considerably from each other in terms of the temperatures at which the transitions occur and the intensity of the transitions[8].

One of the advantages of thermoplastic elastomers is that they can be recycled-indicating that inter-chain bonding in TPE consist of thermo-reversible cross-links arising out of physical interactions like hydrogen bonding, charge transfer complexes, ion-dipole interactions and ion-ion interactions.

Thermoplastic vulcanizates are alloys of polyolefin thermoplastics and fully vulcanized rubber. The cross-linked rubber phase in TPVs gives them a good compression set and excellent dynamic properties. They have good chemical resistance against water, acids and bases and the main advantage which they present is that the rubber used as basis for their preparation can be recycled rubber.

1.3 NMR Methods Used on Polymer Study

1.3.1. NMR Phenomenon

Nuclear Magnetic Resonance spectroscopy has become a method of a great importance for every aspect of the structure and properties of macromolecules. Shortly after the discovery of nuclear resonance in bulk matter[9, 10] it was observed by Alpert (1947) that natural rubber at room temperature gives a proton line width more like that of a liquid than of a solid, but that the resonance broadens markedly at temperatures approaching the glass temperature. This was recognized as being related to the presence (and cessation) of micro-Brownian motion. NMR methods developed rapidly after these initial observations, and solution-state analysis of polymer microstructure has evolved into de one of the primary methods for the chemical characterization of polymers. With the exception of some early wideline proton NMR studies of polymer dynamics, the development of solid-state NMR analysis is a more recent development. But, since most polymers are used as solids, the solid-state NMR analysis of polymers has become increasingly important. These studies are of current interest since they can often provide the connection between the molecular structure and the macroscopic properties.

The NMR phenomenon is possible because in addition to the charge and mass, many nuclei possess spin, or angular momentum. Since the spinning charge generates a magnetic field, there is a magnetic moment associated with this angular momentum. According to the principles of quantum mechanics, the maximum experimentally observable component of the angular momentum of a nucleus possessing a spin is a half-integral or integral multiple of $h/2\pi$, where h is the Planck's constant. This maximum component is **I** and it is called the spin quantum number. There are $2\mathbf{I} + 1$ possible orientations or states of the nucleus. The most two important nuclei in the polymers field are protons and carbons (^{13}C) and they both have $\mathbf{I} = 1/2$, so the possible magnetic quantum numbers are $+1/2$ and $-1/2$.

In the absence of any external magnetic field the nuclei are spinning randomly in their atomic or molecular environment, but when placed in a strong external field ($\mathbf{B_0}$) they behave like small magnets and orientate themselves with respect to the magnetic field. For protons and

carbons there are two possible alignments, either with the field, or against it. These two spin states differ very slightly in energy, and it is this energy difference that can be supplied by the radio frequency radiation allowing the nuclear spins to change their state, see Figure 1.3.

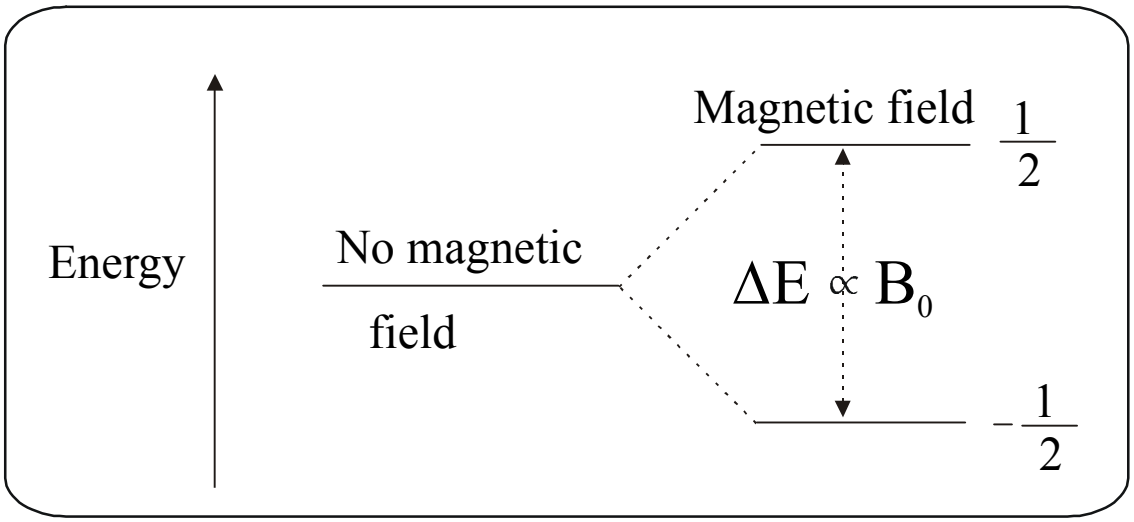

Figure 1.3 Energy description of the NMR phenomenon

The energy difference (ΔE) between spin states is directly proportional to the magnetic field strength, and because

$$\Delta E = h\nu \qquad \textbf{(1.1)}$$

the frequency of resonance ν, is also directly proportional to the strength of the external magnetic field. The proportionality constant can be shown to be $\gamma/2\pi$ where γ is the *magnetogyric ratio* of the nucleus.

The two quantities that determine the observation frequency for NMR signals are the magnetogyric ratio γ and the magnetic field strength B_0. The sensitivity depends both on the magnetogyric ratio and the natural abundance. Protons have the highest sensitivity because they have the highest magnetogyric ratio and natural abundance. At a field strength of 9,3 T (1 tesla

= 10^5 gauss) the NMR signals are observed at 400 MHz. The carbons sensitivity is very low, but in solid state NMR there are techniques, like cross polarization or dipolar decoupling, for improving the sensitivity and therefore we can record very good carbon spectra.

1.3.2 Magic Angle Spinning

From the view point of spectral resolution the liquid state NMR and the solid state NMR are very different. The resonance line width in liquid state is much narrow than for the corresponding solid sample. An illustrative example in this sense is the case of the water sample: the proton resonance line width for water measured at room temperature is 0.1 Hz, and the corresponding line width for ice is about 10^5 Hz. The reason for this difference it is well known and it due to the anisotropic spin interactions which take place in solids. The molecular motion in an isotropic liquid effectively removes many of the nuclear spin interactions, which leads to simple NMR spectra.

The anisotropic spin interactions which lead to broad and overlapping spectral lines in the spectra of the solid samples are chemical shift anisotropy, dipolar couplings and quadrupole interactions (for the case that the nucleus itself is not symmetric, resulting in a non-symmetric nuclear charge distribution, i.e., an electric quadrupole moment).
It can be shown[11, 12] that the magnitude of any of the above anisotropic interactions have a very specific angular dependence with respect to

1. the static field (chemical shift anisotropy)
2. other nuclear spins (dipolar interactions)
3. surrounding electric field gradients (quadrupole interactions).

In the case of nuclei with a spin quantum number I = ½ (e. g., ^{1}H and ^{13}C) the quadrupole moment is zero. The term $(3\cos^2\theta - 1)$ is one of the key term describing the orientational dependence of these anisotropic interactions in each of the respective Hamiltonian operators. Depending upon the type of interaction being considered, the angle θ has a different meaning. In the case of dipole-dipole interaction the angle is between the vector joining two dipoles and

the direction of $\mathbf{B_0}$ magnetic field, and for chemical shift anisotropy interactions θ it is considered to be between the principal axis of shielding tensor and $\mathbf{B_0}$.

If we spin the sample about an axis, which makes an angle ϕ with the applied field, then θ, the angle which describes the orientation of the interaction tensor fixed in a molecule within the sample, varies with time as the molecule rotates with the sample. Under this conditions, the average of the term $(3\cos^2\theta - 1)$ is

$$\left\langle 3\cos^2\theta - 1 \right\rangle = \frac{1}{2}(3\cos^2\phi - 1)(3\cos^2\alpha - 1) \qquad \textbf{(1.2)}$$

where the angle α is between the principal z-axis of the shielding tensor and the spinning axis, ϕ is the angle between the applied field and the spinning axis and θ is the angle between the principal z-axis of the interaction tensor and the applied field $\mathbf{B_0}$. The angle α is fixed for a given nucleus in a rigid solid, but like θ is takes on all possible values in a powder sample. The angle ϕ is under our control and we can set it to 54.74^0 (*magic angle*). Then $(3\cos^2\phi - 1) = 0$, and so the average, $\left\langle 3\cos^2\theta - 1 \right\rangle$ is zero as well. By fast spinning rate θ is averaged rapidly compared with the anisotropy of the interaction and the interaction anisotropy averages to zero. This technique averages the anisotropy associated with any interaction which causes a shift in the energies of the Zeeman spin functions, such as chemical shift anisotropy and heteronuclear dipolar coupling and has also an effect on homonuclear dipolar coupling.

Apart from mechanically spinning the sample at magic angle (MAS: Magic Angle Spinning)[13,14], we can obtain narrower spectra by manipulation of the spins using radio frequencies pulses (MP: Multiple Pulse narrowing techniques)[15]. There are also methods which combine this two techniques like CRAMPS (Combined Rotation and Multiple Pulse Spectroscopy)[16,17] and CP-MAS (Cross-Polarization Magic Angle Spinning)[21] together with dipolar decoupling.

MAS is by far the chief of the applications and it is routinely used in every Solid State NMR laboratory in order to improve the spectral resolution. One inconvenience of the application of

MAS is the presence of the *spinning sidebands* in the spectra. As the sample rotates in a linear field gradient, a typical nuclear spin passes through a magnetic field that is modulated in intensity, $B_0 + B_m \cos \omega_m t$, and since this spin precesses at its instantaneous Larmor frequency, its resonance frequency is frequency modulated. Viewed in the frequency domain, this corresponds to the introduction of a set of spinning sidebands on each side of the main resonance, at distances equal to integral multiples of the spinner frequency. All the sidebands are weak in comparison with the intensity of the central resonance, and only the first-order sidebands have appreciable intensity, but they can interfere with the identification of signals.

The intensity of spinning sidebands may be reduced by increasing the spinning rate. In the present, the spinning frequency continues to increase dramatically with increasing B_0.[18] For the case that technically it is not possible to spin fast enough one may apply a special pulse sequence known as Total Suppression of Spinning Sidebands (TOSS)[19].

Although we have not addressed at all this application in our present work it is worthwhile mentioning that spinning sidebands can be successfully used to determine anisotropies and asymmetries of nuclear spin interactions.

MAS is a nondestructive technique which can be applied to any material in solid state: polymers, semiconductors, metals, biological samples. For our work this technique was of great help. At only 2kHz spinning speed we can separate, in carbon spectra, every NMR resonance of EPDM, see Figure 1.4 and Figure 1.5. As we will see in the following chapters these was especially important in dealing with PP/EPDM blends because some EPDM peaks are well separated from the PP resonances, giving us the possibility to characterize the rubber phase without the superposition of the signals coming from the polypropylene matrix.

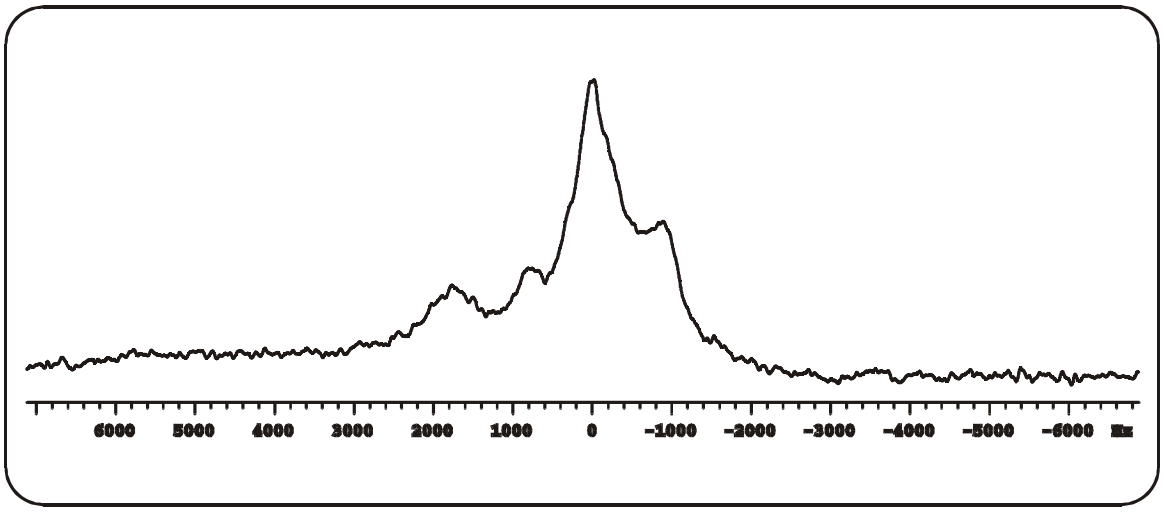

Figure 1.4 Single pulse carbon NMR spectra of EPDM recorded without spinning

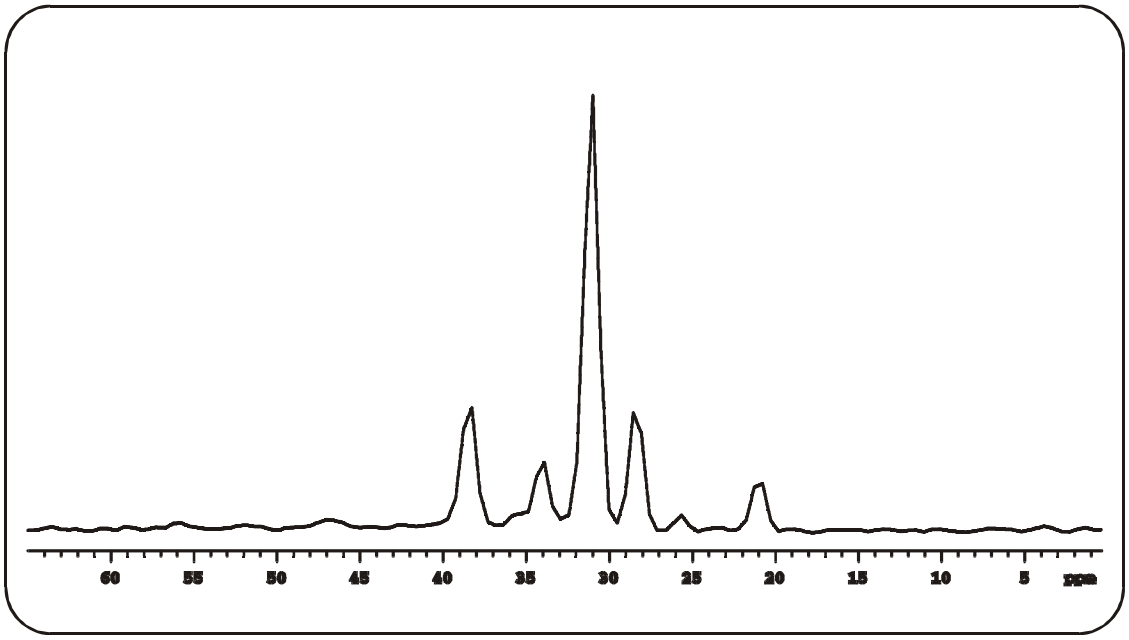

Figure 1.5 Single pulse carbon NMR spectra of EPDM recorded by spinning the sample at 2.5kHz

1.3.3 Dipolar Decoupling

Decoupling was first proposed by Bloch[20] and it is now an essential component of many high-resolution solid-state NMR experiments. This technique may be discussed under the two heads of *homonuclear* or *heteronuclear* depending on whether the two spins or two groups of spins are of the same or different species.

The heteronuclear coupling is responsible for much of the broadening in solid-state NMR spectra. It involves, in the case of our system to study, the coupling of proton spins to the detected carbon spins. This interaction can be removed and narrower lines can be obtained by applying MAS (as we sow in Section 1.3.2) or by simply acquiring the ^{13}C NMR signal at the same time as applying a radio frequency field at the ^{1}H Larmor frequency. The ^{1}H radio frequency must be sufficiently strong . A field of *ca.* 10^{-3} tesla (10 gauss) must be used for the removal of direct dipole-dipole ^{13}C-^{1}H couplings in solids, corresponding to *ca.* 40 kHz expressed as a frequency. For removing the J-coupling in solution, only *ca*. 1 gauss decoupling field is necessary.

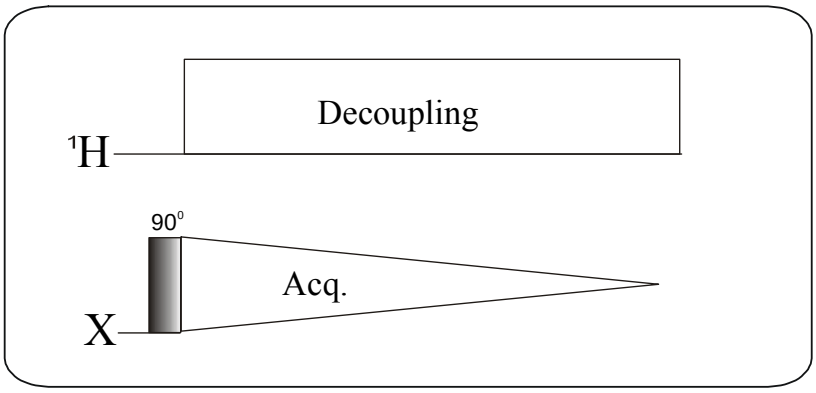

Figure 1.6 High-power decoupling. This removes the effects of ^{1}H dipolar coupling from the NMR spectrum of nuclei X.

1.3.4 Cross Polarization

The first difficulty in obtaining good carbon spectra is due to the low natural abundance of the isotope ^{13}C – only 1,07%. The second difficulty in the way of getting satisfactory solid-state spectra is the fact that spin-lattice relaxation times can be very long, so that the multi-pulse methods are not very efficient. This problem has been solved by an ingenious technique which transfer the magnetization from protons to ^{13}C spins. The transfer, known as *cross polarization*[21], occurs in the rotating frame of reference by using the pulse sequence represented in Figure 1.7.

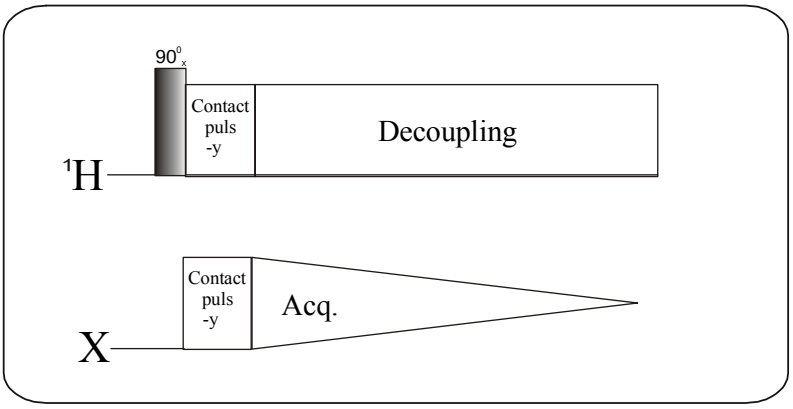

Figure 1.7 The cross polarization pulse sequence

Firstly, a 90^0 pulse must be applied on protons channel and ^1H magnetization must be spin-locked in the y direction of the rotating frame. At this point the radio frequency in the ^{13}C channel is switched on, and the amplitude of the magnetic field B_{1C} adjusted so that the Hartmann-Hahn matching condition[22] is fulfilled

$$\gamma_H B_{1H} = \gamma_C B_{1C} \qquad \textbf{(1.3)}$$

This condition implies that in their respective rotating frames of reference the protons and carbons precess at equal rates and that the effective energies are comparable, thus allowing a rapid transfer of magnetization induced by the flip-flop term in the dipolar Hamiltonian.

2 Samples, Previous Work and DSC Measurements

This chapter describes the samples used for this work and the way they were obtained. The non-NMR methods like Differential Scanning Calorimetry and Dynamic Mechanical Analysis, used usually for polymer characterization are briefly introduced. The previous work of this study consists in sample preparation and DMA results. The results of DSC measurements for representative sample are discussed.

2.1 Samples and non-NMR Methods

2.1.1 Ethylene-Propylene-Diene-Monomer (EPDM)

At room temperature, polyethylene is a partial crystalline plastomer, but on heating, it passes through an "elastomeric" phase. By incorporating in the polymer chain elements which inhibit crystallization, the melting temperature and therefore the elastomeric phase can be reduced considerably to below room temperature. Such amorphous and curable materials can be considered as rubbers, and they can be obtained by co-polymerizing ethylene and propylene with certain catalysts of the Ziegler-Natta type. The resulting, so-called EPMs are amorphous and rubbery, but they do not contain un-saturation, therefore, they can only be cross-linked with peroxides. If, during co-polymerization of ethylene and propylene, a third monomer, a diene, is added, the resulting substance, EPDMs, will have un-saturation, and it can then be vulcanized with sulfur[2].

In the production of EPM and EPDM rubber the following parameters are considered[7]

- concentration ratio of ethylene and propylene (amorphous or segmented grades);
- co- or terpolymerization (EPM or EPDM);
- type and amount of termonomer (vulcanization properties, mechanical properties);
- solution and suspension polymerization (highest obtainable molecular weight);
- molecular weight (differences in Mooney viscosity and processibility);
- processibility, price.

Copolymers, which contain between 45 and 60% ethylene, are completely amorphous.

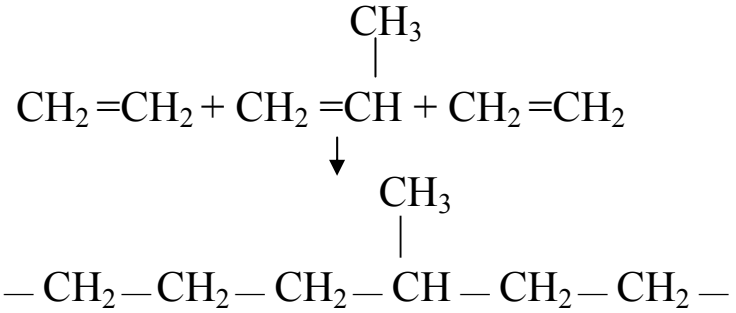

Figure 2.1. The principle of ethylene and propylene copolymerization

At higher ethylene contents of the order ranging between 70 to 80%, the polymers contain long ethylene sequences, which are partially crystalline. These polymers are referred to as "sequential" grades, and their processing behavior differs considerably from that of the normal amorphous grades. The partially crystalline domains form thermally reversible physical cross-links, which, as with the thermoplastic elastomers, give the elastomers an already high mechanical strength without chemical cross-links. At higher temperatures though, this strength deteriorates[7].

The choice of a suitable termonomer poses several problems. Firstly, the two sets of double bonds of the diene should have different reactivities, so that one will co-polymerize with the second remaining un-reacted in the polymer chain, enabling it to be used in subsequent vulcanization reactions. The other requirement is that of a high reactivity of the second double bond in sulfur vulcanization reactions. In the production of commercial rubbers the most used diene are the following: dicyclopentadiene (DCP), ethylidene norbornene (ENB) and trans-1,4 hexadiene (HX).

Sulfur vulcanization is technologically the most important chemistry employed in the production of diene elastomer vulcanizates. It is agreed that the accelerator and activators react to generate an active accelerator complex. This complex reacts with the unsaturated elastomer by substituting a labile allylic hydrogen atom, which results in the attachment of accelerator residues to the elastomer chain, namely, pendent sulfur or cross-link precursor. This intermediate is converted into a sulfur cross-link either via disproportionation with a second pendent sulfur structure or by allylic substitution of the un-saturation of a second elastomer chain. During accelerated sulfur vulcanization dialkenylsulfides are predominantly formed, indicating that the un-saturation is not consumed during reaction but that it activates the α-position, whereas during un-accelerated sulfur vulcanization mixtures of dialkenylsulfides, dialkylsulfides and alkenylalkylsulfides are formed. If a prolonged vulcanization is performed network maturation reactions may occur. The sulfidic cross-link may exude sulfur, resulting in cross-link shortening, and it may be converted into cyclic sulfides[23].

Recently, high-resolution carbon solid-state NMR measurements with ENB unsaturation of EPDM fully isotopically enriched with ^{13}C were performed[24]. It was found that sulfur cross-linking take place at the allylic positions of the ENB and the substitution at the 9-position of ENB is always preferred over the two 3-positions. In turn, the substitution at the 3-exo position is always preferred over the 3-endo position, which is different from earlier studies.

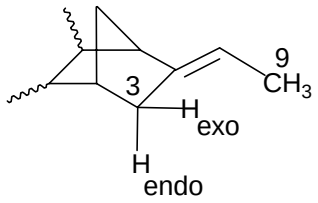

Figure 2.2. Ethylidene norbornene (ENB)

Among the samples chosen for study in this work is EPDM Buna EP G 5567 (Bayer AG, ML (1+4) 125 ^{o}C = 46, ENB 5%, Etylene 66%, Propylene 29%, M_w=620 000g/mol) vulcanized according with tree different recipes, see Table 2.1. EPDM is cross-linked by accelerated sulfur vulcanization. With respect to ultimate and dynamic properties sulfur-vulcanized EPDM is superior to peroxide-cured EPDM as a result of the dymanic

Table 2.1 The recipes for the vulcanization of EPDM ([a]per hundred rubber)

composition	*EPDM_A (phr)*[a]	*EPDM_B (phr)*	*EPDM_C (phr)*
EPDM	100	100	100
Sulfur	1	1	1
TMTD	0,5	0,5	0,5
ZDEC	0,3	0,5	0,5
MBTS	0,3	-	-
ZnO	-	-	3
Stearic acid	-	-	1

rearrangement of sulfidic cross-links during sulfur vulcanization, yielding a rubber network which is relatively free of internal stresses.

Using ethylidene norbornene (ENB) as termonomer it is possible to introduce 4 to 15 double bounds for each 1000 carbon atom chain length, with the polymer remaining free of gel[2]. This is a low amount of un-saturation and sulfur vulcanization of EPDM is rather slow and a relatively large amount of accelerators is needed. The tetramethylthiuranium disulfide (TMTD) and dibenzothiazyl disulfide (MBTS) were used as accelerators. For development of the full activity of accelerators, addition of ZnO and stearic acid is necessary.

The isotherms of vulcanization represented in the graphic below shows that EPDM C sample presents the highest cross-linked density[25].

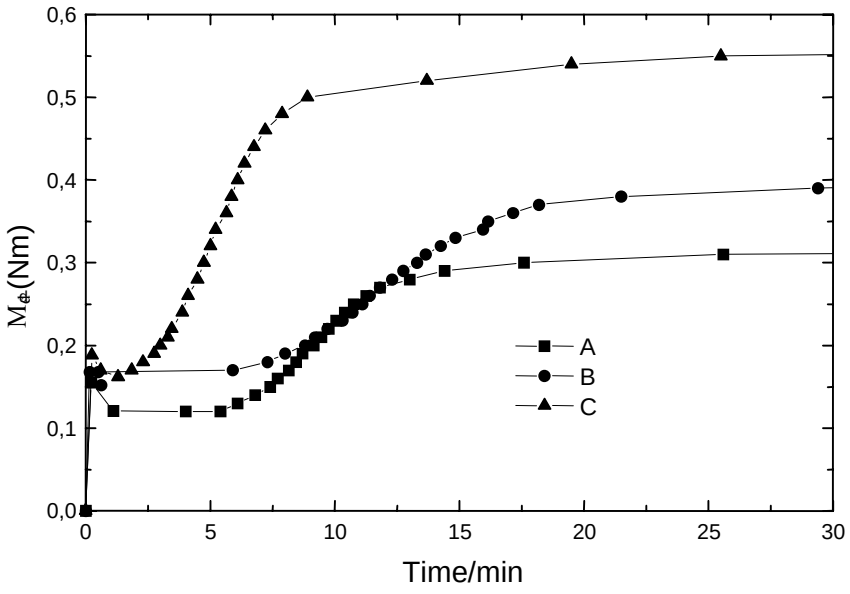

Figure 2.3 The isotherms of vulcanization for EPDM A, -B and -C
(Göttfert elastograph, temperature 160^0 C)

From EPDM's properties we mention that it has a very high resistance against heat, light, oxygen and ozone as a result of his fully saturated polymer backbone. The high

performance/price ratio explains the fact that EPDM rubber is by volume the largest non-tire elastomer (approx. 1000 kton/yr) [26]. Its main applications are to be found in automotive sealing systems, in building and construction and in a variety of technical products (tubes, seals etc.).

2.1.2 The Blends of Polypropylene/Ethylene-Propylene Diene Monomer

Because it is possible to blend EPDM and polypropylene (PP), for example, in any ratio, there is theoretically a continuous spectrum from elastified PP to EPDM reinforced with thermoplastics. Where the PP component predominates, which is by far the chief field of application, PP constitutes the continuous phase with uniformly and finely dispersed rubber segments. With a very high EPDM component, by contrast, the structure reverses and the material is a PP-reinforced EPDM. The properties of the blends containing a high quantity of PP depend on the quantity of EPDM and the uniformity and size of the micro-heterogeneous rubber phase. They have a relatively low level of elasticity, display a low elongation at break and high values for compression set. They have only a low-level elastomeric character in the service temperature range, making them difficult to classify them as TPEs in the true sense of the term[2].

Through dynamic cross-linking in situ of EPDM with PP during mixing, elastomeric alloys (TPOs) can be made with rubber-elastic behavior over a wide range of temperatures (- 40 ^{o}C to + 125 ^{o}C). The rubber elastic behavior of such elastomeric alloys is quite different from that of non-crosslinked EPDM/PP blends. The morphology of *in situ* cross-linked polymer blends differs from those of non-cross-linked ones. The distribution of rubber particles is much finer and, therefore, the heterogeneous phase distribution is much better for the TPOs. The properties of the fully crosslinked elastomer particles do not change even at processing temperatures up to 180 ^{o}C - 225 ^{o}C [27]. In general the properties of each individual TPO type depend, apart from the EPDM and the polyolefine types, also on the blend ratios, the degree of cross-linking and kind of compounding of EPDM phases, and, of course, of the micro-heterogeneous phase distribution of EPDM in polyolefines. These products can replace covalently cross-linked elastomers in a lot of applications and they fill the gap between elastomers and thermoplastics.

Fully or partially cured thermoplastic polyolefinic systems are called thermoplastic vulcanizates or TPVs.

The UV and ozon resistance of TPOs and TPVs is excellent and they are resistant also in most inorganic chemicals as well as in a lot of polar organic solvents like break liquids, but not in aliphatic and aromatic solvents in which they exhibit a great volume swell. TPOs also have good abrasion resistance and excellent electrical insulation properties. The compression set resistance between low minus degrees up to approximately 70 ^{o}C is low and it will rapidly be enlarged above 100 ^{o}C, coming at 125 ^{o}C near to 100%.

For the present study two series of blends were prepared, each of them composed of isotactic polypropylene (PP – Huels AG Verstolen P7000, 46% crystallinity) in different ratios (-30%, 50% and 70%) and the three different ethylene propylene-diene terpolymers (EPDM_A, EPDM_B and EPDM_C). The former (PP%_A, PP%_B and PP%_C) contain EPDM vulcanized powder (diameter < 80 μm) mixed at high temperature with PP, while the latter (PP%N_A, PP%N_B and PP%N_C) were obtained by additional dynamic cross-linking *in situ* of EPDM during mixing.

All the PP/EPDM blends were produced through a melting mixing process in a 60 cm^3 Brabender Plasticorder, equipped with a pair of high shear roller-type rotors. The Brabender is connected to a computer to allow monitoring of mixing properties such as torque and temperature as well as control mixing parameters. The starting temperature of the electrically heated chamber was 190 ^{0}C, the filling grade 0,67, the total mixing time 10 minutes and the rotor speed was set at 100 rpm. The polypropylene was introduced into the mixer during the first two minutes and after another two minutes the rubber powder was added. In the case of additionally cross-linked blends a vulcanization system was added. The vulcanization system used is Struktol 120 (Schill & Seilacher) and is composed by 83% soluble sulfur, 16% organic dispersing agent and 1% inorganic dispersing agent.

2.1.3 Non-NMR Methods

2.1.3.A. Differential Scanning Calorimetry

Differential Scanning Calorimetry (DSC) is a technique which is part of a group of techniques called Thermal Analysis (TA). Thermal Analysis is based upon the detection of changes in the heat content (enthalpy) or the specific heat of a sample with temperature. As thermal energy is supplied to the sample its enthalpy increases and its temperature rises by an amount determined, for a given energy input, by the specific heat of the sample. The specific heat of a material changes slowly with temperature in a particular physical state, but alters discontinuously at a change of state. As well as increasing the sample temperature, the supply of thermal energy may induce physical or chemical processes in the sample, e.g. melting or decomposition, accompanied by a change in enthalpy, the latent heat of fusion, heat of reaction etc. Such enthalpy changes may be detected by thermal analysis and related to the processes occurring in the sample.

Among the thermal analysis techniques the DSC is the one with the most widespread applications. In DSC the energy difference (heat enthalpy) between the sample and the reference is measured. The sample is very small (3-20mg) and is placed in a small aluminium vessel (pan). An empty pan is always used as a reference. When the sample is heated up at a constant rate, any kind of change in its calorimetric properties will cause a temperature difference between the sample and the reference. In the DSC apparatus the measured temperature difference is controlling the electrical power to the sample and the reference in order to keep them at the same temperature. In this technique the difference in the power supply to the sample and reference is recorded. This means that a peak area from the output recording directly corresponds to the heat consumed or produced by the sample[28].

The typical application for DSC is determination of: important transition temperatures like T_g and T_m , heat of fusion of a crystalline phase and the degree of crystallization, heat capacity, rate of cross-linking reactions, miscibility in polymer blends, structural relaxation like enthalpy relaxation during physical aging.

2.1.3.B Dynamic Mechanical Analysis

Dynamic Mechanical Analysis (DMA) is a thermal analysis technique used to measure changes in the viscoelastic response of a material as a function of temperature, time, or deformation frequency. DMA is particularly useful for qualitatively characterizing the glass transition temperature and other sub-Tg transitions of polymer and composite materials.

Polymeric materials have *viscoelasticity,* which is a combination of viscosity and elasticity in varying amounts. When this viscoelasticity is measured dynamically, there is a phase shift between the force applied (stress) and the deformation (strain) which occurs in response. The tensile stress σ and the deformation (strain) ε are related via the elasticity modulus E as follows

$$\sigma = E\,\varepsilon \qquad \textbf{(2.1)}$$

If the stress is applied in a sinusoidal fashion, the measurements are represented as a complex modulus E*

$$E^* = E' + iE'' \qquad \textbf{(2.2)}$$

DMA measures the amplitudes of the stress and strain as well as the phase angle (δ) between them. This is used to resolve the modulus into an in-phase component - the storage modulus (E') - and an out-of-phase component - the loss modulus (E").

$$E' = E^*\cos\delta \qquad \textbf{(2.3)}$$
$$E'' = E^*\sin\delta$$

A useful quantity is the damping factor or loss tangent (tan δ) which is the ratio E"/E' and is the amount of mechanical energy dissipated as heat during the loading/unloading cycle.
The loss tangent is zero for a perfectly elastic material and infinite for a perfectly viscous one[29].

2.2. Results and discussions

2.2.1 Previous Results

For dynamically vulcanized blends the variation of tensile properties with the composition is illustrated in Figure 2.4. The elongation at break increases with the rubber content and with the increase of cross-link density in the EPDM[25].

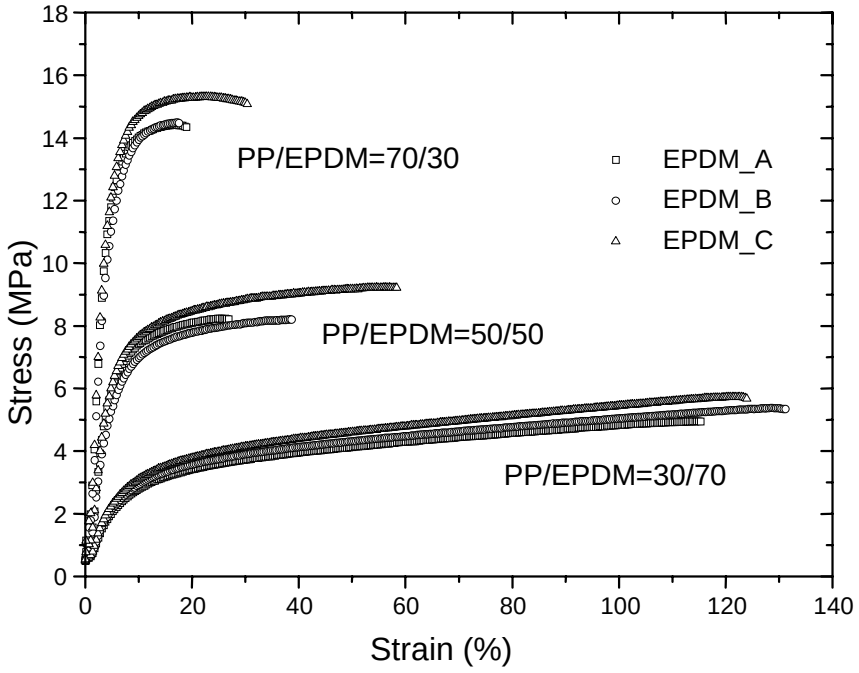

Figure 2.4 Stress-strain plots for blends containing different quantities and kinds of EPDM (Zwick 1425, $L_E = L_0 = 50$ mm, $v_T = 200$ mm/min)

The dynamic mechanical properties were determined using Eplexor 150 N at a heating rate of 1 ^{0}C/min. The temperature range chosen was from -120 ^{0}C to 160 ^{0}C. The plots were recorded for blends with different PP/EPDM content (30/70, 50/50, 70/30) before and after vulcanization in order to detect the effects of dynamic vulcanization process. The storage modulus versus temperature curves, as given in Figure 2.5, shows the characteristic biphasic structure of the blends. The modulus is decreasing, as expected, with increasing the rubber content[25].

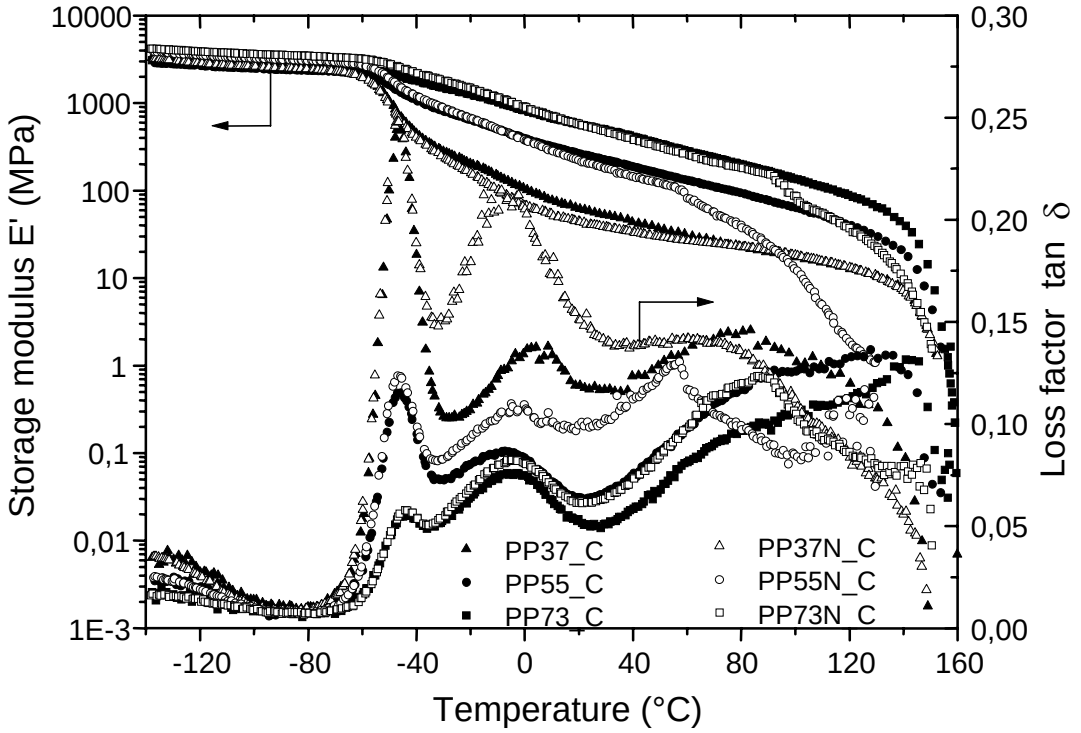

Figure 2.5 The variation of storage modulus and loss tangent with temperature for the blends which contain different percentage of EPDM_C and the corresponding dynamically vulcanized blends (PP%N_C) [25]

2.2.2 Results from DSC Measurements

The DSC measurements were performed using a DSC 7 instrument (Perkin-Elmer) with DSC (TMDSC) software option. The sample mass was about 10-15 mg. The DSC was calibrated at zero heating rate according to the GEFTA recommendation. For all the measurements the heating and cooling rates were 10 K/min. Nitrogen gas with a flow rate of about 20 ml/min was purged to the cell.

Differential scanning calorimetry measures the heat flow into or from a sample as it is heated, cooled and/or held isothermally. In principle the technique provides valuable information on

softening temperatures (T_g), melting temperatures, heats of melting, percent crystallinities, and re-crystallization (temperatures and heats). In the present work we performed DSC measurements in order to answer to the following questions: a) does EPDM contain crystalline parts, and b) is DSC technique able to reveal differences between the non-crosslinked blends and the cross-linked ones?

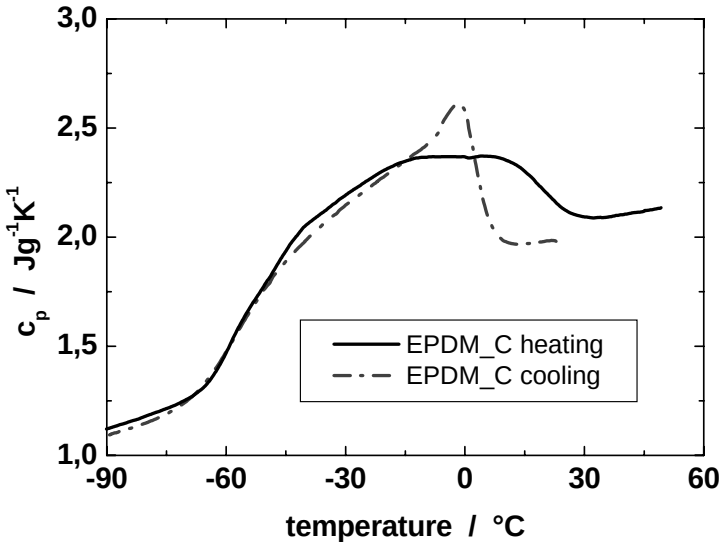

Figure 2.6 DSC results on sample EPDM_C during heating and cooling process[25a]

As we can see in Figure 2.7. the softening and the melting processes are both present, but the corresponding peaks are partially overlaped. However, it is clear that EPDM sample contains crystalline parts.

The Figures 2.7 and 2.8 clearly shows that DSC cannot distinguish between the blends with different amount of cross-link density in the rubber phase. The samples PP73N_C (70% polypropylene) and PP37N_C (30% polypropylene) are the blends which were dynamically vulcanized.

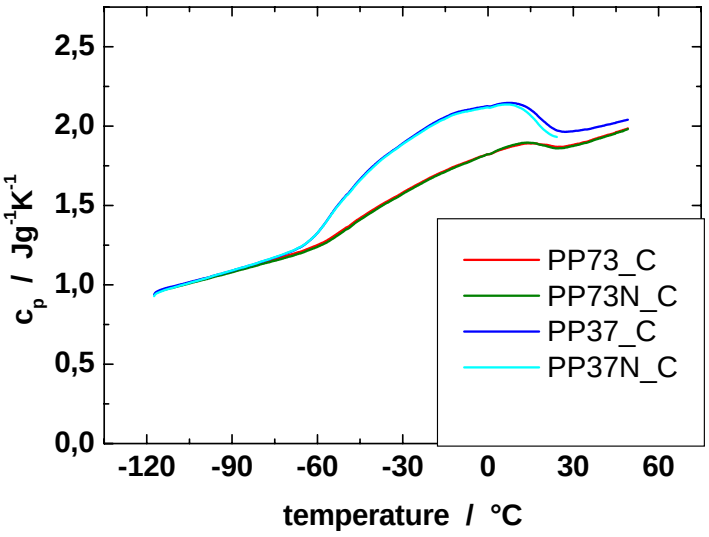

Figure 2.7 DSC results on blended samples during heating segment[25a]

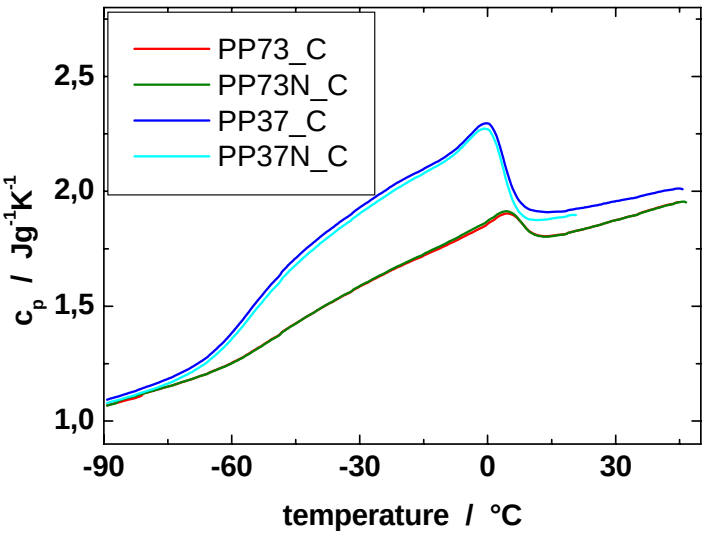

Figure 2.8 DSC results on blended samples during cooling segment[25a]

3 Proton NMR on Cross-linked Polymers

The type of molecular motion of a polymer sample is encoded in the shape of the transversal relaxation (T_2) curve. T_2 is therefore sensitive to the physical environment of the probe molecule. The most important application of this property is the determination of the mean molecular mass between two cross-linked points (M_c). The theory behind the "decoding" process and two practical methods for determination of the M_c values, together with the corresponding results calculated for rubber samples (EPDM's) are presented in this chapter. Also, we demonstrate the impossibility to apply the same procedure for determining the cross-link density of the rubber phase in a blended sample starting from proton T_2.

3.1 Dipolar Residual Coupling and Proton NMR Relaxation

3.1.1 Introduction

The goal of the most studies is the establishment of the relationship among the molecular structure, dynamics and physical properties of final materials. A useful application is connected with the determination of the material cross-link density, which is responsible for important mechanical features of elastomers. An important advantage of the NMR methods, in comparison with the most conventional methods such as swelling and stress-strain measurements is that NMR is a non-destructive technique. And more than that, as we will see through the following chapters, in some cases, the NMR is the only technique that can be applied in order to determine the material cross-link density.

During vulcanization process a certain amount of chemical cross-links are formed and, as a consequence, the degree of freedom of the molecules is decreasing. The change of molecular mobility can be well monitored indirectly by NMR relaxation. A lot of progress has been made in the field of elastomer characterization using spin-spin (T_2) NMR relaxation. Some well-established NMR methods like Hahn-echo and its derivates, for example the "reduced WISE"[30] (^{13}C-edited proton transverse relaxation), the "sine correlation echo", introduced by Callaghan and Samulski[31], and the stimulated echo used by Kimmich et.al.[32], deliver valuable information about the structure and the relaxation behavior of elastomers. Usually, for the interpretation of the transversal NMR relaxation results are used two well-known models: Gotlib model[33, 34] and Sotta-Fülber model[35]. The main difference between the two models consists in the assumption of a distribution either of the end-to-end distances of the polymeric chains (Sotta-Fülber) or of the dipolar interaction under consideration (Gotlib-model).

In the present work we determined the cross-link density of EPDM using Gotlib-model and Litvinov method[36]. The results are compared with swelling experiments data. We will also explain and demonstrate why these methods are not suitable in the case of blends consisting in polypropylene and EPDM.

3.1.2 The Transverse NMR Relaxation

While in liquid state the NMR relaxation times, i.e. spin-lattice relaxation (T_1) and spin-spin relaxation (T_2), can be considered equal, in solid state they have different values. The study of T_1 and T_2 can lead to valuable knowledge about molecular structure and motion and chemical rate processes. This work is concerned with transversal relaxation (T_2) and considers the information related to the polymeric structure and dynamics.

In the present chapter we present the theoretical and experimental aspects of proton transverse relaxation. The following treatment can be actually extended also to ^{13}C transversal relaxation.

Protons are spin ½ nuclei and consequently, when placed in an external magnetic field, they align independently of each other parallel or anti-parallel to the external field. The ratio of parallel spins to the anti-parallel ones is given by the Boltzmann distribution

$$\frac{n_+}{n_-} = \exp(\frac{\Delta E}{kT}) = \exp(\frac{\gamma \hbar B_0}{kT}) \qquad \textbf{(3.1)}$$

Both energy levels are nearly equally populated, because the energy difference is very small in comparison with thermic movements (kT). At T=300 K and a magnetic field of 18.7 T (800 MHz) the excess in the lower energy level is only 6.4 of 10000 particles for protons. This is the main reason for the inherently low sensitivity of NMR when compared to optical spectroscopic methods. However, we obtain a slight resultant magnetization in the positive z direction, see Figure 3.1, after mathematically pairing the magnetic moments of the nuclei, up with down. This magnetization is known as the bulk or macroscopic magnetization **M** and is defined as follows

$$M = \sum_{protons} \mu \qquad \textbf{(3.2)}$$

where μ is the magnetic moment vector of a proton. It is the evolution of this macroscopic magnetization which is recorded in the spectrometer. In thermal equilibrium only magnetization along the axis of the magnetic field exists (by definition z), because the x and y components sum up to zero.

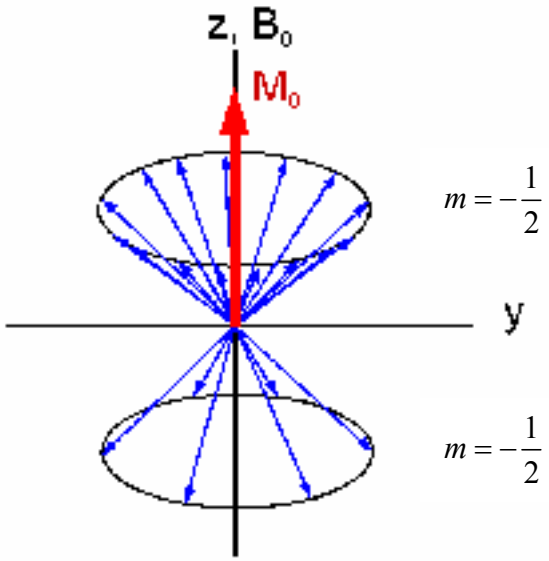

Figure 3.1 Macroscopic magnetization for a protons system

For the mathematical description of NMR spectroscopy a rotating coordinate frame is used, the rotation frequency of which equals the Larmor frequency of the nuclei. All nuclei rotating with the Larmor frequency are fixed in this coordinate frame. the time dependency of the macroscopic magnetization **M** is described by the Bloch equation:

$$\frac{dM}{dt} = \gamma(M \times B_{eff}) \qquad \textbf{(3.3)}$$

The time dependence of the magnetization vector **M** results from the interaction of the magnetization with the effective external magnetic field B_{eff}. In the rotating frame the contribution of B_0 to B_{eff} is cancelled out (for nuclei with the Larmor frequency ω_0), i. e. B_{eff} equals zero as long as only the static external field B_0 is applied.

Transversal magnetization can be created by applying an additional magnetic field B_1 which is perpendicular to B_0. This B_1 field is actually a radio frequency pulse. If the radiation frequency is equal to the Larmor frequency of the nuclei the field causes a rotation of the equilibrium magnetization $\mathbf{M_z}$ around the x axis (cross product, $B_{eff} = B_1$). The z magnetization can be completely transformed to y magnetization by a 90° pulse[37].

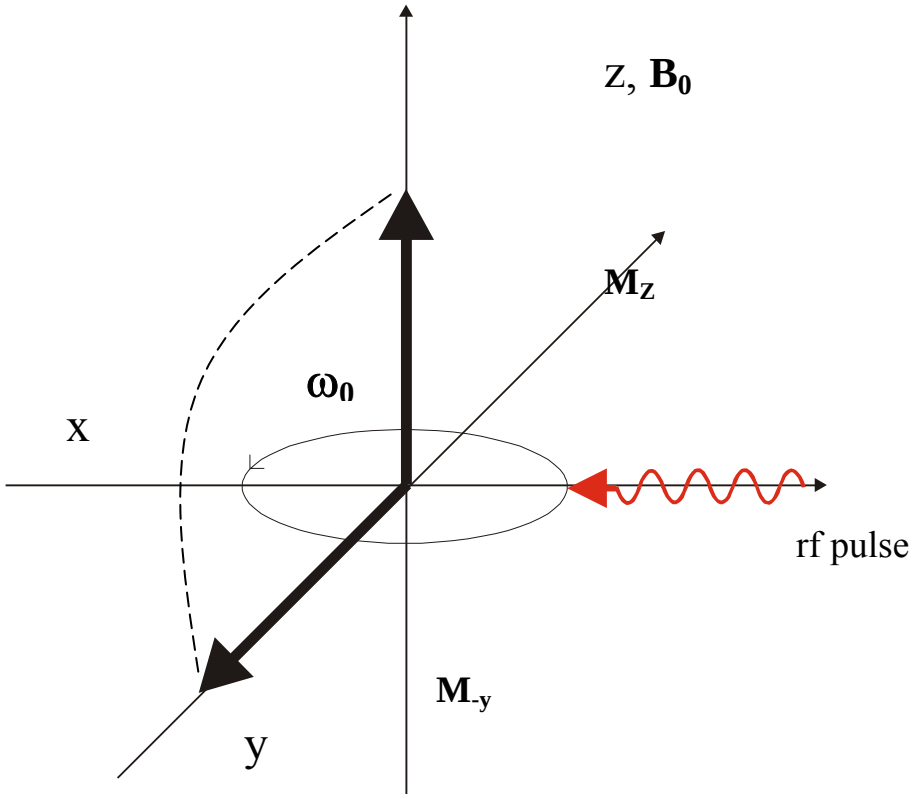

Figure 3.2 Rotation of magnetization by a radio frequency pulse

The observable quantity **M** consists of precessing spins which rotate about the magnetic field at the Larmor frequency. Immediately after the applied 90^0 pulse the magnitude of the bulk magnetization starts to decrease because of the effect of dephasing due to inhomogeneity of B_0. The individual protons are experiencing slightly different magnetic fields and therefore the spins comprising **M** would precess at frequencies perturbed from that of ω_0. The spins experiencing a stronger local magnetic field than B_0 will precess faster than the bulk magnetization. The Figure 3.3 illustrates this process.

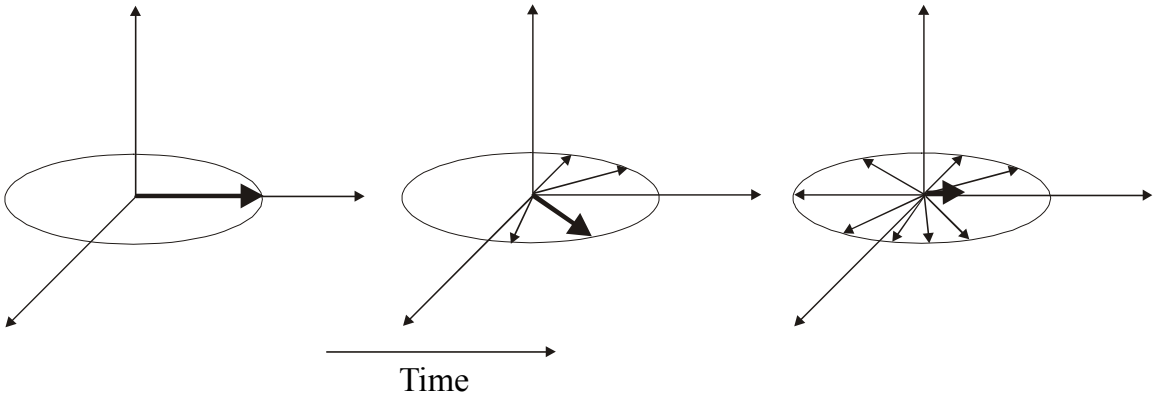

Figure 3.3 Decay of the transverse magnetization **M** as the precessing spins dephase as a result of the magnetic field inhomogeneity.

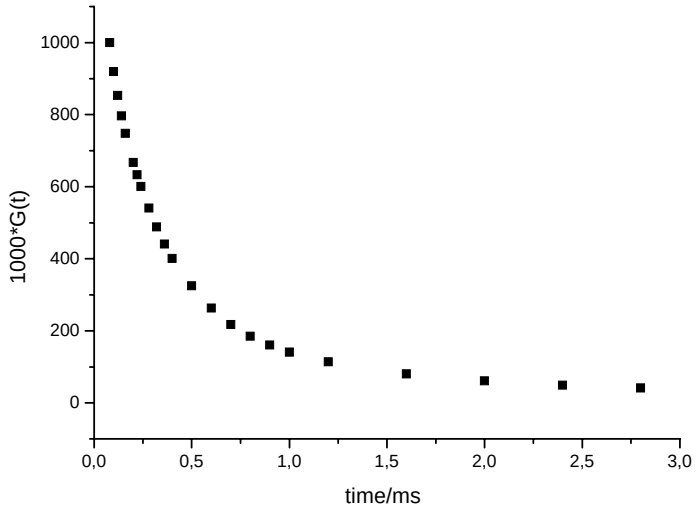

Figure 3.4 The decay of transverse magnetization observed experimentally.

Experimentally we record the free induction decay (FID) G(t) which is actually the quantity **M** as a function of time and it can be defined as

$$G(t) = M(t) / M(0) \qquad \textbf{(3.4)}$$

3.1.3 Transverse Relaxation Function

Protons possess a magnetic dipole moment. Consequently there are dipolar fields around the nuclei that perturb the magnetic field experienced by neighboring spins. The nuclei in a spin-spin interaction are taken to be a vector distance **d** apart, with its orientation being specified by the angle $\alpha(t)$ that **d** makes with the static field, see Figure 3.5.

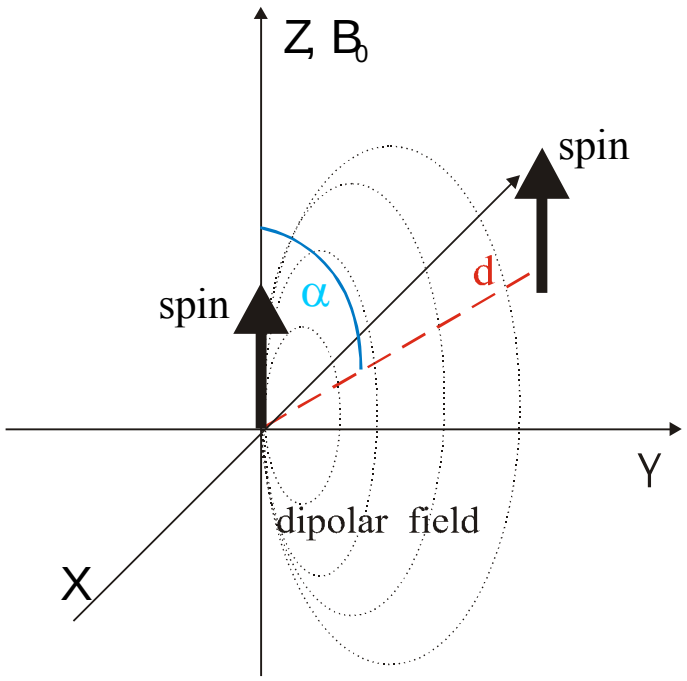

Figure 3.5 Dipolar interaction of a spin pair

A dipolar field falls off as $\mathbf{d}^{-3}$, so in some polymers, above the glass transition temperature, the system of protons may be approximately considered as a collection of isolated spin pairs attached to polymer chains' backbones, see Figure 3.6. It is worth mentioning that fast uncorrelated motion generates a slow-decaying signal. This improves the above approximation since the reorientation of a proton pair is uncorrelated to that of the surrounding spin pairs. The dominant dephasing term for amorphous polymers is thus taken to be the internal isolated spin pair dipolar interaction.

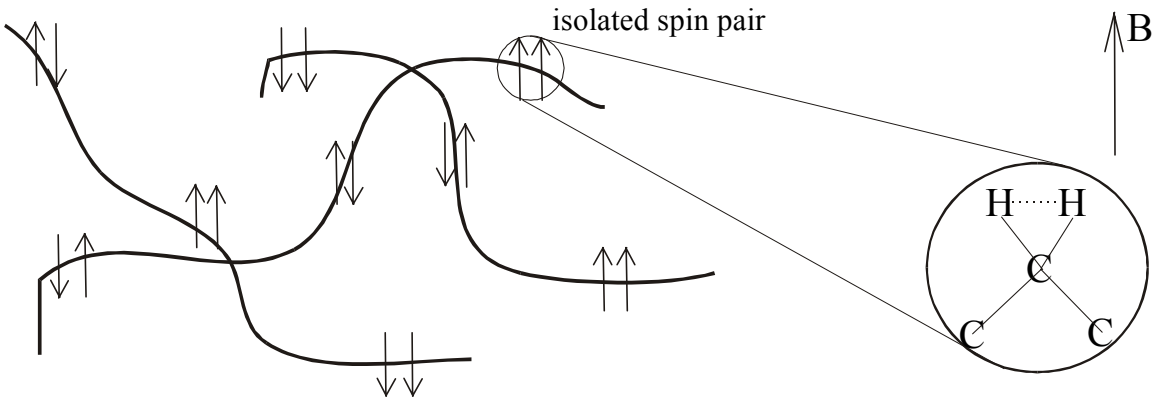

Figure 3.6 A polymer melt as a collection of isolated spin pairs

The angular frequency of precession ω for a particular proton can be written as a term corresponding to the applied field plus some time dependent perturbation from this

$$\omega(t) = \omega_0 + \Delta\omega(t) \qquad \textbf{(3.5)}$$

For a single spin the oscillating transverse components of magnetization m_x and m_y can be described by

$$m_x = m\cos(\omega(t)t) \qquad \textbf{(3.6)}$$
$$m_y = m\sin(\omega(t)t)$$

where m is a constant involved with the magnitude of the magnetic moment.

A term $M(t)$ can be defined as

$$M(t) = m_x(t) + im_y(t) \qquad \textbf{(3.7)}$$

The above expressions satisfy the oscillator equation

$$\frac{dM(t)}{dt} = i\omega(t)M(t) \qquad \textbf{(3.8)}$$

Substituting in for ω(t) from **(3.5)** and integrating up this differential equation yields

$$M(t) = M(0)\exp(i\omega_0 t) \times \exp\left[\int_0^t i\Delta\omega(t')dt'\right] \qquad \textbf{(3.9)}$$

In a polymer melt there are many protons pairs and the result bulk magnetization will be the cumulative sum of all these individual magnetic moments. This is in essence an average value denoted by $\langle ... \rangle$, to give

$$\langle M(t)\rangle = M(0)\exp(i\omega_0 t) \times \left\langle \exp\left[\int_0^t i\Delta\omega(t')dt'\right]\right\rangle \qquad \textbf{(3.10)}$$

The first term in this expression merely specifies the rotation of the spin due to the applied magnetic field. It is the second term that is of interest since this contains information about the perturbation from the static field. This allows us to define the term experimentally recorded as the transverse relaxation

$$G(t) = \mathrm{Re}\left\langle \exp\left[\int_0^t i\Delta\omega(t')dt'\right]\right\rangle \qquad \textbf{(3.11)}$$

To continue the analysis a form is needed for the perturbing term $\Delta\omega(t)$. This can be determined by considering a dipolar field emanating from a proton and the consequent influence on its associate nucleus. Only the perturbation of the z-component of the applied static field is considered. This component specifies the Larmor frequency, with the others merely disturbing the alignment of the magnetization from the z axis. This is unimportant in terms of transverse NMR measurement.

From a consideration of the dipolar field it can be shown that[38]

$$\Delta\omega(t) = \frac{3\gamma^2\hbar\mu_0}{16\pi d^3}(3\cos^2\alpha(t) - 1) \qquad \textbf{(3.12)}$$

where μ_0 is the permeability of a vacuum and $\alpha(t)$ is the angle the vector **d** makes with the applied magnetic field, recall Figure 3.5. This time orientational dependent quality of the interaction permits NMR to monitor chain motion. Combining this form for the interaction of the spin-spin pair with **(3.11)** gives

$$G(t) = \mathrm{Re}\left\langle \exp\frac{3i\gamma^2\hbar\mu_0}{16\pi d^3}\left[\int_0^t (3\cos^2\alpha(t') - 1)dt'\right]\right\rangle \qquad \textbf{(3.13)}$$

This states formally the mathematical problem that the transverse NMR poses. The $\langle ... \rangle$ can be considered as an averaging over all possible bond orientations available to the spin pair in the time interval $0 \rightarrow$ t [1]. This would be an unfeasible task if it were not for the possible replacement of the atomic details, stearic hindrances and fixed bond angles, with an effective Gaussian chain. In a melt the excluded volume interactions of the chain with itself and the environment fortuitously give rise to ideal Gaussian behavior[39]. All the atomic details are then absorbed into an effective average length *b* of a statistical segment. In a similar manner the local dipolar interaction can be viewed at this coarse grained level, as will be discussed in the next Section.

3.1.4 Rescaling of the Dipolar Interaction

The residual part of the dipolar interaction can be described by the scaling concept. It was introduced by Kuhn and Grün[40] and was developed for NMR by Cohen-Addad[41] and Gotlib[42] in the 1970s and Brereton[43] and Sotta and Demco[35] in the 1990s. A short series of N_a monomers is connected together to form a statistical unit **b**. Atomic bond rotations are considered to be fast compared with the same set by the dipolar interaction frequency. This rapid reorientation

averages the NMR term **(3.12)** onto the coarse grained level and reduces its magnitude. This rescaling involves pre-averaging $(3\cos^2\alpha(t)-1)$ over all atomic conformations subject to the constant $\sum_i a_i = b$ (as shown in Figure 3.7). The vector **b** forms a statistical segment similar to the Kuhn step length concept of the Rouse model.

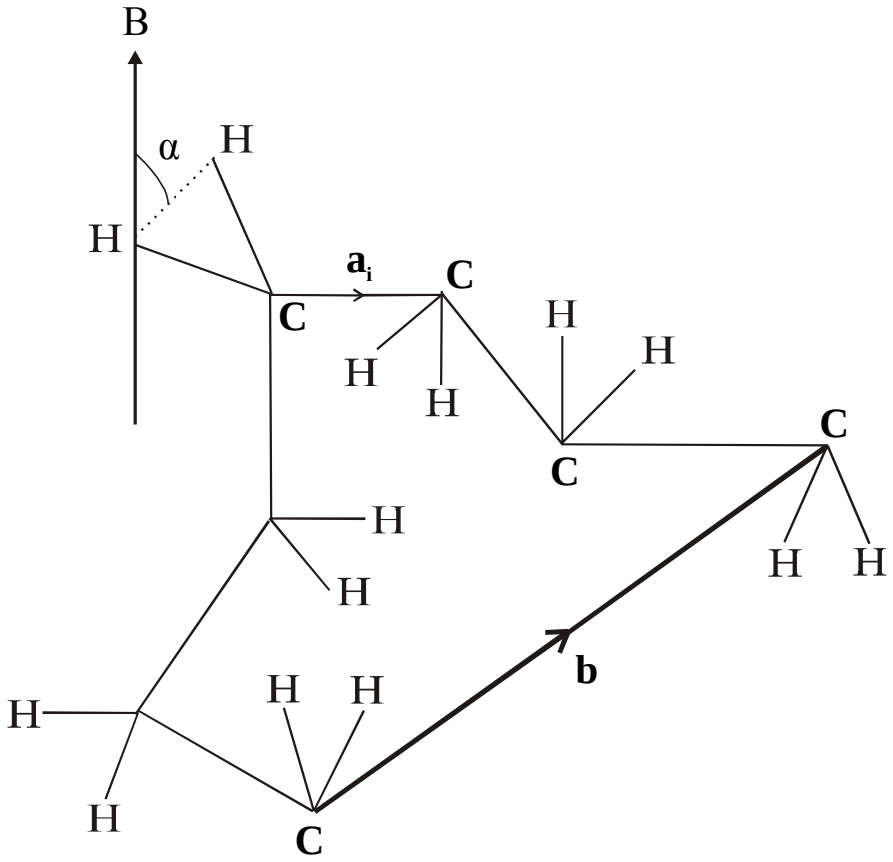

Figure 3.7 A series of N_a monomers is connected together to form a statistical unit **b**

If each monomer behaved as a freely joined rigid rod then the pre-averaging can be accomplished. The leading term is[44]

$$\left\langle 3\cos^2\alpha(t)-1\right\rangle_{\sum_i a_i=b} = k\frac{1}{N_a}\frac{2b_z^2-b_x^2-b_y^2}{b^2} \qquad \textbf{(3.14)}$$

where k=3/5. In general the parameter k depends on the model employed.

The transverse relaxation **(3.13)** can now be rewritten using **(3.14**) as[43]

$$G(t) = \mathrm{Re}\left\langle \exp\left[\frac{3\Delta i}{2b^2} \int_0^t \left(2b_z^2(t') - b_y^2(t') - b_x^2(t')\right) dt' \right] \right\rangle \qquad \textbf{(3.15)}$$

where Δ is the rescaled dipolar coupling constant

$$\Delta = \frac{k\gamma^2 \hbar \mu_0}{8\pi d^3 N_a} \qquad \textbf{(3.16)}$$

Δ is treated as an experimental parameter. For a proton pair with the distance apart **d** measured in angstroms

$$\Delta = 1.59 \times 10^4 / (N_a d^3) s^{-1}$$

The description of the polymer molecule at a coarse grained level, by the chain vectors {**b**}, is now assumed to obey Gaussian statistics. In this regime the Cartesian components are independent and allows the problem to be further reduced to[43]

$$g(\Delta, t) = \left\langle \exp\left[\frac{3\Delta i}{2b^2} \int_0^t b_x^2(t') dt' \right] \right\rangle \qquad \textbf{(3.17)}$$

$$G(t) = \mathrm{Re}\left[g(2\Delta, t) g(-\Delta, t) g(-\Delta, t) \right]$$

with the averaging now being taken over all possible conformations available to the sub-molecule **b** in the time interval $0 \rightarrow$ t.

The physics of the polymer melt, cross-links, entanglements and other chain interactions, is introduced into the transverse decay through the averaging denoted by $\langle ... \rangle$ in **(3.17)**. The type of reorientation undergone by the probe molecule is indicative of its environment and can be revealed through the shape of the transverse relaxation curve.

The problem **(3.17)** can be solved between two limits. Firstly fast dynamics where there is no correlation between a bond vector at one time and a later moment. Secondly frozen dynamics when the Gaussian bonds are essentially not re-orientating on the time scale of the NMR experiment. These give two boundaries in which an NMR signal is expected to lie and indicates the sensitivity of the decay curve to the NMR bond motion[44].

The NMR signal varies from a simple single exponential to a complex algebraic decay as the dynamics of the NMR molecule range from fast to slow. This gives a wide scope of possible decays making NMR usefully sensitive to chain reorientation.

3.1.5 The Second Moments Approximation

The second moments approximation was proposed by Anderson and Weiss[45] in 1953 and Brereton[46] discussed in 1991 its validity. Now it is possible to use this simplification within certain known boundaries.

This method was an attempt to solve the problem **(3.17)** presented by the NMR experiment. It made use of a well known statistics result for a random Gaussian variable X, which can be stated as

$$\langle \exp(X) \rangle = \exp\left[\langle X \rangle + \frac{1}{2}\left(\langle X^2 \rangle - \langle x \rangle^2 \right) \right] \qquad \textbf{(3.31)}$$

where $\langle ... \rangle$ indicates an average value found over a Gaussian distribution. In the transverse relaxation problem **(3.31)** is compared with **(3.17)**. From this likening the term X is given by

$$X = \frac{3\Delta i}{2b^2} \int_0^t b_x^2(t')dt' \qquad \textbf{(3.32)}$$

The integral is replaced by a sum over discrete time and the dynamics are taken to be fast. Then X becomes a summation of essentially independent random variables. This then produces the required Gaussian statistics.

The term $\langle X \rangle$ is linear in Δ and so will not survive the construction of G(t) from g(Δ,t) see **(3.17)**. Applying **(3.31)** to the NMR problem and ignoring this linear term gives

$$g(\Delta,t) = \exp\left[\frac{-1}{2}\left(\frac{3\Delta}{2b^2}\right)^2 \int_0^t \int_0^t \left(\left\langle b_x^2(t')b_x^2(t'')\right\rangle - \left\langle b_x^2(t')\right\rangle\left\langle b_x^2(t'')\right\rangle dt'\,dt''\right)\right] \qquad \textbf{(3.33)}$$

Since a Gaussian distribution is completely specified by its mean and variance the 4th order correlation term presented above, $\left\langle b_x^2(t')b_x^2(t'')\right\rangle$, can usefully be rewritten from another standard result

$$\left\langle b_x^2(t')b_x^2(t'')\right\rangle \equiv 2\left\langle b_x(t')b_x(t'')\right\rangle^2 + \left\langle b_x^2(t')\right\rangle\left\langle b_x^2(t'')\right\rangle \qquad \textbf{(3.34)}$$

to give

$$g(\Delta,t) = \exp\left[-\left(\frac{3\Delta}{2b^2}\right)^2 \int_0^t \int_0^t \left\langle b_x(t')b_x(t'')\right\rangle^2 dt'\,dt''\right] \qquad \textbf{(3.35)}$$

This result is the general starting point for a second moments approximation calculation. To proceed a bond correlation function is needed and this can be that of single and multiple relaxation times.

A bond relaxation function that bridges the two limits is that of a single exponential decay

$$\left\langle b_x(t')b_x(t'')\right\rangle = \frac{b^2}{3}\exp\left(\frac{|t'-t''|}{\tau_1}\right) \qquad \textbf{(3.36)}$$

where τ_1 is termed the correlation or relaxation time of the NMR active bond. It indicates the rate of reorientation for the Gaussian link. A small τ_1 implies rapid tumbling. A single relaxation time is somewhat simplistic but it has the key features; at short times ($t \ll \tau_1$) the bond appears frozen, and at long times ($t \gg \tau_1$) the correlation tends to zero, i.e. the chain has successfully completed many reorientations losing memory of its initial conformation.

The Rouse model (multiple relaxations) first appeared in 1953 in a paper by P. E. Rouse and is a mechanical representation of the Gaussian chain[47]. The dynamics are governed by local interactions along the chain and the physical constraint that a polymer cannot pass through itself is ignored. It has been shown valid for low molecular weight polymer melts in rheological experiments and more recently in NMR work[48]. The dynamics are then specified by a spectrum of relaxation times[49].

3.2 Different Methods of Crosslink Density Determination from Proton NMR Relaxation

3.2.1 Gotlib Model

The Gotlib method for determining the mean molar mass between two cross-link points M_c is based, as in the case of other methods (i.e. Sotta, Litvinov and Brereton), on the fact that the transverse NMR relaxation is sensitive to angular anisotropic segmental motion which is spatially inhibited by chemical cross-links and topological hindrances. The persistence of angular correlations on the time scale set by the residual dipolar interactions and the presence of temporary or permanent constraints (entanglements or cross-links, respectively) leads to a non-exponential decay of the transverse magnetization[50]. The shape of the line broadening ("solid-like effect") visualizes the dynamic influence of these constraints.

The residual part of the dipolar interaction is described by the scaling concept, the starting point being the angular dependence of the dipolar interaction

$$\delta\omega(\alpha) = \Delta \cdot P_2(\cos\alpha) \qquad \textbf{(3.37)}$$

where $\Delta = \mu_0 \gamma_H^2 h/(8\pi^2 d^3)$ is the coupling strength, h is the Planck constant, μ_0 is the magnetic moment and γ_H is the proton gyromagnetic ratio. $P_2(\cos\alpha)$ represents the second Legendre polynomial, and α is the angle between the interaction vector d, connecting the two

protons, and the static magnetic field B_0. For an anisotropic rigid lattice of spin pairs the result is $\left\langle P_2(\cos\alpha)^2 \right\rangle = 1/5$, and the second moment $M_2^{rl} = \left\langle (\delta\omega)^2 \right\rangle$ can be calculated as

$$M_2^{rl} = \frac{9}{4}\Delta^2 \left\langle (P_2(\cos\alpha))^2 \right\rangle = \frac{9}{20}\Delta^2 \qquad \textbf{(3.38)}$$

In the case of a very fast anisotropic motion ($\nu >> 10^6$ s^{-1}) of the segment vector **a** in the molecular system around the vector R the second moment can be reduced by pre-averaging to the residual second moment M_2^{Res} of a slow and more isotropic motion (motional averaging). Finally, the residual second moment of the dipolar interaction (general case) is given

$$M_2^{res} = \frac{9}{4}\Delta^2 \left(\frac{K}{n}\right)^2 \frac{1}{5} = M_2^{rl}\left(\frac{K}{n}\right)^2 \qquad \textbf{(3.39)}$$

where *n* is the number of statistical segments (Kuhn statistical segments) consisting in about 5 to 10 backbone bonds[33] and K is a factor which depends on the geometry of the molecule.

The rapid anisotropic segmental motion of the network chains described by a number *n* of freely rotating statistical segments leads to a nonzero average of the proton dipolar interaction if the ends of this chain are fixed. The decay of the transverse proton NMR magnetization of the network chain is described by

$$\frac{M_N(t)}{M_N(0)} = A\exp\left\{-\frac{t}{T_2} - M_2^{res}\tau_s^2\left[\exp\left(-\frac{t}{\tau_s}\right) + \frac{t}{\tau_s} - 1\right]\right\} \qquad \textbf{(3.40)}$$

Here, A is the fraction of network chains in the system, T_2 is the transversal relaxation time related to the fast local motion and τ_s is the slow relaxation time for large scale rearrangements. At this point is introduced[42] a parameter to describe the anisotropy of the rapid motion. This is defined as

$$q = \frac{M_2^{res}}{M_2^{rl}} = \left(\frac{K}{n}\right)^2 \qquad \textbf{(3.41)}$$

The factor K takes the value 3/5 in the case of a Gaussian chain and a direction of the dipolar interaction vector parallel to the chain. In the case of a normal direction of the dipolar interaction vector, like it is usually by C-H bonds of methylen or methyl groups, the factor K is 3/10 and 3/20, respectively.

The motion of free sol chains is assumed to be isotopic and yields to additionally purely exponential decay[37]. Then, by assuming an anisotropic motion for the inter-cross-link chains and the dangling free chain ends, the total NMR relaxation is described by [51, 34]

$$\begin{aligned}\frac{M_N(t)}{M_N(0)} = A\exp\left\{-\frac{t}{T_2} - qM_2^{rl}\tau_s^2\left[\exp\left(-\frac{t}{\tau_s}\right) + \frac{t}{\tau_s} - 1\right]\right\} + \\ B\exp\left\{-\frac{t}{T_2} - q'M_2^{rl}\tau_s\left[\exp\left(-\frac{t}{\tau_s}\right) + \frac{t}{\tau_s} - 1\right]\right\} + C\exp\left\{-\frac{t}{T_{2,sol}}\right\}\end{aligned} \qquad \textbf{(3.42)}$$

The fractions A, B and C represent the parts of magnetization of protons in inter-cross-link chains, dangling ends and sol fraction, respectively. qM_2^{rl} represents the mean residual part of the second moment of the dipolar interaction in relation to the physical and chemical constrains. $q'M_2^{rl}$ is the same as before but much smaller and was introduced by Heuert et al.[34] as a residual part of the second moment due to an assumed anisotropic motion of the dangling chain ends.

The average molecular mass of inter-cross-link chains $M_c = nM_S$ can be determined. M_S is the molar mass of a statistical segment. Because of the influence of physical entanglements in real networks, the value n that is obtained from equation **(3.41)** is not the true inter-cross-link segmental number but an effective one. The influence of entanglements is taken into consideration by correcting the value of q by a net value q_0, which is obtained for the un-cross-linked system. For the mean molar mass between two cross-links M_c it follows[33, 52]

$$M_c = \frac{K}{\sqrt{q} - \sqrt{q_0}} M_s \qquad \textbf{(3.43)}$$

The experiments must be performed at a temperature well above glass transition temperature (T = T_g + 120 K). Good correlation for many different rubbers was obtained between the M_c values estimated from different methods for moderately cross-linked samples with $M_c < 10^4$ g/mol, while agreement between them was poor for loosely cross-linked samples with $M_c > 10^4$ g/mol[50, 53]. Parameters characterizing the network such as M_c, B, T_2 and τ_s showed a similar tendency as swelling and mechanical data[50, 53, 54]. The network parameters evaluated from the different experimental techniques show fair agreement[50].

3.2.2 Litvinov's Method

Litvinov's method for determining the mean molar mass of the network chains from proton transversal relaxation in the vulcanized rubber is based also on Kuhn and Grün model of freely joined chains. It is assumed that the network chain consists of Z statistical segments between the network junctions[42, 55]. As in the case of other models, the T_2 value is determined at a temperature well above glass transition temperature, where a plateau region is detected.

For a Gaussian chain, in which the average, squared distance between network junctions is much shorter than the contour chain length, the T_2^p (transversal relaxation from the plateau region) value is related to Z

$$Z = \frac{T_2^p}{aT_2^{rl}} \qquad \textbf{(3.44)}$$

where a is the theory coefficient, which depends on the angle between the segment axis and the internuclear vector for the nearest nuclear spins at the main chain. For polymers containing aliphatic protons in the main chain, the coefficient a is close to 6.2 ± 0.7[55]. The T_2^{rl} value, which is measured for swollen samples below glass transition temperature, is related to the

strength of intrachain proton-proton interaction in the rigid lattice[56]. The T_2^{rl} value for a C_2Cl_4 swollen EPDM sample equals 10.4 ± 0.2 μs at 140 K[57].

Using the number of backbone bonds in the statistical segment, C_∞, the molar mass of network chain, M_w is calculated

$$M_w = ZC_\infty M_u / n \qquad \textbf{(3.45)}$$

where M_u is the average molar mass per elementary chain unit for the copolymer chain and n is the number of backbone bonds in an elementary chain unit. For the calculation of M_w in the case of EPDM the value of C_∞ at 363 K is 6.62 and is considered for an alternating ethylene-propylene copolymer[58]. It is assumed that the relative contribution of a network chain to the total relaxation function for heterogeneous networks is proportional to the number of protons attached to this chain. The cross-link density is defined by the value $2/fM_w$, where f is the functionality of network junctions by which this chain is fixed.

The maximum, relative error of network density determination by Litvinov's method is estimated to be about 15-25%. This error is composed of absolute errors in the T_2^p and T_2^{rl} values and the inaccuracy of the coefficients *a* and C_∞[57].

3.3 Experimental detection of transverse NMR relaxation

The *spin echo* phenomenon was accidentally discovered and named by Hahn[59]. The corresponding pulse sequence (see Figure 3.8) measure the spin-spin relaxation time (T_2) and represents the most useful building block for eliminating B_0 inhomogeneities.

At time zero a 90^0 pulse is applied along the positive x axis of the rotating frame, causing the magnetization **M** to precess into the positive y axis. The magnetization is the vector sum of

individual spin vectors arising from nuclei situated in different parts of the sample and therefore experiencing slightly different values of the magnetic field B_0, which is never perfectly homogeneous. The individual vectors will begin to fan out since some will be precessing slightly faster and some slightly slower than the rf field frequency ν_0.

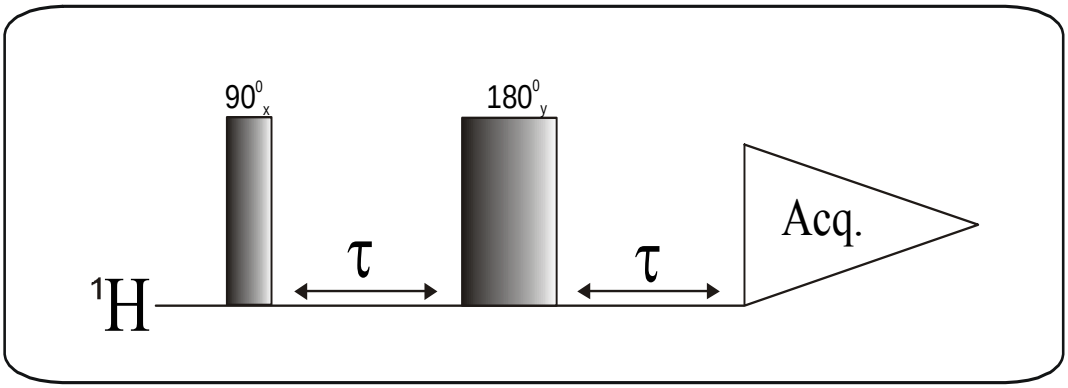

Figure 3.8 Hahn-echo pulse sequence.

After a time period τ is applied an 180^0 pulse which rotates the spins vectors into the –y axis. Since they continue to precess in the same sense, they will be now rotating together rather than fanning out. After a second interval τ they will refocus, meaning that all vectors simultaneously attain the same negative emission phase signal form corresponding to an inverted spin population. Together with the magnetic field inhomogeneity the τ-180-τ sequence refocuses also the chemical shift. In this way the correct phases are restored. However the chemical shift information are again contained in the decay following the echo.

The signal at 2τ is reduced somewhat in intensity because the effects of the true spin-spin relaxation processes are not refocused in the spin echo experiment. Assuming that other phenomena like, for example, spin diffusion are negligible for 2τ time interval, the intensity of the signal is proportional with the factor $\exp(-2\tau/T_2)$. Therefore the transverse relaxation time can be measured accurately using the Hahn-echo pulse sequence.

The phase cycling of the 180^0 pulse in a spin echo experiment is called *exorcycle*. If the phase of the 180^0 pulse is varied through the sequence {x, y, -x, -y}, the magnetization refocuses along the {y, -y, y, -y}. If the four signals are simply co-added, they would cancelled each other, but if the receiver phase is adjusted in order to follow the refocused magnetization {y, -y, y, -y} the signal will add up. In spectrometer encoding, the phase cycle would be written as:

- 0 1 2 3 (for the 180^0 pulse)
- 0 2 0 2 (for the receiver).

For the present work all proton transversal relaxation time were carried out on a Varian INOVA widebore spectrometer operating at 400 MHz for protons. The applied repetition time of 3-4 s was longer than 5 T_1, where T_1 is the NMR spin-lattice relaxation time. Usually, 40 values of $I(2\tau)$ were measured in the time interval 2τ from 80μs to 120 ms, where $I(2\tau)$ is the amplitude of an echo signal after the second pulse in the pulse sequence. The temperature for all experiments was set to 80 ^{0}C.

3.4 Results and Discussions

3.4.1 Determination of the Network Density for EPDM Samples

In order to determine the mean molar mass between two cross-linked points for the EPDM samples, the proton transversal relaxation decay was recorded for each cross-linked sample as well as for the corresponding uncross-linked EPDM. As expected, the EPDM_C shows the fastest decay, indicating the highest amount of cross-links.

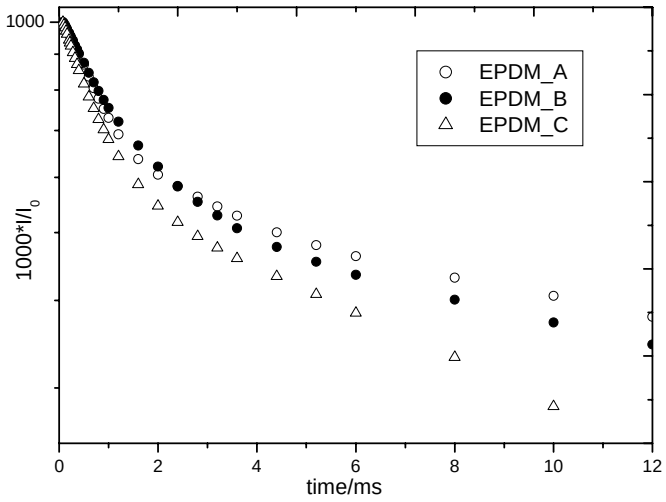

Figure 3.8 Transversal relaxation decay for EPDM_A, EPDM_B and EPDM_C

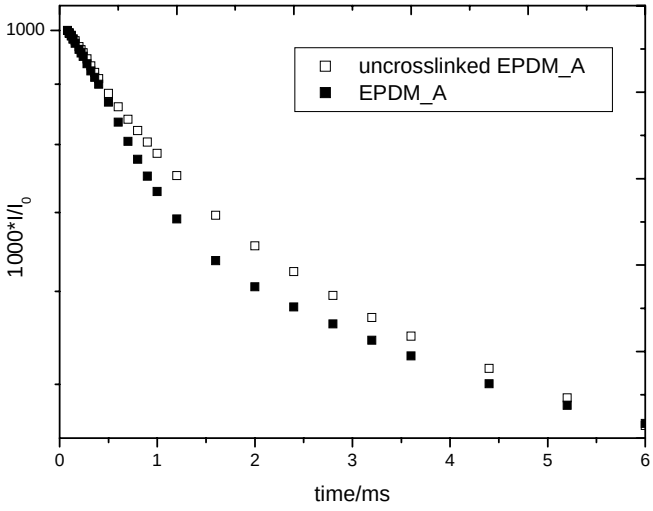

Figure 3.9 Transversal relaxation decay for EPDM_A and corresponding uncross-linked sample

In Figure 3.9 we represent the results of the transversal relaxation measurements for EPDM_A and EPDM_A before cross-linking. Due to the cross-liking process the transversal magnetization decay for EPDM_A is faster. The same behavior is observed for all EPDM samples.

The mean molar mass (M_c) between two cross-linked points was determined by applying the Gotlib model as well as by applying the Litvinov's method. Following the Gotlib model we fit all T_2 decays using a function adapted from the equation 3.42.

$$y = A\exp\left\{-\frac{x}{T_2} - qM_2^{rl}\tau_s^2\left[\exp\left(-\frac{x}{\tau_s}\right) + \frac{x}{\tau_s} - 1\right]\right\} + B\exp\left\{-\frac{x}{T_2}\right\} + C \qquad \textbf{(3.42.a)}$$

After determining the parameter qM_2 we apply the formula 3.43 and we obtained the results listed in Table 3.1 together whit the M_c values obtained using Litvinov's method.

In Figure 3.10.b we show the fitting procedure indicated by Litvinov. We used a double exponential function and we calculated the M_c values according with the formula 3.44 and 3.45. The parameter T_2^p is determined by fitting and the other parameters are taken from the literature[55].

Table 3.1 The results of M_c values determination by different methods

sample	*M_c(g/mol) Gotlib Model*	*M_c(g/mol) Litvinov's Method*
EPDM_A	2910	1396
EPDM_B	3666	1847
EPDM_C	2541	1039

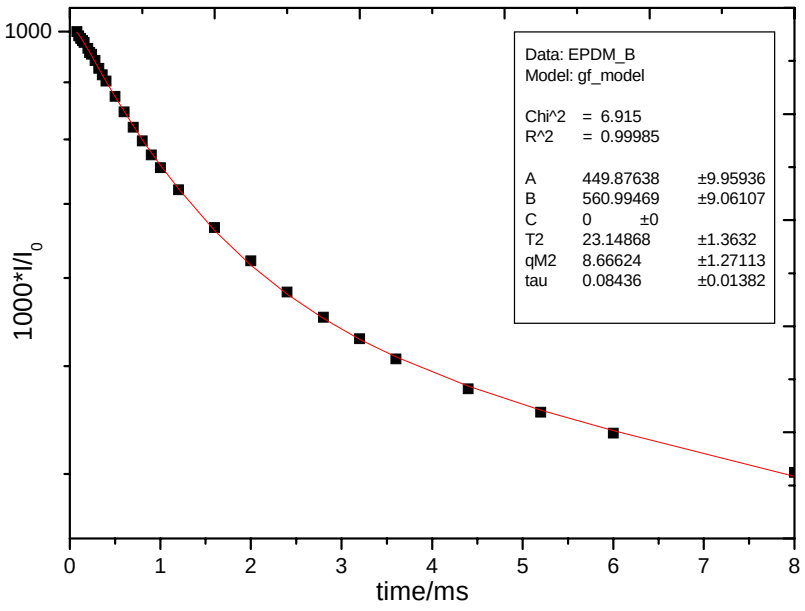

Figure 3.10.a T_2 decay for EPDM_B fitted with the function **(3.42.a)**

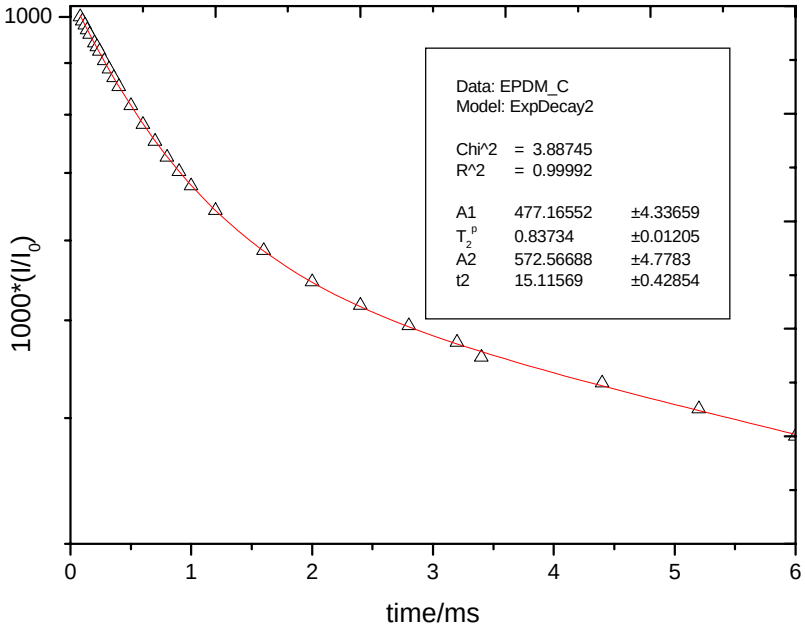

Figure 3.10.b T_2 decay for EPDM_C fitted with double exponential function

3.4.2 T_2 Results for PP/EPDM Blends – The influence of PP

In this Section we will demonstrate that the mean molar mass between two cross-linked points for rubber phase in blended samples cannot be determined from proton transversal relaxation, neither by Gotlib model nor by Litvinov's method. For this purpose we measured the T_2 for all PP/EPDM blends as well as for pure polypropylene.

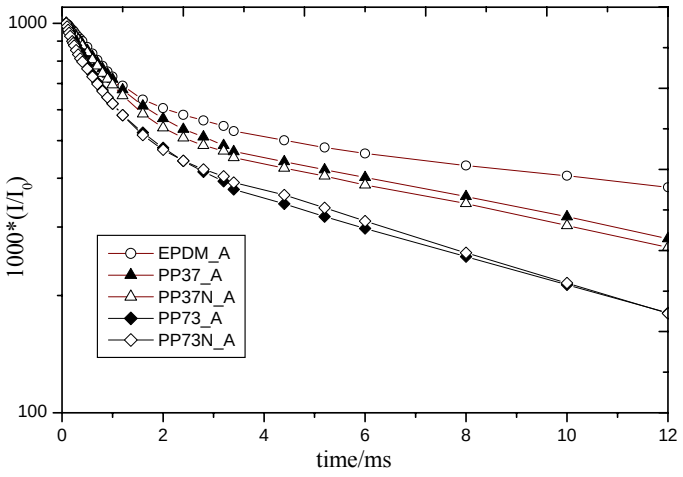

Figure 3.11 T_2 decay for blends containing 70% EPDM_A (PP37_A) and 30% EPDM_A (PP73_A) and for the corresponding dynamically cross-linked blends (PP37N_A and PP73N_A)

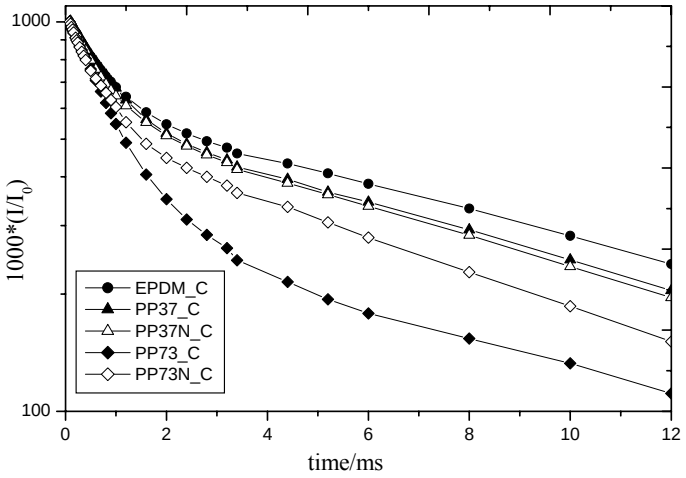

Figure 3.12 T_2 decay for blends containing 70% EPDM_C (PP37_A) and 30%EPDM_C (PP73_C) and for the corresponding dynamically cross-linked blends (PP37N_C and PP73N_C)

Figures 3.11 and 3.12 show the proton transversal relaxation of different blends, including dynamically cross-linked samples. The T_2 decay is faster with the increase of polypropylene content. The additionally cross-linked blend, PPN73_C, present a higher mobility (slower T_2 decay) than the corresponding blend (PP73_C) obtained only by mechanically mixing the rubber with polypropylene. This behaviour is due to the influence of the cross-linking agents (Struktol) on polypropylene matrix.

The measurements performed for pure polypropylene at 80 ^{0}C (see Figure 3.13) reveal that the complete relaxation of these sample occur only after 2 ms. The time domain 0-2ms is of the maximum interest when we want to estimate the cross-link density, no mater by which proton relaxation NMR method, but here, both phases in the blend have a contribution to the signal.

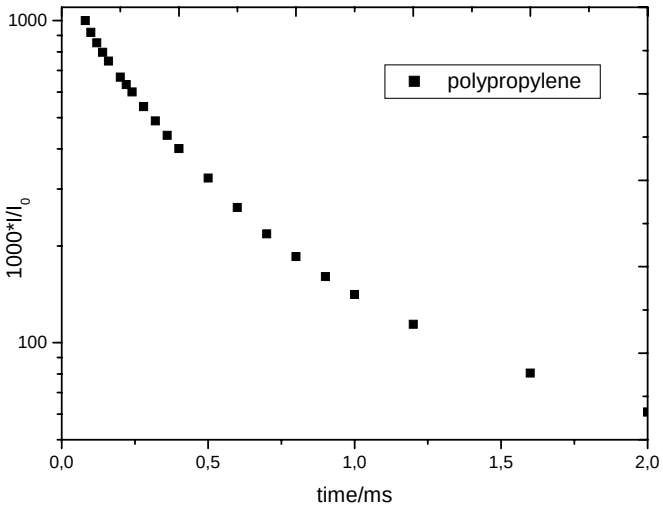

Figure 3.13 T_2 decay for pure polypropylene

The experimental and the simulated T_2 curves for to different blends are presented in Figure 3.14. The former were obtained by adding the signal from pure EPDM_A with the signal from pure polypropylene. The difference between the results (for both blends taken into consideration) leads to the conclusion that the interface between the rubber phase and polypropylene matrix plays un important role and the signal which came from this part of the sample is higher than we actually expected. Therefore it is clear that we cannot estimate

accurately, by means of proton NMR relaxation, the mean molar mass of the rubber phase in a blend which contain polypropylene.

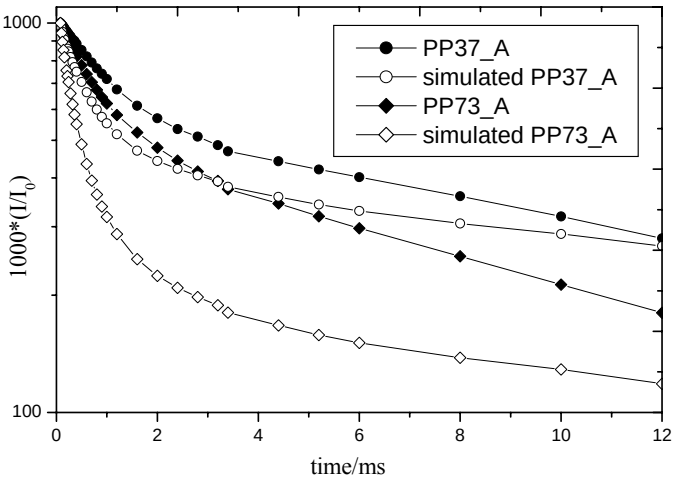

Figure 3.14 Experimental and simulated T_2 decay for the blends which contain 70% EPDM_A and 30% EPDM_A

4 Spin-echo, Spin-echo Double Resonance (SEDOR) and Rotational-echo Double Resonance (REDOR) applied on polymer blends

The next logical step after analyzing and concluding upon the results of proton transversal relaxation decay on our samples, is to apply the spin-echo technique on carbon channel. The main advantage of carbon measurements is the chemical site resolution, meaning that we can analyze the signal of the rubber phase free of polypropylene signal superposition. As we are mainly interested in getting information about cross-link density, the residual heteronuclear dipolar coupling is needed. Therefore the results of carbon spin-echo experiments have to be analyzed together with the SEDOR curves. To overcome the effect of the MAS conditions on heteronuclear dipolar coupling, the REDOR pulse sequence is applied. The results of all the above mentioned techniques are presented and discussed in this chapter.

4.1 Introduction

In the last chapter we demonstrated that the rubber phase in a plastic matrix (EPDM/PP blends) can be poorly characterized by proton NMR. As the other consecrated methods, like DMA and swelling measurements, present difficulties in getting rid of the polypropylene influence on their results, ^{13}C high- resolution magic angle spinning solid-state magnetic resonance spectroscopy seems to be the most appropriate technique for determining the cross-link density of blended samples.

All the following measurements are based on the fact that the carbon spectra of all blends (including the blends which contain 70 % polypropylene) present three EPDM resonances, which are well separated from the PP resonances, see Figure 4.1. A detailed assignment is presented in the Section 5.4.1.

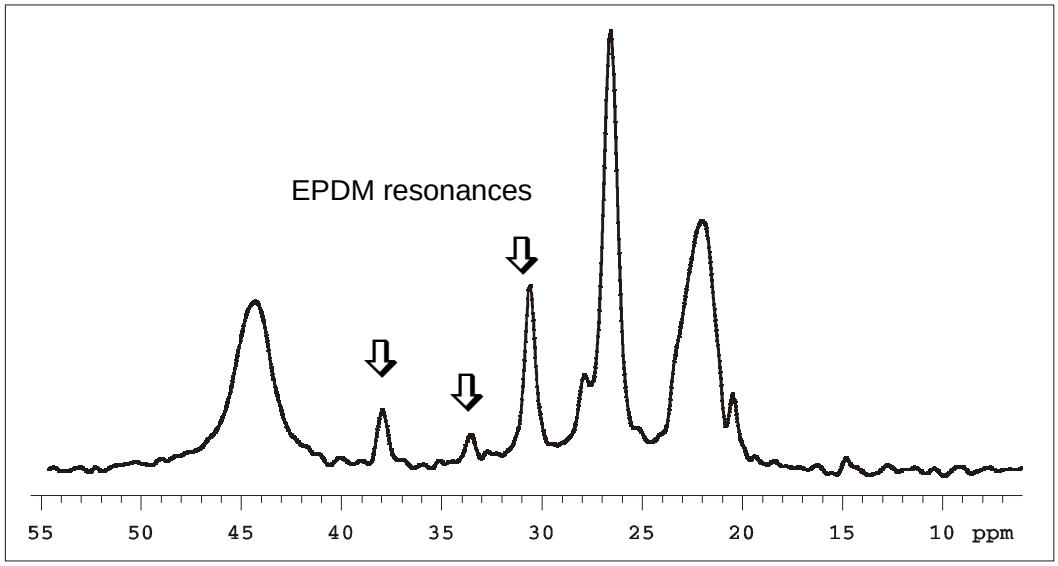

Figure 4.1 Carbon spectra of the blend PP37_A

Information about heteronuclear dipolar coupling (residual heteronuclear dipolar coupling in the case of polymers) and implicitly about cross-link density of the blended samples can be determined by applying the consecrated recoupling techniques like Spin-echo Double Resonance (SEDOR) and Rotational-echo Double Resonance (REDOR).

4.2 Theoretical Background

4.2.1 The Principle of SEDOR

In a ordinary ^{13}C spin-echo experiment the information about heteronuclear coupling is removed, but this can be reintroduced by applying simultaneously a 180^0 pulse on the both cannel (carbon and proton). This is actually the SEDOR pulse sequence and was first introduced by Kaplan and Hahn[60] in 1958. This basic double-resonance, solid-state NMR experiment was used to show that two unlike nuclei were physically near to each other. Later, Slichter provided a description of this experiment[61].

If the proton spins are near to a carbon spin, then carbons experience a local magnetic field, H_{loc}, generated by the proton spins. A component of this field can be parallel or anti-parallel to the applied Zeeman field. During the time period τ, between the 90^0 and 180^0 pulses of a simple spin-echo experiment (recall Figure 3.8) applied on carbon channel, the magnetization of the observed spins dephases because of the interaction with the dipolar magnetic field generated by the proton spins. After the 180^0 pulse, H_{loc} is unchanged and the carbon spins magnetization begins to rephase and the result is the formation of a *full* spin-echo after another τ period. The amplitude of the *full* spin-echo is

$$M_{x,1}(2\tau) = M_i e^{-2\tau/T_2} \qquad \textbf{(4.1)}$$

where M_i is the observed spins signal intensity following the 180^0 pulse and T_2 is the transversal relaxation time. Information about heteronuclear dipolar coupling can be derived, in principle, from carbons T_2, but as in the case of proton transversal relaxation, analysis is very much model dependent and therefore does not provide satisfactory results. The solution is to perform another experiment with an 180^0 pulse on proton channel simultaneously applied with the one on carbon channel. The effect of this pulse is a change in sign (see Figure 4.2) of the local magnetic field experienced by carbons during the second half of the spin-echo experiment. As a result, the carbon-proton dipolar interaction will not refocus and we will acquire a *reduced* echo with the following amplitude

$$M_{x,2}(2\tau) = M_i e^{-2\tau/T_2} \cos(2\tau\omega_D) \quad \textbf{(4.2)}$$

where $\omega_D = \omega_{D_0} \cdot P_2(\cos\theta)$ and θ is the angle between R and B_0. ω_D is inversely proportional to the cube of the internuclear distance and is a measure of the ^{1}H-^{13}C dipolar interaction. Transversal relaxation effects and B_0 inhomogeneities can be eliminated if we perform both experiments (Hahn-echo and SEDOR) and if we consider the ratio of the difference of the two signals to the *full* signal. For a single crystallite[62], the this ratio is

$$\frac{\Delta M_x(2\tau)}{M_{x,1}(2\tau)} = 1 - \cos(2\tau\omega_D)\,;\ \omega_D = \omega_{D_0} \cdot P_2(\cos\theta) \quad \textbf{(4.3)}$$

In the case of a powder sample an average over all angles is needed

$$\frac{\Delta M_x(2\tau)}{M_{x,1}(2\tau)} = \left\langle 1 - \cos 2\tau\omega_D(\theta) \right\rangle \quad \textbf{(4.4)}$$

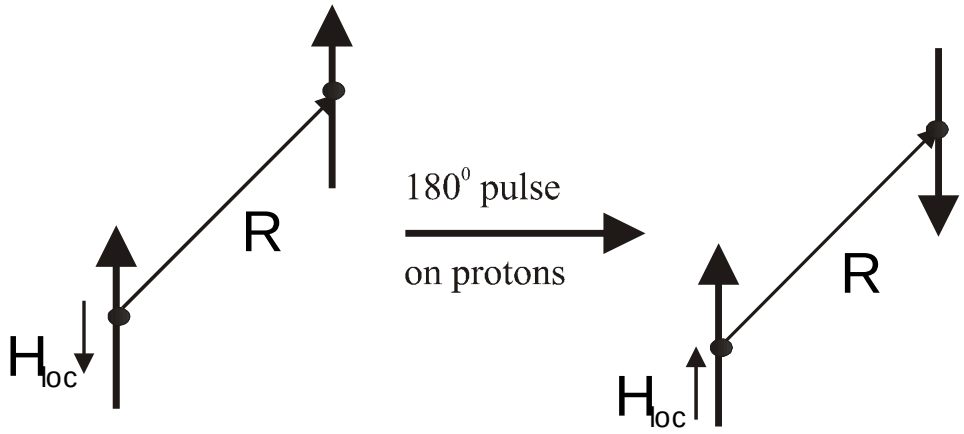

Figure 4.2 The effect of 180^0 pulse applied on proton channel

The SEDOR experiment in combination with spin-echo is very attractive because the equation 4.3 depends only on the dipolar interaction and the effects of relaxation and chemical shift anisotropy are not included. This kind of experiments can be also performed for many coupled nuclei like, for example, cupper and cobalt[63], platinum and carbon[64] and others.

4.2.2 The Principle of REDOR

Rotational-echo Double Resonance[62, 65] (REDOR) is currently the most used technique for determining the heteronuclear dipolar couplings in rotating solids. Original application is for isolated heteronuclear two-spin systems, like ^{13}C and ^{15}N, and recently REDOR was applied also to ^{1}H-^{13}C systems[66]. The basis of this method is the application of equally spaced 180^0 pulses on proton channel twice per rotor period. They serve to recouple the dipole-dipole interaction, which was averaged out under MAS conditions.

For a rotating powder sample the average value of the dipolar interaction is zero over each rotor cycle (T_r). Therefore the dipolar interaction has no effect on the detected signal from the spin echo experiment applied simultaneously with the sample rotation, see Figure 4.3 A. Similarly with the result of the spin-echo experiment for the static sample, the signal recorded here is the *full* signal and accounts for transversal relaxation decay.

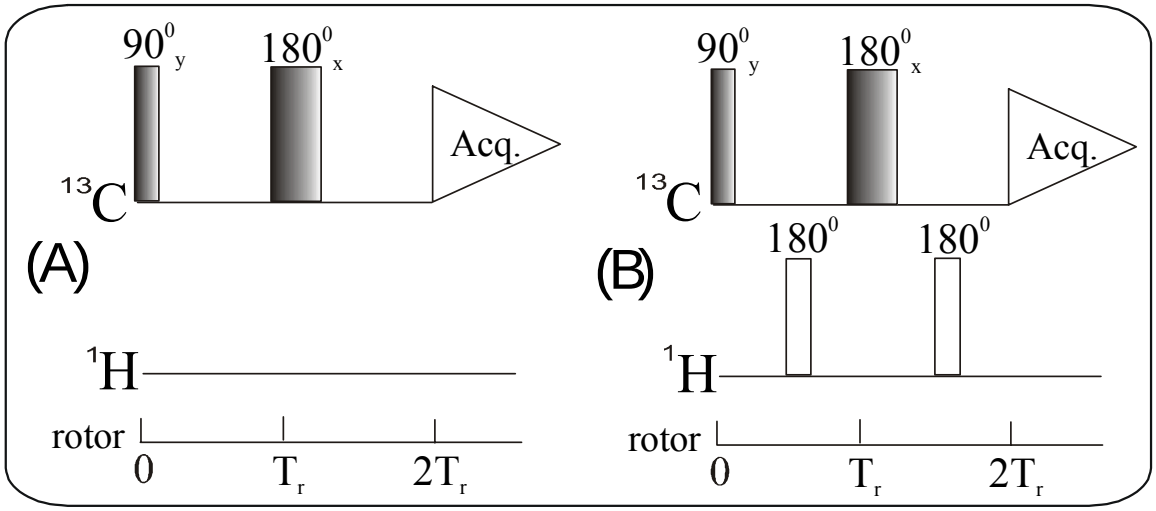

Figure 4.3 Models of REDOR experiments for ^{1}H-^{13}C system

During the first half of the first rotor cycle, the local dipolar field is positive (by convention) and, because of the spatial modulation of the dipolar interaction, will be negative during the second half of rotor period. By applying an 180^0 pulse on carbon channel at $T_r/2$, see Figure

4.3B, the relative sign of local dipolar field can is changed and become positive. Thus, the average local field experienced by carbon spins during the first rotor cycle is positive. The dipolar interaction has a periodic nature and, therefore, during the first half of the second rotor period the local dipolar field of the carbon spins is negative. The 180^0 pulse applied at $3T_r/2$ assure a negative dipolar field for the entire second rotor cycle. Because the average dipolar field experienced by carbon spins is positive for the first rotor cycle and negative for the second one, the carbon spins magnetization does not refocus when we start the data acquisition process. The signal recorded will be a *reduced* signal. Similar to SEDOR, the ratio of the difference to full signals produces an equation[62] for REDOR dipolar dephasing and depends only on C-H dipolar interaction.

4.3 REDOR Pulse Sequence – a Practical Version for Elastomers

A REDOR pulse sequence for ^1H-^{13}C spin system was firstly implemented by Saalwaechter et al.[66] In their version the carbon spins magnetization is created by ramped cross-polarization (CP) step[67], which is recommended under very-fast MAS condition (spinning rate of 25-30 kHz). This high spinning rate is used in order to suppress the influence of homonuclear dipolar couplings. In the case of our sample the very-fast MAS is not needed because the homonuclear couplings for elastomers, especially for EPDM, is weak and has a value of several kHz. Moreover we did not used cross polarization at all because by applying this procedure to a blend composed from two phases, the signal from the rigid part (polypropylene) will be over-emphasized and actually we are interested to analyze the signal from the mobile part (rubber phase). Additionally, the CP signal of the rubber phase, i.e. EPDM, is smaller than the signal obtained with an 90^0 pulse.

Figure 4.4 illustrates the pulse sequence implemented by us. The recoupling 180^0 pulse traines are applied on proton channel. The 90^0 pulses on carbon channel used by Saalwaechter et al. for cleaning the spectra from unwanted signal contributions are not needed in the case of our samples, see Figure 4.5. The two-pulse phase-modulated (TPPM)[71] decoupling was used in both cases.

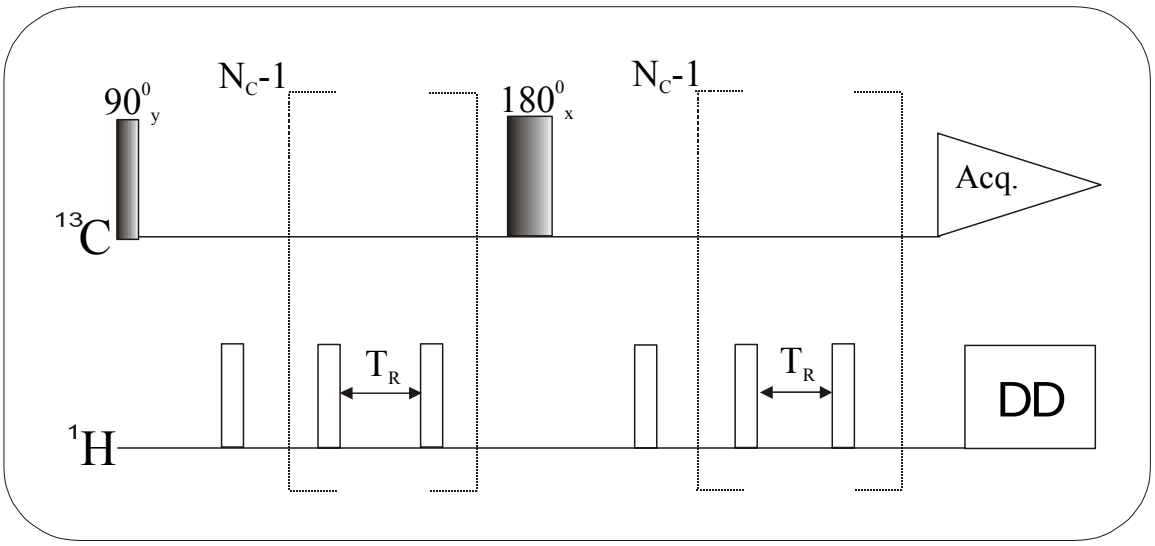

Figure 4.4 REDOR pulse sequence for ^1H-^{13}C system. N_c represents the number of cycles and T_R is the rotation period.

4.4 Experiments-Results and discussions

Solid state ^{13}C NMR spectra were recorded at 100 MHz ^{13}C Larmor frequency with a Varian Inova-400 spectrometer. A Varian double-resonance MAS probe was used with 7 mm zirconia rotors and Torlon caps. For all NMR experiments the temperature was set to 80 ^0C, which corresponds to approximately T_g + 120 ^0C for EPDM, and T_g + 95 ^0C for the PP, respectively, with T_g – the glass transition temperature. This enhances the mobility of the polymer chains leading to a better spectral resolution for rubber materials[68]. For all carbon measurements presented in this chapter the repetition time was 4 s and the spinning speed was 2 kHz. The spectra were acquired under TPPM proton decoupling at 50 kHz.

For spin-echo and SEDOR were recorded 57 values of $I(2\tau)$ in the time interval 2τ from 20 μs to 36 ms, where $I(2\tau)$ is the amplitude of an echo signal after the second pulse in the pulse sequence. The applied magnetic field on carbon channel was adjusted for each sample and the value was approximately 55 kHz. The 180^0 pulse on proton channel, for SEDOR experiment

was about 12 μs and its exact value depended also on the measured sample. The same value was usually taken for the ^{1}H 180^{0} pulses used in REDOR experiments. The number of scans was 518 for spin echo and SEDOR and 64 for REDOR measurements.

As presented in the introductory part of this chapter, the carbon spectra of blended samples present three peaks coming from EPDM, which are free from the polypropylene signal. From the view point of the experiments presented here, the analysis of each of them has to give the same results therefore we will present here only the experimental curves corresponding to the resonance from 31 ppm. We have chosen this resonance because it presents the best signal to noise ratio.

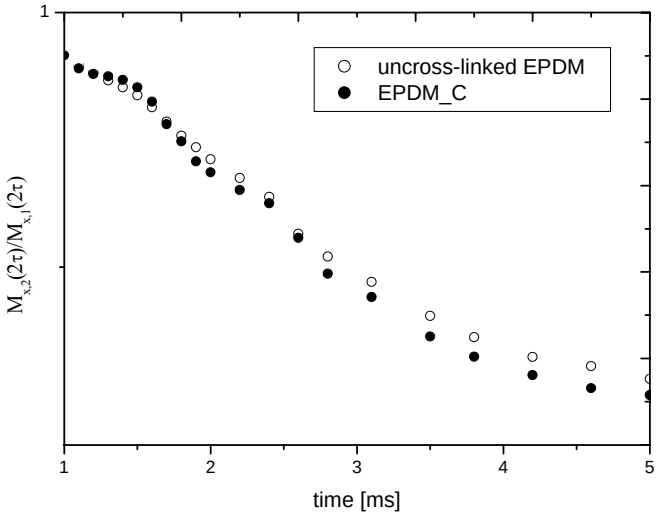

Figure 4.5 The SEDOR curves for an uncross-linked EPDM and EPDM_C

The results of spin-echo and SEDOR experiments for an uncross-linked sample and for EPDM_C are presented in Figure 4.5. From all our sample, this two have the highest difference between the cross-links densities, because the former must have no chemical cross-linked points and the latter must present the highest amount of chemical cross-links. As it can be observed, the difference between the two curves is very small therefore we cannot distinguish between smaller differences in cross-links densities, as it is the case of our blends.

The sensitivity of SEDOR and REDOR experiments is, in principle, the same. In Figures 4.6a and 4.6b we can clearly remark that there is now detectable difference between the REDOR curves of blends PP37_C and PP37N_C.

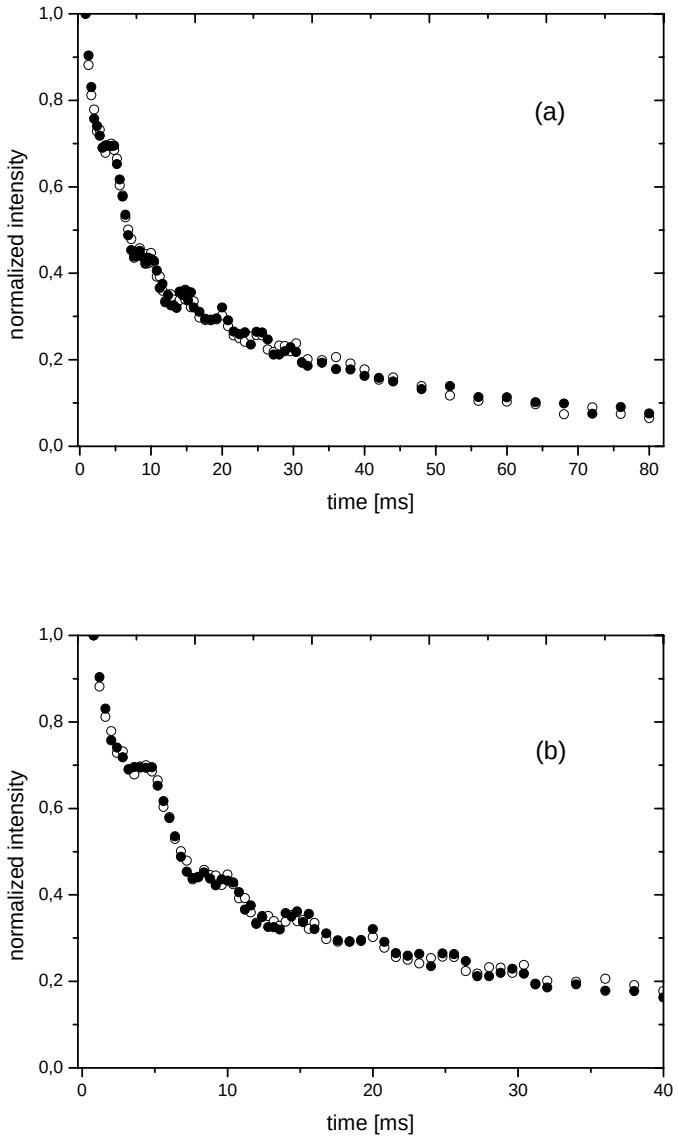

Figure 4.6 The REDOR curves for two of the investigated blends: PP37_C (open circles) and PP37N_C (filled circles); the hole time range is shown in (a) and an expansion from 0 to 40 ms is presented in (b)

5 Characterization of Crosslinking in EPDM/PP Blends from ^{1}H-^{13}C Polarization Transfer Dynamics

A new approach for characterization of the rubber phase in polymer blends by means of ^{1}H-^{13}C polarization transfer dynamics is introduced in this chapter. Its validity is demonstrated for our PP/EPDM blends. After a short presentation of the theoretical background, the experimental aspects for recording process of cross-polarization (CP) and depolarization (iCP) curves are explained in details. First we analyzed the experimental results according to the thermodynamic model developed by Mehring and then we employed the model of residual dipolar coupling under permanent cross-linking.

5.1 Introduction

As we demonstrated in the previous Sections, the high-resolution techniques are indispensable to selectively investigate structural and dynamical properties of the desired component in a blend. The most common ^{13}C solid-state NMR methods used to date, like spin-echo, SEDOR and REDOR, failed in providing information about cross-linking in the case of our compounds.

Here we would like to introduce a new approach for solid-state NMR characterization of cross-linking in polymer blends from the analysis of ^{1}H-^{13}C polarization transfer dynamics. It extends the model of residual dipolar couplings under permanent cross-linking, typically used to describe ^{1}H transverse relaxation techniques, by considering a more realistic distribution of the order parameter along a polymer chain in rubbers. Based on numerical simulations, this extended model was shown to explain for all the characteristic features of the cross-polarization (depolarization) curves measured on such materials.

The occurrence in some cases of transient dipolar oscillations, and the large CP scaling factor observed experimentally in the CP build-up curves of rubbers, are inconsistent with models used in the past to describe CP dynamics in the presence of fast molecular motion. For this reason, cross-polarization techniques in elastomers were commonly considered as being not very quantitative, despite their advantage of providing chemical site resolution.

The validity of the new approach developed here was demonstrated using the example of the CP build-up curves measured on a well resolved EPDM resonance line in a series of EPDM/PP blends. The improvements in CP data analysis are particularly important for investigating blends of great technological potential, like thermoplastic elastomers.

.

5.2 Short description of Cross-polarization Process

The direct nuclear magnetic dipole-dipole interactions is averaged to zero in liquids due to rapid rotational and translational diffusions leading to a good NMR spectral resolution, but no such motions prevails in rigid solids, the above interactions being a source of spectral broadening. To overcome this inconvenience, usually, a combination of techniques like cross polarization (CP), magic angle spinning (MAS) and dipolar decoupling is applied.

The cross-polarization technique is applied, usually, to improve the signal of the dilute spins like ^{13}C, ^{29}Si, ^{15}N by transferring the polarization from protons via dipolar interaction between the two spin species. Cross polarization requires two steps: firstly, the proton spin system must have a appropriate state for the magnetization transfer and then the two spin system must be put into efficient contact to allow the polarization transfer to occur. The proton spins are initially spin-locked which effectively assigns them a very low spin temperature in the rotating frame and allow the polarization transfer. After this preparation step, the cross polarization is brought about by switching on a resonant ^{13}C (or other dilute spin) radio frequency field with an amplitude satisfying the Hartmann-Hahn[22] matching condition ($\gamma_H B_{1H} = \gamma_C B_{1C}$). This simultaneous double-frequency irradiation of proton and carbon spins gives them the same effective precession frequency around their B_1 fields. This conditions being full filed, the two species can exchange energy. The energy exchange is mediated by the heteronuclear dipolar coupling[12].

The effect of different type of motions, like macroscopic sample rotation, molecular reorientation and molecular conformational changes, on CP process was first discussed by Pines et al.[21] Later, Fülber et al.[69] analyzed the influence of molecular motion on the heteronuclear cross-polarization rate for an application to cross-linked elastomers. When cross polarization is carried out in the presence of magic angle spinning the rate of CP can be affected by MAS when its frequency becomes comparable to the proton-proton secular dipolar linewidth[70]. Thus the match condition under magic angle spinning is $(\omega_H - \omega_C) = \pm \omega_R$ or $\pm 2\omega_R$, the so-called *sideband match conditions*.

5.3 Experimental

5.3.1 Recording Cross-polarization and Depolarization Curves

The cross-polarization, depolarization and depolarization under spin locking experiments were performed at 100 MHz ^{13}C Larmor frequency with a Varian Inova-400 spectrometer. As in the case of other carbon measurements a Varian double-resonance MAS probe with 7 mm zirconia rotors and Torlon caps was used. The temperature was kept to 80^0 C.

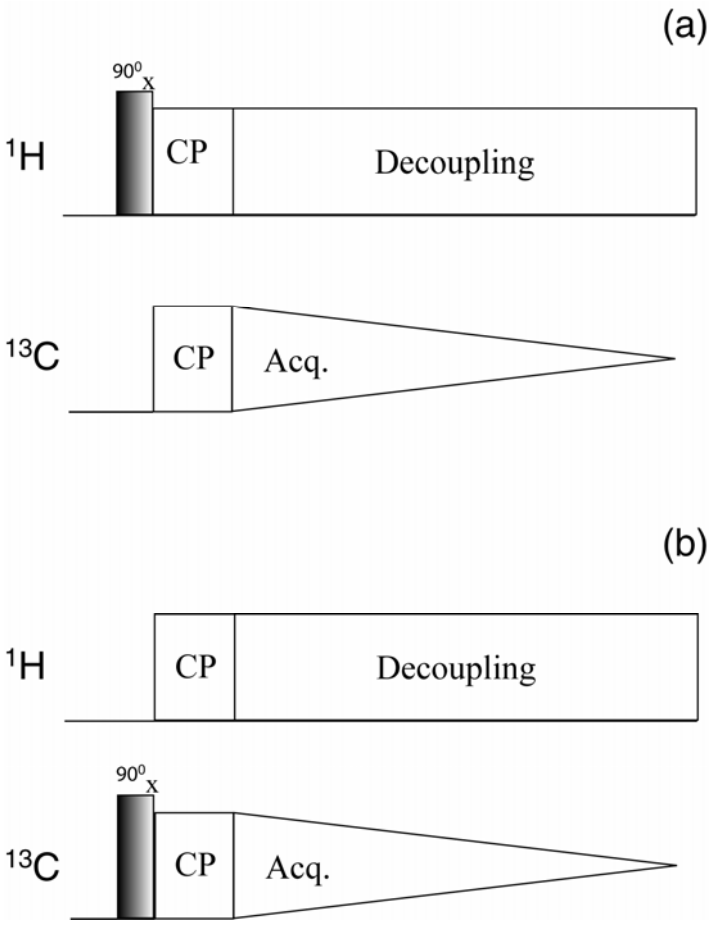

Figure 5.1. Schematic representation of the **(a)** CP-MAS and **(b)** iCP-MAS pulse sequences used to acquire the ^{13}C NMR spectra

Standard cross-polarization magic-angle-spinning (CP-MAS) experiments (Fig. 5.1.a) were performed at a spinning frequency of 2.5 kHz, using a ^{1}H 90^{0} pulse length of 6 μs. The ^{13}C NMR spectra were acquired under two-pulse phase-modulated[71] (TPPM) ^{1}H decoupling at 50 kHz by averaging 128 scans with a recycle delay of 4 s. The CP transfer was optimized for 30 kHz ^{1}H *rf* field for the contact pulse and approximately 32.5 KHz on the ^{13}C channel. The experimental determination of magnetization transfer efficiency is presented in the next Section.

CP build-up curves were recorded by incrementing the length of the contact pulse from 0 to 30 ms: this was done in steps of 25 μs at short times, while for times larger than 4 ms the value of the increment was progressively increased, so that in the end a total number of 42 points was employed to define the CP build-up curves.

The ^{13}C depolarization curves were recorded in an inverse cross-polarization experiment (iCP-MAS) – see Fig. 5.1.b. The iCP experiment has an important advantage over the CP one: by applying the 90^{0} pulse on carbon channel all ^{13}C spins are polarized, therefore we are sure that we record the signal for all carbon spins. In the CP experiment the polarization transfer from protons to ^{13}C, take place selectively and the more mobile ^{13}C spins are, most likely, not polarized. The same experimental parameters as in the case of CP-MAS were used, except that a different phase cycle was employed which eliminates the contribution of the initial ^{1}H longitudinal polarization. The phase cycling is

- X, -X, Y, -Y, -X, X, -Y, Y (for the 90^{0} pulse on carbon channel)
- Y, Y, -X, -X, -Y, -Y, X, X (for the radiofrequency field applied on proton and carbon channel, respectively)
- X, -X, Y, -Y, -X, X, -Y, Y (for the receiver).

Direct one-pulse ^{13}C spectra were acquired for the all samples using the same experimental conditions. They were used to quantify the intensity scaling under the interference of the molecular motion with the coherent CP transfer process. The ^{13}C resonances in the recorded NMR spectra are calibrated, as usually, with respect to TMS.

5.3.2 The Determination of Magnetization Transfer Efficiency

For a solid sample, the CP transfer rate it higher with decreasing mobility. In a static sample the maximum transfer rate is at the Hartmann-Hahn match. This is not the case if the sample is spinning.

It has been reported for adamantane that the static C-H coupling is amplitude modulated by the MAS and that the homonuclear proton coupling is frequency modulated, giving rise to a dependence of transfer rate an the carbon spin locking radio frequency. The maximum transfer rate occur when the carbon spin locking radio frequency is offset from the exact Hartmann-Hahn match by integrals of the spinning frequency[70, 72].

All cross-polarization measurements for determining the magnetization transfer efficiency were made by using a 30 kHz ω_H. ω_C was varied as desired. Usually the contact time was fixed at 2ms. This experiments were used in order to optimize the parameters for CP curves and were performed for each sample. Illustrative examples for two different PP/EPDM blends are shown in the figure below. The plots correspond in each case for an EPDM resonance.

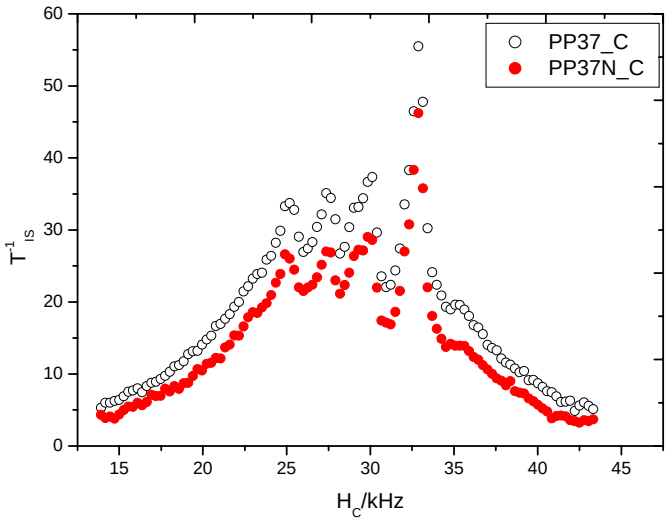

Figure 5.2 Plot of magnetization transfer efficiency vs. ω_C with ω_H maintained at 30 kHz for two different blends

5.4 Results and discussions

5.4.1 Carbon CP-MAS Spectra

Representative ^{13}C CP-MAS spectra of PP, EPDM_A and PP55_A samples are shown in Fig. 5.3. The three distinct resonances in the PP spectrum correspond to the CH_3 (22 ppm), CH_2 (44.5 ppm), and CH (27 ppm) carbons, respectively. They are all slightly asymmetric, which is typical for partially amorphous materials. Narrower and more symmetric lines are obtained in the spectrum of EPDM_A due to its increased molecular mobility.

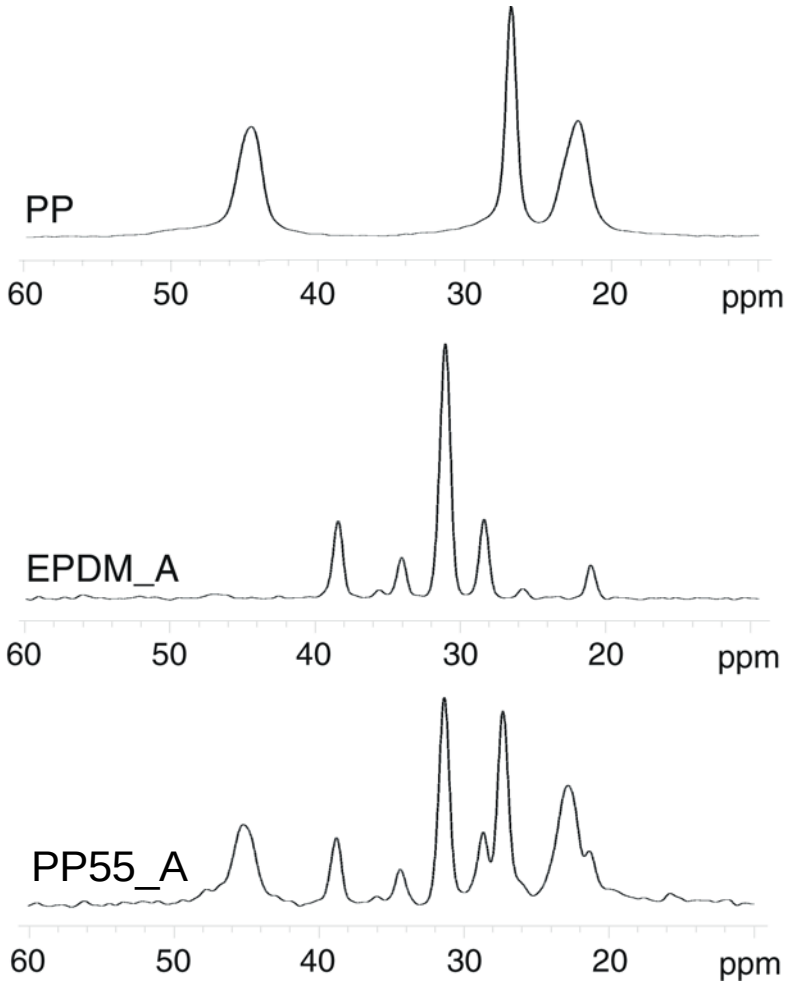

Figure 5.3 ^{13}C NMR spectra acquired by CP-MAS at 2.5 kHz sample spinning and a temperature of 80^0C on polypropylene (PP), EPDM rubber vulcanized according to the recipe A in Table 1, and a blend obtained by mixing equal amounts of the two components (PP55_A).

The EPDM sample resonances are assigned as follows[73]: the 21, 38, and 34 ppm lines come from the CH_3, CH_2, and CH carbons in propylene, while the ethylene resonances are located at 28 ppm and 31 ppm, both corresponding to CH_2 groups. Almost the same line positions are obtained in the CP-MAS spectra of the all blends.

As can be seen from the PP55_A spectrum in Fig. 5.3, except for the EPDM resonances at 31, 34 and 38 ppm, the other EPDM lines are partially or fully overlapped with PP lines. Thus, for a reliable analysis of CP and iCP dynamics one is confined to working on these three resonances. In the following, however, the results will be illustrated only on the ethylene 31 ppm line because its increased S/N ratio enables one a more accurate comparison between the different blends.

5.4.2 Cross-polarization and Depolarization Curves

The measured CP-MAS build-up curves are shown in Figure 5.4a. As described in the Experimental Section, they are recorded using a total number of 42 points for contact pulse durations ranging from 0 to 30 ms. Normalization is done with respect to the integral intensity of the corresponding line in the ^{13}C MAS spectrum acquired by one-pulse excitation.

According to the labeling scheme defined in Section 2.1.2, the two different symbols represent blends containing EPDM vulcanized according to the two different recipes, namely PP%_A (circles) and PP%_C (triangles), whereas open and filled symbols correspond to the normal, and to the additionally cross-linked (with "N") samples, respectively. A typical behavior of CP dynamics was obtained in the all cases, where the short-time raise of the build-up curves is dominated by ^{1}H-^{13}C polarization transfer process driven by residual dipolar interaction recoupled at Hartmann-Hahn matching, while after reaching the saturation level their evolution is governed mainly by spin-lattice relaxation in the rotating frame. Both regimes are well defined within the contact time range of 30 ms chosen here.

As a distinctive feature, in Figure 5.4a one can see that the transition between them is accomplished in a different manner depending on the type of EPDM elastomer present into the

blend. In particular, a smooth passage from the short-time to the long-time regime characterizes the blends which contain EPDM_A, while in the case of EPDM_C containing blends features which are reminiscent of transient dipolar oscillations [] are also visible in the CP build-up curves. This already indicates differences in the overall structure of their cross-link networks. In addition, one can also see that the amplitude factor of the analyzed line in the CP-MAS spectrum is slightly different across the blends series, ranging from 0.62, in the case of PP37_A sample, to 0.7 for PP37N_C, respectively. These values correspond to a significant CP efficiency reduction compared to the ideal enhancement factor of $\gamma_H/\gamma_C \approx 4$, but they are not unusual for elastomers because of the increased molecular mobility.

Further insights into the polarization transfer dynamics can be drawn from analyzing the short-time behavior of the CP process, where the CP build-up rates mainly depend on the strength of the residual C-H dipolar interactions induced by cross-linking. This dependence is illustrated in Figure 5.4b by expanding the contact time axis in the range 0 – 3 ms. Qualitatively, the results obtained for the PP37_A, PP37N_A and PP37_C samples agree well with theory, where the increased values of the build-up rates correlate with strengthening the residual C-H heteronuclear dipolar couplings, thus implicitly, with increasing the cross-link density. Within this scenario, the PP37N_C blend behaves quite anomalously: although this sample is expected to have the highest cross- link density of the all blends in the series, its corresponding CP build-up rate is approximately the same as that of PP37N_A. Nevertheless, this anomaly can be explained based on the results reported in literature[24]: there, the cross-linking process in EPDM rubber could be studied directly by specific ^{13}C labeling at the allylic positions in ENB, where the sulfur bridges are actually formed during vulcanization. In that study it was found that, under certain conditions, the additional vulcanization can lead to oxidation and reversion of the cross-links and therefore to a reduction in their density. Thus, the decrease in the PP37N_C cross-polarization build-up rate shown in Figure 5.4b clearly indicates the onset of the cross-link reversion process. The fact that such information can be retrieved with good sensitivity based on a much less expensive technique, like CP-MAS on ^{13}C natural abundant samples, must be appreciated.

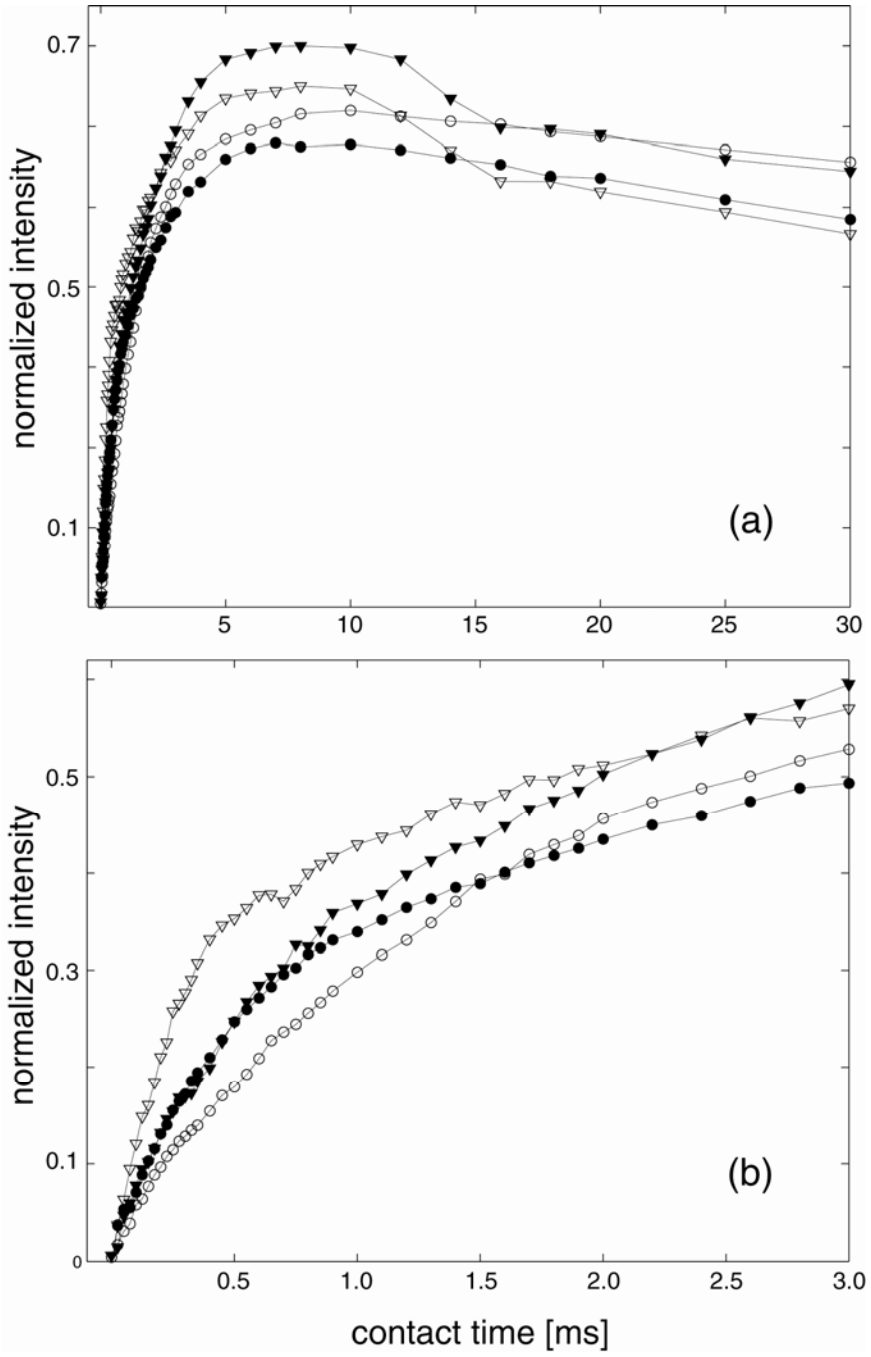

Figure 5.4 The CP-MAS build-up curves for the 31 ppm ^{13}C NMR line of EPDM in the investigated blends: PP37_A, open circles; PP37_C, open triangles; PP37N_A, filled circles; PP37N_C, filled triangles. They are normalized with respect to the intensity of the 31 ppm line in the ^{13}C NMR spectra acquired by one-pulse excitation under the same experimental conditions. In **(a)** the whole mixing time range from 0 to 30 ms is shown, while **(b)** corresponds to a blow up of the short time range from 0 to 3 ms.

Next we present the results of the depolarization (iCP-MAS) and ^{13}C spin-locking (SL) experiments obtained on the same EPDM/PP blends. They are illustrated in the Figures 5.6 and 5.7 where again the intensity variation of the 31 ppm ^{13}C line in the range 0 – 30 ms, and a blow up of the short contact time region, from 0 to 3 ms, are displayed separately.

In a quasi-rigid approximation, the cross-polarization (CP) and depolarization (iCP) processes are equivalent and thus provide the same information on the C-H dipolar couplings responsible for the polarization transfer. This equivalence is illustrated well in the case of pure polypropylene, which is more rigid than EPDM, (see Figure 5.5).

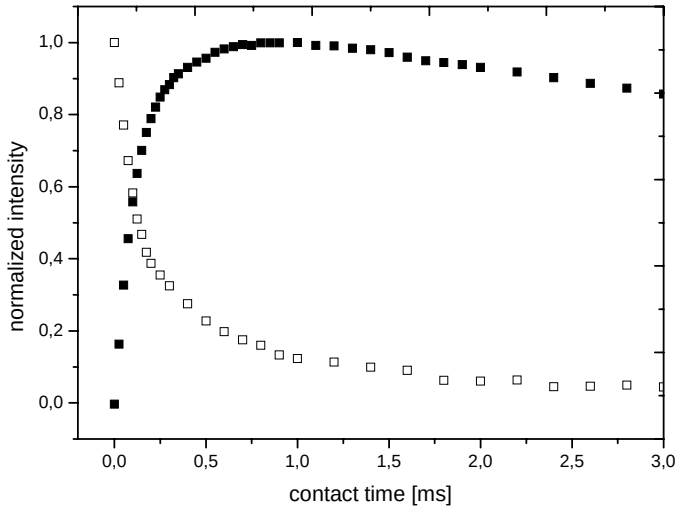

Figure 5.5 The CP-MAS (filled squares) and iCP-MAS (open squares) curves for the 22 ppm ^{13}C NMR line of polypropylene (PP)

However, in the presence of rapid molecular motion, like in elastomers, this symmetry is broken because relaxation will encode the corresponding CP and iCP curves in different ways[12]. This means that a simultaneous analysis of the both curves should in principle increase the accuracy of extracting the residual dipolar couplings, by reducing the number of independent fit parameters. Nevertheless, in the particular case investigated here this procedure seems to be complicated by the relatively strong amplitude modulations in the iCP curves obtained at contact times shorter than 0.5 ms, see Figure 5.6b.

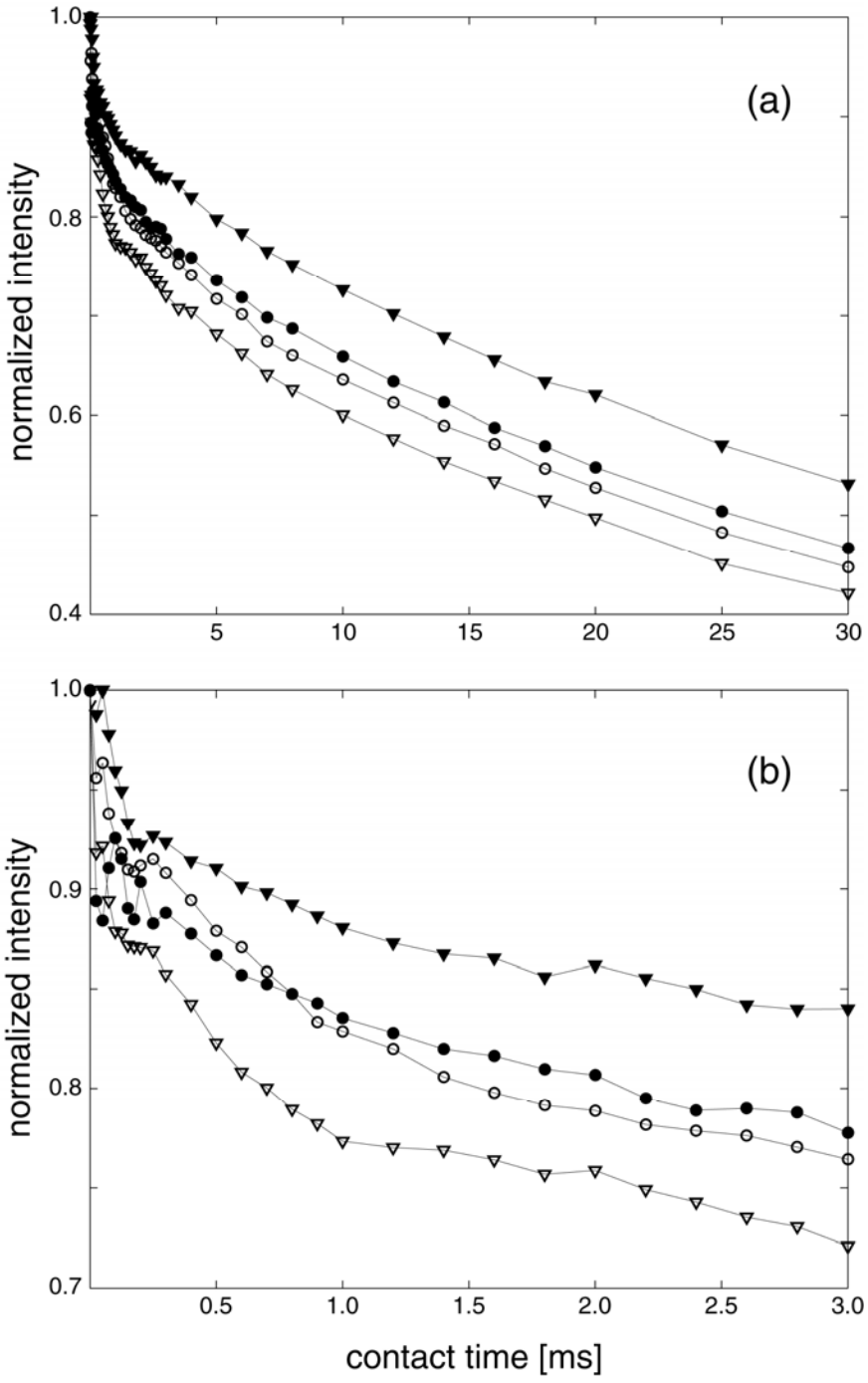

Figure 5.6 The iCP-MAS depolarization curves for the 31 ppm ^{13}C NMR line of EPDM in the investigated blends: PP37_A, open circles; PP37_C, open triangles; PP37N_A, filled circles; PP37N_C, filled triangles. They are normalized with respect to intensity of the 31 ppm line in the ^{13}C NMR spectra acquired by one-pulse excitation under the same experimental conditions (described in the text). In **(a)** the whole mixing time range from 0 to 30 ms is shown, while **(b)** corresponds to a blow up of the short time range from 0 to 3 ms.

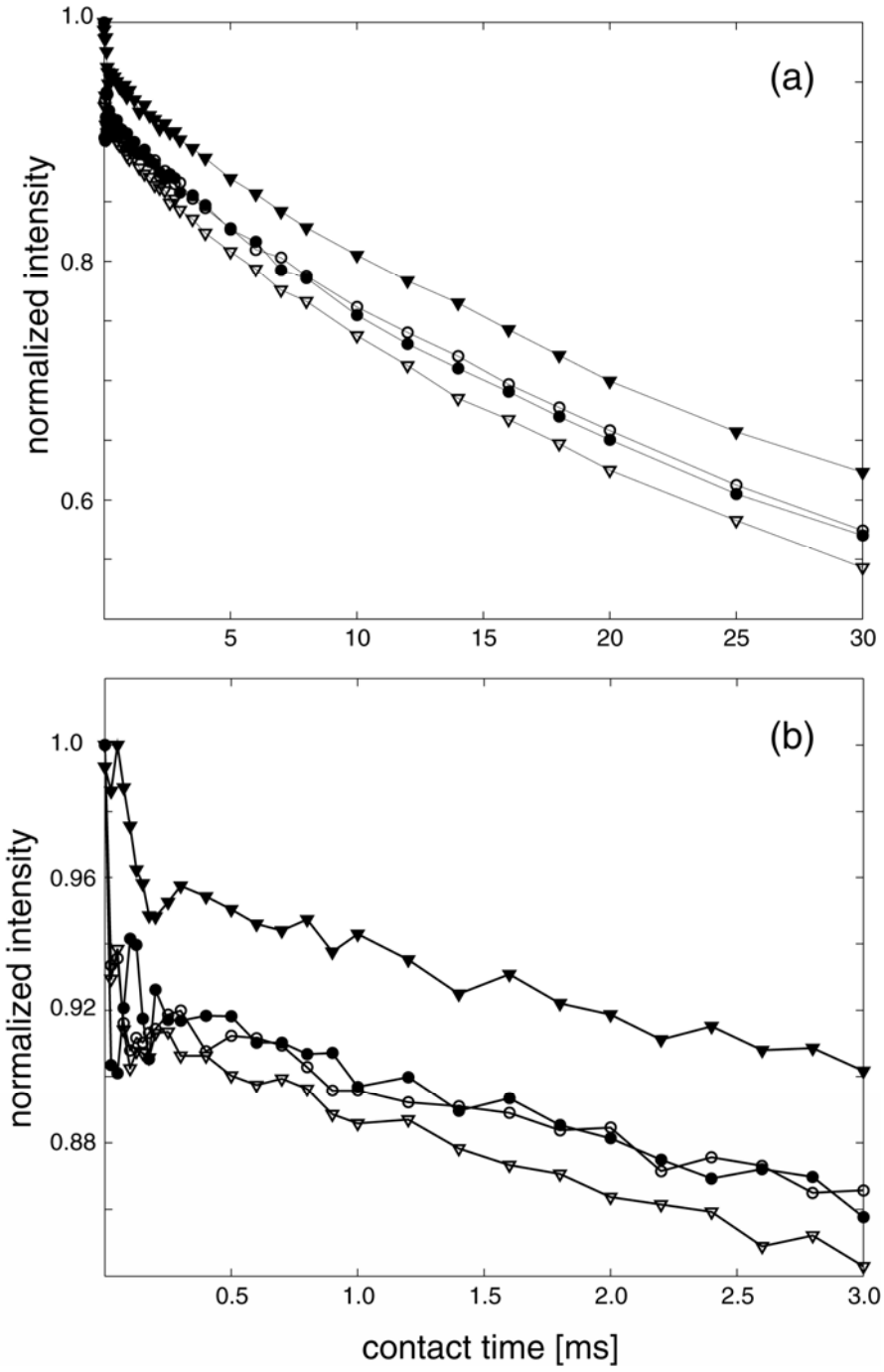

Figure 5.7 The depolarization curves under spin-locking (SL) experiment for the 31 ppm ^{13}C NMR line of EPDM in the investigated blends: PP37_A, open circles; PP37_C, open triangles; PP37N_A, filled circles; PP37N_C, filled triangles. In **(a)** the whole mixing time range from 0 to 30 ms is shown, while **(b)** corresponds to a blow up of the short time range from 0 to 3 ms.

As explained in literature[70] such modulations are not related with the CP process itself, but they are rather a manifestation of the particular features of ^{13}C spin-lattice relaxation in the rotating frame. This is clearly demonstrated by the results illustrated in Figure 5.7b, where a similar behavior was observed also in SL experiments. Thus, unlike the case of direct CP, a reliable estimation of the residual dipolar couplings from the short-time evolution of ^{13}C depolarization curves is no longer possible. On the other hand, the relaxation parameters obtained from the long time iCP decay, could prove useful in simplifying the analysis of the CP build-up curves. However, the information one can actually extract from the above experimental findings depend on the particular model we chose to employ, and this will be thoroughly analyzed in the following sections.

5.5 Analyses and Discussions

5.5.1 The Thermodynamic Model

According to the thermodynamic model developed by Mehring[12], the CP process is characterized by individual ^{13}C transfer rates, $1/T_{CH}$, which considerably depend on static (recoupled) C-H heteronuclear dipolar interactions, but also on the rates of spin-lattice relaxation in the rotating frame corresponding to the given carbon site, $1/T_{1\rho}(^{13}C)$, and to the surrounding protons, $1/T_{1\rho}(^{1}H)$, respectively. The exact functional dependence of the normalized CP build-up curve on these parameters can be extracted from the solution of two coupled rate equations[12] which means that the polarization transfer dynamics is a result of competitive relaxation and transfer processes. Specifically, one has[12]

$$\frac{I(t)}{I_0} = \frac{\alpha}{a_+ - a_-}\left[\exp\left(-\frac{a_- t}{T_{CH}}\right) - \exp\left(-\frac{a_+ t}{T_{CH}}\right)\right] \qquad \textbf{(5.1)}$$

where I(t) and I_0 are the ^{13}C line intensities in the CP-MAS, and one-pulse NMR spectrum, respectively. The a_+ and a_- coefficients are complicated functions of the parameters $\eta_H = T_{CH}$ /

$T_{1\rho}(^1H)$ and $\eta_C = T_{CH} / T_{1\rho}(^{13}C)$, whose explicit expressions can be found in Mehring's book[12]. Their difference, $a_+ - a_-$, defines a scaling by molecular motion of the rigid body CP gain factor, α. Its ideal value is $\alpha = \gamma_H/\gamma_C \approx 4$, but in practice, however, this is typically not larger than $\alpha \approx 2.5 \div 3$[74].

The main disadvantage of the thermodynamic model comes from the dependence of the normalized intensity $I(t)/I_0$ on three independent parameters, such that a fit with the relation (1) of a measured CP build-up curve could lead to ambiguities in extracting the corresponding relaxation- and transfer rates. The analysis however can be simplified in a regime of fast molecular motion, where the $T_{1\rho}$ relaxation times are considerably larger than T_{CH}, thus η_H (η_C) $\rightarrow$ 0. In elastomers this can be reached at temperatures well above the glass transition temperature, T_g. Under these conditions, the eq. (5.1) can be approximated through[12]

$$\frac{I(t)}{I_0} = \frac{\alpha}{\lambda}\left[1 - \exp\left(-\frac{t}{T_{CH}}\right)\right]\exp\left(-\frac{t}{T_{1\rho}(^1H)}\right) \qquad \textbf{(5.2)}$$

with the new scaling factor given by

$$\lambda = 1 - \eta_H + \eta_C \approx 1 \qquad \textbf{(5.3)}$$

According to the above relations, such a regime can be easily identified in practice. In particular, the signal amplitude is not significantly scaled compared to its rigid approximation value, $\alpha \approx 2.5 \div 3$, whereas the CP curves are characterized by a slow decay, with the rate $1/T_{1\rho}(^1H)$, at long contact times and a much faster build-up at short times, with the rate $1/T_{CH}$. Similar relationships can be found for the iCP case as well, except that the long-time behavior of the depolarization curve is governed by ^{13}C spin-lattice relaxation in the rotating frame, namely, this will decay with the rate $1/T_{1\rho}(^{13}C)$. Consequently, the relaxation and transfer parameters can be conveniently extracted now by separately fitting the two extreme time domains in the polarization (and depolarization) transfer process.

Table 5.1 Spin-lattice relaxation times and CP transfer times obtained by the best fits of the measured CP and iCP data with the simplified relations [Mehring] which characterize the fast molecular motion regime in elastomers

sample	$T_{1\rho}(^1H)$ *[ms]*	$T_{1\rho}(^{13}C)$ *[ms]*	T_{CH} *[ms]*
PP37_A	110	58.9	3.4
PP37_C	105	52.3	3.8
PP37N_A	120	56.5	4.1
PP37N_C	118	52.8	3.9

The temperature used in the present investigation is significantly larger than T_g of EPDM, so that we expect to be able to analyze the experimental data based on the simplified relationships (5.2) and (5.3), characteristic to the fast motional regime. The slow variation of the CP curves in Figure 5.4, and iCP depolarization curves in Figure 5.6, at contact times larger than 10-15 ms is in perfect agreement with this assumption. The values of the $T_{1\rho}(^1H)$ and $T_{1\rho}(^{13}C)$ spin-lattice relaxation times extracted from fitting the long time parts of these curves with the exponential decay functions $exp[-t/\ T_{1\rho}(^1H)]$, and $exp[-t/\ T_{1\rho}(^{13}C)]$, respectively, are listed in the Table 5.1. For comparing these relaxation times with the corresponding polarization transfer time-constant, T_{CH}, the short time parts of the CP build-up curves have been also fitted with the functions $c_k\{1 - exp[-t/\ T_{CH,k}]\}$, where c_k are the measured amplitude scaling factors, while *k* labels different samples in the series. The resulting fit values are also shown in Table 5.1.

The T_{CH} transfer times we obtained are indeed much smaller than the both spin-lattice relaxation times in the rotating frame, so that for the all four blends the condition expressed by the eq. (5.3) are fulfilled, and hence a fully effective polarization transfer by CP is expected, with $c_k \approx \alpha \approx 2.5 \div 3$. This result is however in large disagreement with the measured amplitude factors. In particular, the significant amplitude scaling we obtained experimentally, with c_k ranging between 0.6 and 0.7, does not fit at all with the prediction of the thermodynamic model. In addition, the transient oscillations observed between 5 and 10 ms in the CP curves of

the PP37_C and PP37N_C blends (see Figure 5.4a) also cannot be explained within this theoretical framework.

5.5.2 The Model of Residual Dipolar Interaction under Permanent Cross-Linking

At the other extreme, compared to the thermodynamic treatment, one can employ a theoretical model where the coherent nature of the CP-MAS process is better taken into account. Using such an approach is definitely more suitable here due to the weak influence of relaxation upon CP in the fast motional regime. Within this model, the effect of intense molecular motion is assumed to consist only of scaling the rigid-body dipolar couplings by the so-called order parameter, $\langle P_2 \rangle$[41], which is due to topological constraints induced by cross-linking in elastomers. Specifically, the molecular motion is rendered anisotropic with respect to the axes connecting consecutive cross-link points (either sulfur bridges, or physical entanglements of the polymer chains), considered fixed on the time-scale of the polarization transfer process. Taking a linear chain of N statistical segments, fixed at its extremities, the dipolar coupling constant between any two spins, j and k, is given by $\langle \omega(j,k) \rangle = \omega_0(j,k) \langle P_2 \rangle$, with $\omega_0(j,k)$ the rigid-body coupling constant, and where the exact relationship between the order parameter and N essentially depends on the adopted statistical chain model[38, 43, 51].

As we sow in chapter 3, the model of residual dipolar couplings under permanent cross-linking proves quite successful in explaining the shape of ^{1}H transverse relaxation curves acquired by Hahn echo technique in rubbers. These curves consist of two distinct components: a fast decaying part assigned to inter-crosslink chains, which are characterized by a finite $\langle P_2 \rangle$, and a slow decaying component, attributed to the dangling ends. The latter are supposed to have an isotropic, liquid-like, motion and thus characterized by an order parameter $\langle P_2 \rangle = 0$. The weighting factor for each contribution is a direct measure of the corresponding fraction from the two distinct proton environments present into the sample.

Applying the same arguments also to the analysis of the build-up curves in Fig. 5.5, the large drop in the CP efficiency can be attributed to the ^{13}C nuclei located in dangling ends, where the order parameter is assumed zero, and cannot be cross-polarized.

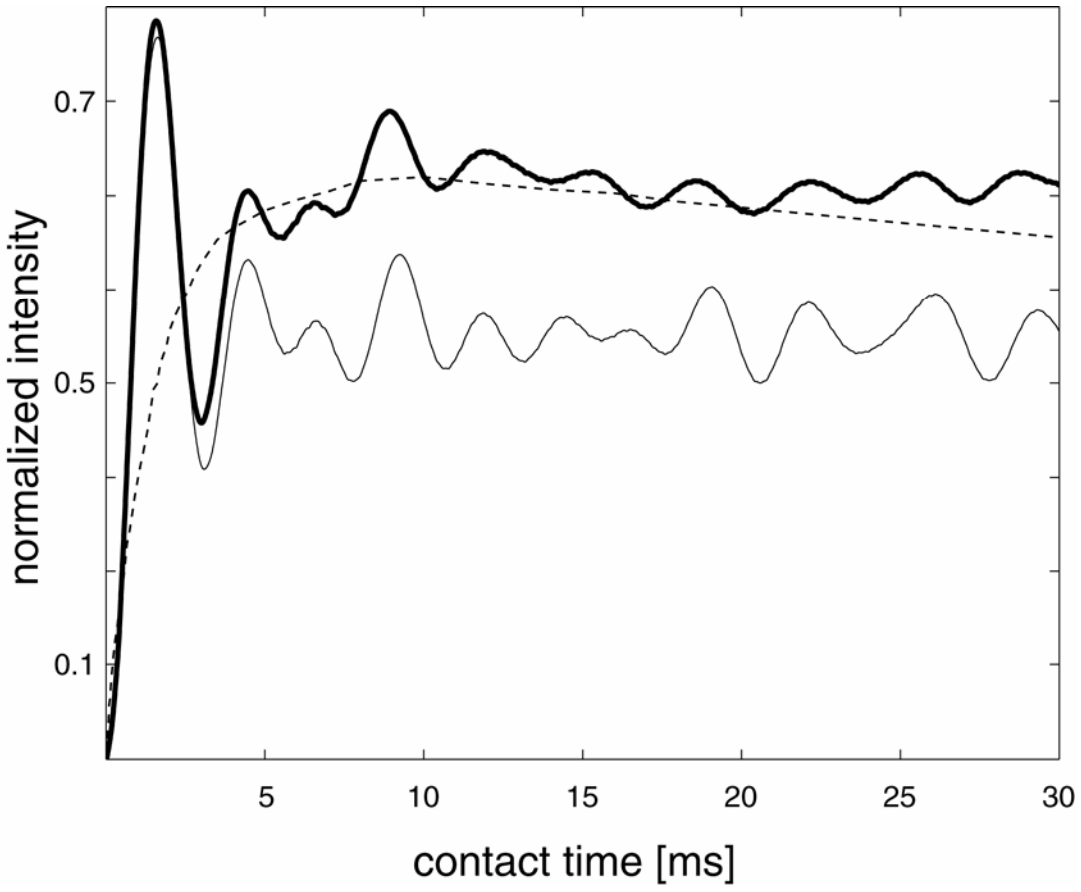

Figure 5.8 Simulated CP-MAS build-up curves on a -**C**H_2- (thin line), and a –CH_2-**C**H_2-CH_2- spin system (thick line), compared to the measured curve on the PP37_A blend (dotted line). The spinning frequency was considered the same as in the experiment, ν_R = 2.5 kHz. All the dipolar couplings were scaled uniformly with an order parameter of $\langle P_2 \rangle = 0.023$, to approach the experimental build-up rates in blends. Also, the amplitude of the simulated curve on the extended spin system was scaled by a factor of 3.96, in order to reproduce the real CP efficiency in PP37_A blend[75].

A CP build-up curve is thus generated only by the remaining carbons, that is, by the ^{13}C nuclei from inter-crosslink chains. Such a situation can be modeled for instance by numerical simulations in an appropriately defined C-H spin system, where all the static dipolar couplings are scaled uniformly by the same order parameter, $\langle P_2 \rangle$. In the end, the computed curve has to

be multiplied by a weighting factor representing the fraction of carbons located in inter-crosslink chains.

An important issue within the above procedure is to define an appropriate spin system which on the one hand is sufficiently large to reproduce all the characteristic features of the polarization transfer process, while on the other hand is not too extended, such that one can keep the computational time within reasonable limits. Unlike rigid organic solids, the case of elastomers is more advantageous from this point of view: in choosing an optimal spin system size one can safely confine to protons which are located in the same polymer chain around a given ^{13}C position, because the fast molecular motion will effectively average to zero the inter-chain dipolar couplings. Given these considerations, in Figure 5.8 one illustrates the results of CP-MAS numerical simulations performed on a -**C**H_2- (thin line), and a –CH_2-**C**H_2-CH_2- system (thick line), where only the central carbon (marked in bold) is considered a ^{13}C isotope. The CP curves were computed using an order parameter of $<P_2>=0.023$, for which the CP build-up rate was found to be close to the measured rates in the PP/EPDM blends (see the dotted line). Comparing these examples of a two-, and a six-proton reservoir, one can draw the following conclusions: *(i)* the short-time raising parts of the CP curves almost coincide, which means that CP dynamics here is dominated by the residual dipolar couplings between the given carbon and its directly bonded protons, *(ii)* the quasi-equilibrium value of the transferred polarization at large mixing times, however, depends also on the spatial extension of the proton network around the central ^{13}C nucleus, and *(iii)* the dephasing under ^{1}H-^{1}H multi-spin dipolar interactions (or, equivalently, the relaxation of zero-quantum coherences in the tilted rotating frame) is not very effective in smoothing out the transient dipolar oscillations, which are quite pronounced even in the case of a six-proton reservoir. Extending the simulations to a larger chain fragment would not lead to essentially new features, because the distances from the central ^{13}C nucleus to the added protons are too large to cause significant changes in the polarization transfer dynamics within the investigated time scale. Therefore, all the simulations below will be performed on the seven-spin system defined above.

Comparing the simulated CP curves with the measured ones, it is obvious that there are still major inconsistencies between them. Whereas the order parameter is relatively easy to adjust for approaching the experimental CP build-up rates, the weak damping of transient oscillations

under ^{1}H-^{1}H multi-spin dipolar interactions cannot explain for the smooth CP curves typically obtained in practice, see Figure 5.5. In addition, the scaling factor of about 4 we had to apply upon the simulated curves in order to reproduce the actual CP efficiency is unrealistically large, because this would mean that more than 75% of the rubber material is confined into dangling ends. In the following we demonstrate that these discrepancies are mainly a consequence of the simplified assumptions on which the model is build.

To remove the observed inconsistencies, obviously, a more realistic picture of the way in which molecular motion affects the residual dipolar couplings in elastomers must be considered. In terms of a distribution of residual dipolar couplings along a polymer chain, the case treated above is equivalent with an order parameter distribution function, $J(\langle P_2 \rangle)$, which is delta-peaked around two distinct values: a finite value, $\langle P_2 \rangle_0$, for nuclei inside inter-crosslink chains, and zero for nuclei located in dangling ends. This is illustrated in Figure 5.9 by the dotted line, where the amplitudes of these peaks are proportional with the corresponding fraction of the two types of carbon nuclei. However, a more natural extension of this model would be to consider instead a distribution function where the two infinitely narrow peaks of the previous approximation are replaced by broader peaks (for simplicity, we chose here Gaussian peaks) centered on the same values of the order parameter, namely, $\langle P_2 \rangle = 0$ and $\langle P_2 \rangle = \langle P_2 \rangle_0$, respectively. Here, variations in the cross-links density will not only affect the actual value of $\langle P_2 \rangle_0$, as in the former simplified approximation, but are expected to cause changes also in the peak widths and intensities.

In the roughest approximation, a possible connection between the structure of the cross-link network in a rubbery sample and particular features of its corresponding order parameter distribution function can be drawn based on the natural assumption that the widths of the two peaks are a measure of flexibility along the polymer chain. For instance, the more rigid a segment of an inter-crosslink chain is in its rapid molecular reorientation around the anisotropy axis, the narrower should be the corresponding peak centered on $\langle P_2 \rangle_0$. At higher cross-link densities, the average chain length between two cross-link points will decrease, which is expected to result in an increased rigidity of the statistical segments along the chain. Thus, within this picture, a narrowing of the peaks in the $J(\langle P_2 \rangle)$ distribution function is obtained at

larger cross-links densities by restricting the relative motion between statistical segments along a polymer chain.

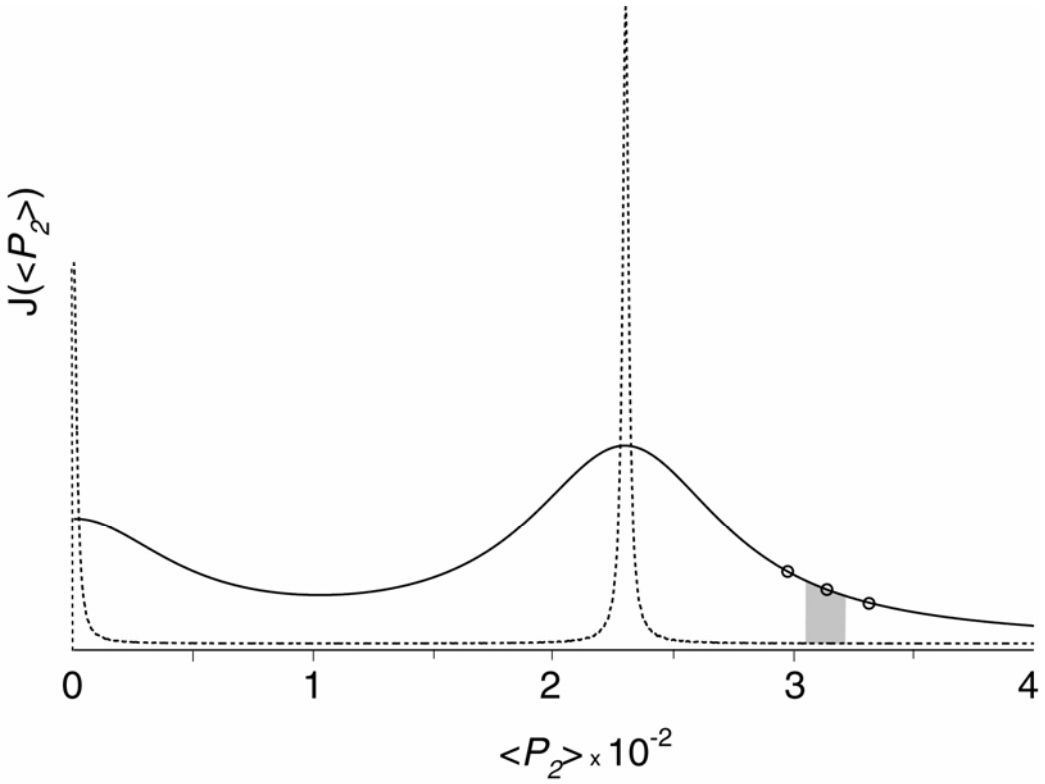

Figure 5.9 The order parameter distribution functions $J(\langle P_2 \rangle)$ corresponding to the two distinct approximations discussed in the text[75]

A more quantitative analysis, like establishing exact relationships between different statistical chain models in rubbers and the shape of the resulting order parameter distribution function is beyond the purpose of the present investigation. Therefore, in the remainder of this work we will confine to analyze the sensitivity of the CP curves to changes in characteristic parameters of the corresponding distribution functions, $J(\langle P_2 \rangle)$. To accomplish this, first, a series of 45 CP build-up curves was generated by numerical simulations performed on the $-CH_2$-**C**H_2-CH_2- system described above. Each of them corresponds to a different value of the order parameter within the range $\langle P_2 \rangle = 0.0005 \div 0.125$. To construct a resultant build-up curve, these 45 individual contributions were added together with weighting factors given by the area under

$J(\langle P_2 \rangle)$ between two consecutive points, as illustrated by the shaded region in Figure 5.9. The total integral intensity of $J(\langle P_2 \rangle)$ was normalized to one.

Subsequently, an algorithm for finding distribution functions which generate CP build-up curves with a given shape was constructed and applied. In particular, a scan through a large number of distinct values for the $J(\langle P_2 \rangle)$ characteristic parameters was performed taking the experimental PP37_A CP curve as target function. The result is shown in Fig. 8b by dotted line, and the characteristic parameters of the $J(\langle P_2 \rangle)$ distribution function which generates this particular CP curve are $\langle P_2 \rangle_0 = 0.03$, $\Delta\langle P_2 \rangle = 0.02$, $\Delta\langle P_2 \rangle_0 = 0.04$ and $I/I_0 = 3/7$, where $\Delta\langle P_2 \rangle$ and I, represent the width and intensity of the Gaussian peak centered on $\langle P_2 \rangle = 0$, while $\Delta\langle P_2 \rangle_0$ and I_0 are the same parameters for the $\langle P_2 \rangle_0$ peak, respectively. In addition, an overall scaling factor of ¾ was applied to the resulting CP curves in Figure 5.10b to account for the difference between the CP gain factor achievable in practice, and the ideal factor, which characterize the numerical simulations.

As can be easily seen from the Figure 5.10b, all the main features of the measured CP curves on blends PP37_A and PP37_C are reproduced quite well using the proposed model. In particular, the significant drop in CP efficiency, the complete smoothing of the transient dipolar oscillations, and an approximately similar CP build-up rate, could all be obtained using the order parameter distribution function displayed by dotted line in Figure 5.10a.

Keeping the analysis on a qualitative ground, the effect of increasing the cross-link density will be investigated next using the CP curve and the $J(\langle P_2 \rangle)$ distribution function, represented by dotted line in Figures 5.10a and 5.10b, as reference curves. According phenomenological interpretation provided above, an increase in cross-link density could lead to *(i)* narrower Gaussian peaks in the $J(\langle P_2 \rangle)$ function, *(ii)* smaller I/I_0 ratios, and *(iii)* larger $\langle P_2 \rangle_0$ values, respectively. The major changes we obtained by performing all these parameter variations were, indeed, a progressive development of transient dipolar oscillations in the resultant CP curves, and also an increase in their build-up rates. This result agrees well with the trend observed experimentally on going from blends obtained by mixing PP with EPDM to additionally cross-linked blends.

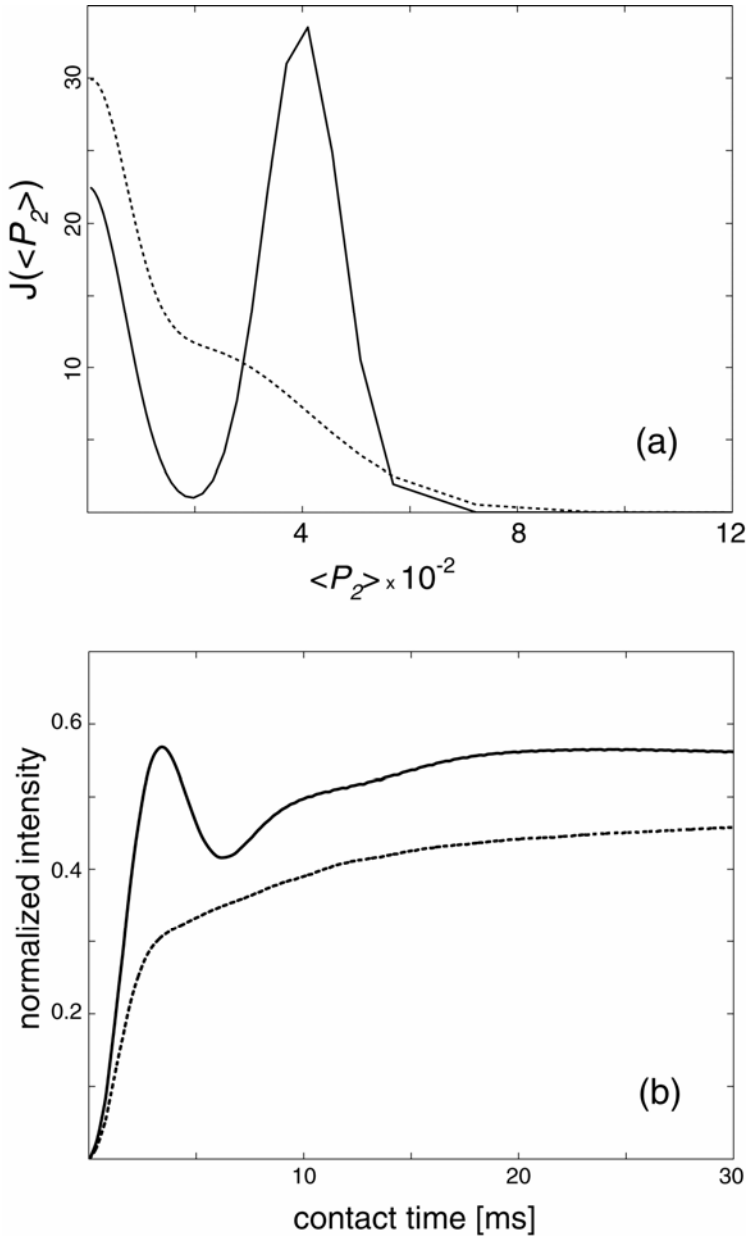

Figure 5.10 (a) The order parameter distribution functions $J(\langle P_2 \rangle)$ evaluated for 45 discrete values of the order parameter $\langle P_2 \rangle$ ranging between 0.005 and 0.125; they are made up of two Gaussian peaks, centered on $\langle P_2 \rangle = 0$ and $\langle P_2 \rangle_0 = 0.03$ (dotted line), and on $\langle P_2 \rangle_0 = 0$ and $\langle P_2 \rangle_1 = 0.04$, respectively. The other parameters are $\Delta\langle P_2 \rangle = 0.01$, $\Delta\langle P_2 \rangle_0 = 0.04$, intensities ratio 3/7 (dotted line), and $\Delta\langle P_2 \rangle = 0.01$, $\Delta\langle P_2 \rangle_0 = 0.01$, intensities ratio 2/3 (continuous line). In both cases, the total integral intensity of the $J(\langle P_2 \rangle)$ function was normalized to one. **(b)** The CP build-up curve generated by the above two distribution functions. These curves were constructed according to the algorithm defined in the text.

One of such theoretical CP curve is illustrated in Figure 5.10b with continuous line: it was generated using an order parameter distribution function (represented in Figure 5.10a also by continuous line) with the following parameters: $\langle P_2 \rangle_0 = 0.04$, $\Delta\langle P_2 \rangle = 0.01$, $\Delta\langle P_2 \rangle_0 = 0.01$ and $I/I_0 = 2/3$.

Finally, it is worth mentioning that distinctive features in the resultant CP build-up curve are not equally sensitive to the all $J(\langle P_2 \rangle)$ characteristic parameters. In particular, it was found that the occurrence of transient dipolar oscillations is more sensitive to decreasing $\Delta\langle P_2 \rangle_0$, i. e., to reducing the order parameter dispersion within inter-crosslink chains, whereas the build-up rate is mostly responsive to changes in the $\langle P_2 \rangle_0$ and I/I_0 values. These findings also constitute an important point of our analysis, because they provide a possible explanation for the fact that the build-rate in PP37N_C sample is smaller than in PP37_C, even though the presence of the transient oscillation in the CP curve of the former would indicate a larger cross-link density.

However, the values of the theoretical parameters do not exactly agree with the experiment. Partly, this could originate from the relatively small number of distinct $\langle P_2 \rangle$ values used for constructing a resultant CP curve, and partly it can be explained by the actual degree of validity for our samples of the assumptions on which the model is built.

In principle, the M_c values for blended samples can be obtained from this results analog with the calculations performed for the case of proton transversal relaxation for pure EPDM. The parameter q from eq. (3.43) have to be identified with $\langle P_2 \rangle^2$.

CONCLUSIONS

Solid-State Nuclear Magnetic Resonance methods were used to characterize the rubber phase in PP/EPDM blends. ^{1}H transverse relaxation techniques are routinely used to characterize cross-linking in rubbers because only a short acquisition time is needed, and the interpretation of the measured ^{1}H signal in terms of characteristic structural features of the investigated material is considered not to be very complicated. The cross-link density can be conveniently extracted based on the model of residual dipolar couplings induced by permanent cross-linking. However, we employed two different models to determine the network density in EPDM rubber and we proved that the results are very much dependent on the method.

Serious problems arouse when we wanted to apply the ^{1}H transverse relaxation techniques on polymer blends, where the signal usually contains multiple contributions coming from morphologically and dynamically distinct regions of the sample, which are impossible to disentangle from each other, as it is the case of our blended samples. With the help of numerical simulations and the measurements of the pure EPDM and pure PP we have demonstrated that the signal from polypropylene superimpose in a non-linear way the signal from rubber phase making impossible a correct estimation of network density of the rubber contained by this blended materials. We also showed that the inter-phase between the two regions with different mobility has a significant contribution to the proton signal.

The use of ^{13}C NMR techniques, such as spin-echo with detection on carbon channel, spin-echo double resonance (SEDOR), rotational echo double resonance (REDOR), cross-polarization (CP-MAS) or depolarization (iCP-MAS) represents the best alternative in the case of our system to study. They offer the advantage of chemical site resolution, thus selectivity in addressing distinct components of a blend. The residual C-H heteronuclear dipolar interactions are recoupled allowing, in principle, the estimation of the cross-link density for the EPDM network. REDOR proved to be not sensitive to small differences in cross-link density and therefore not useful in analyzing the effect of additional cross-linking process on blended samples.

Despite its advantages, the analysis of heteronuclear polarization transfer dynamics in terms of structural information in elastomers is commonly considered as being not very quantitative, due to the complicated way in which molecular motion interferes with the coherent polarization transfer process. In the present work it was shown that the existing theoretical models of CP dynamics in the presence of molecular motion are indeed unable to accurately describe all the characteristic features of the CP build-up (or iCP depolarization) curves observed experimentally on these materials.

According to the thermodynamic model developed by Mehring, the measured CP (iCP) curves are the result of competitive polarization transfer and spin-lattice relaxation in the rotating frame processes. The extraction of the polarization transfer rate, $1/T_{CH}$, from such curves in elastomers is preferable within the so called fast motional regime, i. e., at temperatures well above the glass transition temperature, where relaxation has only a marginal influence upon the short-time polarization transfer dynamics. However, even in this regime the thermodynamic model proves to be too simplistic. In particular, it cannot explain for the large amplitude scaling factor commonly obtained in practice, and also for the occurrence in certain cases of transient dipolar oscillations in the resultant CP curves.

The model of residual dipolar couplings under permanent cross-linking is better suited from this point of view to describe CP dynamics in elastomers, because of the dominant coherent character of polarization transfer process in the fast motional regime. The simplest approach (typically used to analyze ^{1}H transverse relaxation data) considers the rigid body dipolar couplings scaled under molecular motion by the so called order parameter, which in elastomers is assumed to have only two distinct values: a finite value for the inter-crosslink chains, and zero for dangling ends, respectively. Based on numerical simulations we have shown here that, in its simplified form, this model can only provide a rough approximation of the real CP dynamics. In particular, the weak damping of the transient dipolar oscillations under ^{1}H-^{1}H multi-spin dipolar interactions, predicted by the model, is in large disagreement with the experimental facts.

Theory and experiment can be reconciled assuming a more realistic distribution of the order parameter across the sample. For this purpose, we have derived an extension of the model

where the delta-peaked order parameter distribution function of the previous approach is replaced by a superposition of two broad Gaussian peaks. The extended model was shown to easily account for the all features observed in the resultant CP curves. For instance, the complete (or partial) damping of transient dipolar oscillations, the values of the CP build-up rate, and amplitude scaling factor, strongly depend on the characteristic parameters of the Gaussian peaks associated with the two dynamically distinct domains in rubbers. Coming from the other side, the exact shape of the order parameter distribution function depends on structural and dynamical properties of the sample. Thus, provided that an adequate statistical chain model is available, changes in the characteristic features of the measured CP curves can be easily analyzed in terms of structural information. In any case, even in its abstract form, the extension of the theoretical model developed here clearly demonstrates that ^{1}H-^{13}C polarization transfer dynamics is a source of useful quantitative information, contrary to what was believed in the past.

The validity of the new CP data analysis model was demonstrated using the example of the CP build-up curves measured on a well resolved EPDM resonance line in a series of EPDM/PP blends. The build up rates, as well as the presence (or not) of transient dipolar oscillations, proved quite sensitive to changes in the cross-link network induced by different EPDM vulcanization conditions. A simple phenomenological approach was employed here to explain the observed behavior based on the extended model of residual dipolar couplings under permanent cross-linking. Specifically, the occurrence of transient oscillations is most probably associated with an increased rigidity of the statistical segments in their relative motion along the polymer chain, while the values of the build-up rate correlate with the cross-link density.

REFERENCES

(1) Hofmann, W., *Rubber Technology,* **1990**, Oxford University Press, UK.

(2) Coran, A. Y.; Patel, R., *Rubber Chem. Technol*., **1980**, 5, 141.

(3) Painter, P. C.; Coleman, M. M., *Fundamentals of Polymer Science,* **1994,** Technomic Publishing Co., Lancaster.

(4) Birley, A. W.; Haworth, B.; Batchelor, J., *Physics of Plastics*, **1992**, Hanser Publishers, Munich.

(5) Kunn, T. H., *Rubber World*, **1985**, 192, 5, 20.

(6) Kresja, M. R.; Koenig, J. L., *Rubber Chem. Technol*., **1993**, 66, 376-410

(7) Hoover, F. I., *Rubber World*, **1990**, 220, 24

(8) Sperling, L.H., *Introduction to physical polymer science*, **1992**, John Wiley & Sons, New York.

(9) Purcell, E. M.; Torrey, H. C.; Pound, R. V., *Phys. Rev*., **1946**, 69, 37.

(10) Bloch, F.; Hansen, W. W.; Packard M. E., *Phys. Rev*., **1946**, 69, 127.

(11) Abragam, A., *Principles of Nuclear Magnetism,* **1961**, Clarendon Press, Oxford.

(12) Mehring, M., *Principles of High Resolution NMR in Solids,* **1983**, Springer-Verlag, Berlin.

(13) Andrew, E. R.; Bradbury, A.; Eades, R. G., *Nature*, **1958**, 182, 1659.

(14) Lowe, I.J., *Phys. Rev. Lett*., **1959**, 2, 285.

(15) Waugh, J. S.; Huber, L.M.; Haeberlen, U., *Phys. Rev. Lett*., **1968**, 20, 180.

(16) Gerstein, B. C.; Chou, C.; Pembleton, R. G.; Wilson, R. C., *J. Phys. Chem*., **1977**, 81, 565.

(17) Dec, S. F.; Bronnimann, C. E.; Wind, R. A.; Maciel, G. E., *J. Magn. Reson*., **1989**, 82, 454.

(18) Samoson, A.; Tuherm, T.; Gan, Z., *Solid State Nucl. Magn. Reson*., **2001**, 20, 130.

(19) Dixon, W.T., *J. Chem. Phys*., **1982**, 77, 1800.

(20) Bloch, F., *Phys. Rev*., **1954**, 93, 944.

(21) Pines, A.; Gibby, M. G.; Waugh, J. S., *J. Chem. Phys*., **1973**, 59, 569.

(22) Hartmann S. R.; Hahn, E. L., *Phys. Rev*., **1962**, 128, 2042.

(23) Litvinov, V. M.; De, P. P., *Spectroscopy of Rubbers and Rubbery Materials*, **2002**, Rapra Technology LTM, Exeter, UK.

(24) Winters, R.; Heinen, W.; Verburggen, M. A. L.; Lugtenburg, J.; van Duin, M.; de Groot, H. J. M., *Macromolecules,* **2002**, 35, 1958.

(25) Menge, H.; Ilisch, S.; Aluas, M., *Kautschuk Gummi Kunststoffe*, **2002**, 55, 3, 86.

(25a.)Hempel, E., unpublished results.

(26) International Institute of Synthetic Rubber Producers, *Worldwide Rubber Statistics*, **1998**, Houston, TX, USA.

(27) Jacob, C.; De, P.; Bhowmick, A. K.; De, S. K., *J. Appl. Polym. Sci*., **2001**, 82, 3304.

(28) Höhne, G. W. H.; Hemminger, W. F.; Flammersheim, H. J., *Differential Scanning Calorimetry*, **2003**, Springer-Verlag, 2nd Rv&Enl edition.

(29) Ward, I. M.; Hadley, D. W., *An Introduction to the Mechanical Properties of Solid Polymers*, **1993**, John Wiley & Sons Ltd., Chichester.

(30) Fülber, C.; Demco, D. E.; Weintraub, O.; Blümich, B., *Macromol. Chem. Phys*., **1996**, 197, 581.

(31) Callaghan, P. T.; Samulski, E. T., *Macromolecules,* **1997**, 30, 113.

(32) Kimmich, R.; Fischer, E.; Callaghan, P.; Fatkullin, N., *J. of Magn. Res. A*, **1995**, 117, 53.

(33) Simon, G.; Schneider, H., *Makromol. Chem. Macromol. Symp.,* **1991**, 52, 233.

(34) Heuert, U.; Knörgen, M.; Menge. H.; Scheler, G.; Schneider, H., *Polymer Bulletin,* **1996**, 37, 489.

(35) Sotta, P.; Fülber, C.; Demco, D. E.; Blümich, B.; Spiess, H. W., *Macromolecules,* **1996**, 29, 6222.

(36) Litvinov, V. M.; Barendswaard, W.; van Duin, M., *Rubber Chemistry and Technology*, **1998**, 71, 105.

(37) Abragam, A., *Principles of Nuclear Magnetism*, **1961**, Clarendon Press, Oxford.

(38) Brereton, M. G., *Macromolecules*, **1991**, 24, 6160.

(39) Flory, P. J., *The Journal of Chem. Phys*., **1949**, 17, 303.

(40) Kuhn, W.; Grün, F., *Kolloid Z. Z. Polym*., **1942**, 101, 248.

(41) Cohen-Addad, J. P., *J. Chem. Phys*., **1974**, 60, 2440.

(42) Gotlib, Yu. Ya.; Lifshitz, M. I.; Shevelef, V. A.; Lishanskij, L. S.; Balanina, I. V., *Polym. Sci. URSS*, **1976**, 10, 2630.

(43) Brereton, M. G., *Macromolecules*, **1989**, 22, 3667.

(44) Cohen-Addad, J. P.; Domard, M., *J. Chem. Phys*., **1981**, 75, 4107.

(45) Andreson, P. W.; Weiss, P. R., *Review of Modern Physics*, **1953**, 25, 269.

(46) Brereton, M. G., *J. Chem. Phys*., **1991**, 94, 213.

(47) Rouse, P. E., *J. Chem. Phys*., **1953**, 21, 1272.

(48) Brereton, M. G.; Ward, I. M.; Boden, N.; Wright, P., *Macromolecules*, **1991**, 24, 2068.

(49) Doi, M.; Edwards, S. F., *The Theory of Polymer Dynamics*, **1983**, Clarendon Press, Oxford.

(50) Klueppel, M.; Menge, H.; Schmidt, H.; Schneider, H.; Schuster, R. H., *Macromolecules,* **2001**, 34, 8107.

(51) Gronski, W.; Hoffman, U., *Rubber Chem. Technol.,* **1992**, 65, 63.

(52) Menge, H.; Hotopf, S.; Poenitzsch, St.; Richter, S.; Arndt, K.; Schneider, H.; Heuert, U., *Polymer* **1999**, 40, 5303.

(53) Knoergen, M.; Menge, H.; Hempel, G.; Ries, M. E.; Schneider, H., *Polymer,* **2002***,* 43, 4091.

(54) Menge, H.; Hotopf, S.; Heuert, U.; Schneider, H., *Polymer*, **2000**, 41, 3019.

(55) Fry, C.; Lind, A. C., *Macromolecules*, **1988**, 21, 1292.

(56) Simon, G.; Baumann, K.; Gronski, W., *Macromolecules*, **1992**, 25, 3624.

(57) Litvinov, V. M.; Barenswaard, W.; van Duin, M., *Rubber Chemistry and Technology*, **1998**, 71, 105.

(58) Richter, D.; Farago, B.; Butera, R.; Fetters, L. J.; Huang, J. S.; Ewen, B., *Macromolecules*, **1993**, 26, 795.

(59) Hahn, E. L., *Phys. Rev*., **1950**, 80, 580.

(60) Kaplan, D. E.; Hahn, E. L., *J. Phys. Radium*, **1958**, 19, 821.

(61) Slichter, C. P., *Principles of Magnetic Resonance*, **1990**, Springer-Verlag.

(62) Gullion, T., *Magn. Reson. Rev.*, **1997**, 17, 83.

(63) Lang, D. V.; Boyce, J. B.; Lo, D. C.; Slichter, C. P., *Phys. Rev. Lett*., **1972**, 29, 776.

(64) Makowka, C. D.; Slichter, C. P.; Sinfelt, J. H., *Phy. Rev. Lett*., **1982**, 49, 379.

(65) Gullion, T.; Schaefer, J., *Adv. Magn. Reson*., **1989**, 13, 57.

(66) Saalwaechter, K.; Spiess, H. W., *J. Chem Phys*., **2001**, 114, 13, 5707.

(67) Metz, G.; Wu, X.; Smith, S. O., *J. Magn. Reson*., **1994**, 110, 219.

(68) Mori, M.; Koenig, J. L., *A Review of High-Resolution NMR Studies of Vulcanized Elastomers* in *Annual Reports on NMR Spectroscopy,* **1997**, Academic Press, New York.

(69) Fuelber, C.; Demco, D. E.; Bluemich, B., *Solid State Nucl. Magn. Reson*., **1996**, 6, 213.

(70) Stejskal, E. O.; Schaefer, J.; Waugh, J. S., *J. Magn. Reson*., **1977**, *28*, 105.

(71) Benett, A. E.; Rienstra, C. M.; Auger, M.; Lakshmi, K. V.; Griffin, R. G., *J. Chem. Phys.,* **1995**, *103*, 6951.

(72) Curran, S. A.; Padwa, A. R., *Macomolecules*, **1987**, 20, 625.

(73) Da Silva, N. M.; Tavares, M. I. B.; de Menezes, S. M. C., *J. Appl. Polym. Sci*., **1996**, 60, 1419.

(74) Ray, S.; Ladizhansky, V.; Vega, S., *J. Magn. Reson.,* **1998**, 135, 237.

(75) Aluas, M.; Filip, C., in press.

Acknowledgements

This work would not have been possible without the support and decisive guidance of a few people. This is the place and opportunity for me to thank them for making my years of research fruitful.

First I would like to express my most sincere gratitude to Professor Horst Schneider. He was the one who encouraged me to join his research group at Halle-Wittenberg University, offered me the first insights on what NMR actually means and made my staying in Halle something to remember for the rest of my life. He was, and in many ways still is, the best "Chef" I could have asked for.

Second on my list is Günter, a man of infinite patience, as he has proven numerous times. Always in good mood, he tried to do his best in guiding my work. He was instrumental in getting me moving forward at a time when I thought I was stuck in an impossible research project. I want also to thank him for all his good suggestions related to this work and for the critical reading of the manuscripts.

Detlef, a magician of technology. He helped whenever I had troubles with the spectrometers in our lab. And troubles were many, sometimes at impossible hours. In one instance he came at seven o'clock in the morning in a weekend day to help to get my work back on the line.

Then there is Manfred, a true friend. He was the one to take me see various places in Germany, making several of my weekends more interesting and enjoyable.

I cannot miss on Karin. She took care of me by providing me with lots of useful information that is valuable for any foreigner coming to Germany. It was comfortable to know that she was there, in the lab, ready to help if asked.

I want also to thank Maxim. We shared the "misery" of being Ph.D. students in a foreign country probably the same way. But he, being a genius, had to help me whenever I needed and asked for it, whether it was about my computer, my research or some other problems.

Further, I have to mention Adnan, the colleague with whom I shared office during the time I wrote my Ph.D. thesis. I have to thank him for keeping as quiet as possible when I most needed it, and for being such a nice and responsive person.

I would also like to thank Uwe and all of my colleagues for their help and encouragements.

I am particularly indebted to Dr. Claudiu Filip for the many interesting and fruitful discussions and for his invaluable guidance through the last part of my research work. Without his input many of the things I achieved would not have been possible.

I would also want to thank my parents for being so supportive all these years of being far away from them and my home.

CURRICULUM VITAE

PERSONAL

Name**:**	**Aluas**
Given name:	**Mihaela**
Date of birth:	**27th of December, 1974**
Place of birth**:**	**Hida, Romania**
Gender:	**Female**
Nationality**:**	**Romanian**
Marital status:	**Married**

EDUCATION

2001 – present	**PhD Student at Martin-Luther University, Halle, Germany**
1998 – 1999	**M. Sc. at „Babes–Bolyai" University, Cluj-Napoca, Romania** **Specialization: Molecular Physics** **Disertation title:** IR and Raman Studies of Theophylline
1993 – 1998	**B. Sc. at Faculty of Physics, "Babes-Bolyai" University, Cluj-Napoca, Romania** **Disertation title**: Vibrational Studies of B_6 Vitamin
1989 – 1993	**High-school, specialization: mathematics and physics.**

WORKING EXPERIENCE

2000 – present	**Researcher at Martin-Luther University, Halle, Germany, Solid State NMR Spectroscopy Department** **Academic duties: - student research stages supervisor in NMR laboratories** **- general physics laboratories supervisor for undergraduate students**
1999 – 2000	**Physics teacher at „Aurel Vlaicu" High-school, Cluj, Romania**

FOREIGN LANGUAGES

		Language competencies, on a scale from 1 to 5			
		Understanding	**Reading**	**Speaking**	**Writing**
Language	**English**	**5**	**5**	**4**	**4**
	German	**4**	**4**	**4**	**3**
	French	**3**	**4**	**2**	**2**

PUBLICATIONS AND POSTERS

Papers

S. Canta, T. Iliescu, D. Maniu, C. Morari, M. Aluas**, O. Cozar, W. Kiefer**
Vibrational Studies of B6 Vitamin.
Vibrational Spectroscopy, 19, 2, 329-334 (1999)

S. Canta, E. Vogel, D. Maniu, **M. Aluas,** T. Iliescu, W. Kiefer
Surface Enhanced Raman Scattering of PP Vitamin on Different Au and Ag Substrates.
J. Mol. Struct., 482, 679-684 (1999)

Papers related to this work

H. Menge, **M. Aluas,** S. Ilisch
Investigation of Physical-mechanical Properties of PP/EPDM Blends.
Kautschuk Gummi Kunststoffe, 55, 3, 86-93 (2002)

M. Aluas, C. Filip
Solid-State NMR Characterization of Cross-Linking in EPDM/PP blends from ^{13}C-^{1}H Polarization Transfer Dynamics
In press

M. Aluas, S. Ilisch, H. Schneider, G. Hempel
Rubber Phase Characterization in PP/EPDM Blends by Means of ^{13}C Solid-State NMR
In preparation

Abstracts (posters) related to this work

1. 24th Discussion Meeting - Magnetic Resonance and Molecular Interactions, Bremen, Germany, 24-27 September 2002.
M. Aluas, H. Menge, H. Schhneider, S. Ilisch, G. Hempel
„Estimation of the Elastomer Structure in Thermoplastic Vulcanisates by NMR"

2. Morphologie und Eigenschaften von Polymerblends, Merseburg, Germany, 26-27 March 2003.
M. Aluas, H. Schneider, S. Ilisch, G. Hempel
„Characterization of EPDM/PP Blends by ^{13}C Solid State NMR"

3. Alpine NMR Conference, Chamonix, France, 14-18 September 2003.
M. Aluas, H. Schneider, G. Hempel
"Selective ^{13}C Investigation in Thermoplastic Elastomers

Eidesstattliche Erklärung

Hiermit erkläre ich an Eides Statt, dass ich die vorliegende Arbeit selbständig und ohne fremde Hilfe verfasst und nur die angegebenen Quellen und Hilfsmittel verwendet habe. Ergebnisse anderer wissenschaftlicher Arbeiten wurden als solche gekennzeichnet. Diese Arbeit wurde bisher weder im In- noch im Ausland in gleicher oder ähnlicher Form in einem Prüfungsverfahren vorgelegt. Ich erkläre hiermit, dass ich mich bis zu dem jetzigen Zeitpunkt noch nie um einen Doktorgrad beworben habe.

Halle (Saale), July 2004 Mihaela Aluas